Control of Wave Systems Based on Reflected Wave Rejection

September 2015

Eiichi Saito

Control of Wave Systems Based on Reflected Wave Rejection

September 2015

A thesis submitted in partial fulfillment of the requirements for the degree of
Doctor of Philosophy in Engineering

Keio University

Graduate School of Science and Technology
School of Integrated Design Engineering

Saito, Eiichi

Acknowledgements

This dissertation is summary of my research from April 2010 to September 2015 as the member of Katsura Laboratory, in Keio University. In the six years since I entered the laboratory, I have had many valuable experiences and I was supported by a lot of people. Here, I would like to express my gratitude to all people who have given me the supports and advices.

First of all, I would like to be deeply grateful from my heart for my supervisor Associate Professor Dr. Seiichiro Katsura, Department of System Design Engineering, Keio University. His dedicated teaching has grown me and provided a lot of precious things. Moreover, his passion for the academic research has inspired me to do research activity actively and to develop the novelty. Besides, he provided a lot of opportunities such as making the presentation of my research at domestic and international conference, participating in exhibitions. I can never imagine that I could accomplish this work without this kind help.

I would like to offer my special thanks to the members of my Ph. D. dissertation committee, Professor Dr. Toshiyuki Murakami, Department of System Design Engineering, Keio University, Associate Professor Dr. Yakoh Takahiro, Department of System Design Engineering, Keio University, Associate Professor Dr. Masayuki Kohiyama Department of System Design Engineering, Keio University.

I would like to show my appreciation to Professors who gave precious comments at the research meetings. I would like to thank Professor Dr. Kouhei Ohnishi in Keio University, and Assitant Professor Dr. Takahiro Nozaki in Keio University.

During my Ph. D. course, I visited and studied in Prof. Roberto Oboe Laboratory in Padova University, Italy, for one year. This visit was supported by the "International Collaborative Research of Perception and Expression Media for Development of Medical Access Space," the one of the programs of" Strategic Young Researcher Overseas Visits Program for Accelerating Brain Circulation ". I would like to thank Proffessor Roberto Oboe in Padova University. He discussed my research with me, and supported my life in Italy.

As my career of research activities, the Japan Society for the Promotion of Science (JSPS) has provided me the financial support. I would like to show my gratitude to the organization. By the support, I could get various opportunities to conduct my research and to make the presentation at the academic conferences.

Let me appreciate everyone who collaborated with and help me in Katsura Laboratory. The things which I obtained at this laboratory are treasurable for me.

Finally, I would like to express my gratitude to my family who bring me up and help me a lot. Your kind and warm-hearted assistance have enabled me to study without any inconvenience, and I would like to thank you from my heart.

September, 2015
Eiichi Saito

Table of Contents

List of Figures

List of Tables

Chapter 1

Introduction

1.1 Background of This Dissertation

1.1.1 Automatic Control of Robots and Machines

Precise motion control of robots and machines has been demanded in various industrial fields for a long time [1, 2]. Both progress of control theory and development of performance of a computer lead to achieve accurate and rapid control of robots and industrial machines [3,4]. In general, to construct a high performance control system, sampling time should be set as short as possible. In recent year, a control system with 5 μs sampling time has been realized and high bandwidth motion control has been achieved by FPGA [5]. In addition, it is now easy to construct a real-time system with about 100 μs sampling time by using a general-purpose computer with some software such as Real-Time Application Interface [6]. With the performance improvement of a computer, control theory of industrial robots and machines has also been developed. In particular, robust control can control accurate and rapid control of them under existence of disturbance and modeling error. Representative methods of robust control are H_∞ control [7, 8], sliding-mode control [9–11], acceleration control based on a disturbance observer [12–14], etc. Although a disturbance observer has a simple structure, robust control of robots and machines can be conducted, and it is friendly to use the observer in the industrial fields. Additionally, the disturbance observer with accurate nominal model can be used as a force sensor [15, 16]. Because the disturbance observer omits the force sensor including some stiffness, the high-bandwidth force control system has been realized [17]. Owing to its simplicity, the disturbance observers have been applied to various applications [18–26].

To improve control performance of robots and machines, not only increasing the control bandwidth but also vibration suppression of mechanical resonances and time-delay compensation should be considered. Particularly, if there are some mechanical constraints such as weight reduction of robots, use of gear, enlarging size of a mechanical system to improve production efficiency, not only first-order resonance but also higher-order resonance is often excited, which prevents the control system from further improvement of control bandwidth. In addition, time delays, existing in a DA converter, a communication system or a sensing device, which are neglected in the past should be considered because its phase-lag characteristic makes the control system unstable. Therefore, this dissertation deals with vibration suppression of mechanical resonance and time-delay compensation to realize high-performance control of robots and machines.

1.1.2 Vibration Control of Resonant Systems

Although various types of vibration control have been researched in the past, vibration suppression methods of mechanical resonance by a linear-control theory can be divided into two methods [27–30]: gain-stabilization method and phase-stabilization method. The gain stabilization means that resonant peak is suppressed by pole-zero cancellation based on small-gain theorem. The gain-stabilization method is often realized by use of a notch filter [31, 32]. A notch filter is often implemented in industrial fields, and typical servo drivers for the AC servo motors have function of use of a notch filter [33–35]. However, disturbance-suppression performance of control system using a notch filter is worse than that of phase stabilization method. In addition, performance of control based on a notch filter is weak against variation of resonant frequency. Hence, control system using a notch filter needs assumption that there is few disturbance at the frequency in which the notch filter is applied. Additionally, an adaptive notch filter [36] which estimates the resonant frequency is often used. On the other hand, the phase-stabilization method stabilizes the resonances by increasing phase margin based on the Nyquist stability criterion. The phase-stabilization method has advantage that it has robustness against variation of resonant frequency because the sensitivity function of the control system becomes low-sensitivity near the resonant frequency. Examples of phase-stabilization method are a state feedback control, velocity feedback, phase-lag or phase-lead compensator. Whether phase-lead or phase-lag compensation is appropriate for stabilizing the resonance depends on coefficient of each vibration mode [37]. The method [38] deals with the case that all the coefficients are same sign, and phase-lead compensation generated by the disturbance observer is conducted to suppress the vibrations in a semi-closed-loop control of a multi-mass resonant

system. In general, when the coefficient of vibration mode are different sign from that of neighbor vibration mode, it is difficult to realize phase stabilization of the two resonances at the same time [39]. Hence, in this case, combination of the gain-stabilization and phase-stabilization method should be used.

It is also important to select which model is used for construction of vibration control. They can be divided into two models: One is a lumped parameter model, the other is a distributed parameter model.

As for the lumped parameter models, there are a two-mass resonant model, a multi-mass resonant model. A N-mass resonant model is composed of N masses and N-1 springs, which are connected in series in general. A two-mass resonant model is the simplest model in lumped parameter models, which considers only a first-order resonant frequency. Owing to its simplicity, there are many conventional methods of the two-mass resonant system in the past [40, 41]. For example, there are a velocity feedback, state feedback control [42–44], H_∞ control [45, 46], μ synthesis [47], coefficient diagram method [48], resonance ratio control [49, 50], integral resonant control [51], self resonance cancellation control [52, 53], etc. Those conventional methods have simple control structures. In particular, resonance ratio control has clear physical meanings. In the field of vibration control of the two-mass resonant system, inertia/mass ratio between motor and load is strongly related to difficulty of vibration control by velocity feedback [54]. The resonant ratio control conducts the reaction torque/force feedback estimated by a reaction force observer [15] to equivalently reduce the inertia/mass ratio. In addition, when the resonance ratio, which is ratio between resonant and anti-resonant frequency, equals to $\sqrt{5}$, good vibration suppression performance can be attained in a position-control case, and it is proved that any two-mass resonant system can obtain good performance under such resonant ratio. This fact has been extended to force control of a two-mass resonant system [55–58]. According to the above, advantage of vibration control based on a lumped parameter model is that they have simple control structure and it is easy to implement and to adjust the control gains. However, because the lumped parameter model based control considers the finite number of resonances, the resonance neglected in the modeling is often excited, which is named as spillover problem [59]. The spillover problem can be solved by adding stabilizing compensator which considers robust stability. H_∞ control is good at design of robust performance and robust stability simultaneously, which is so-called mixed sensitivity problem. However, in this case, the controller becomes complicated structure and it is difficult to understand physical meaning of the controller.

On the contrary, a distributed parameter model is composed of dynamics of not only time but also space, it can consider infinite numbers of resonances. Examples of distributed parameter model for vibration control of resonant system are a wave equation [60] and a equation of Bernoulli-Euler beam [61].

Advantage of a control system based on distributed parameter models is that the spillover problem can be avoided. Although there are various control methods of distributed parameter models [62], in general, the control systems based on distributed parameter models are designed in time-domain [63] because of its complexity. Although a transfer function can be obtained analytically, it is difficult to implement a controller derived from the transfer function because the transfer function is often represented by a fractional-order form [64]. Hence, in this case, the controller derived from a distributed parameter model is approximated, but the spillover problem arises again. The distributed parameter based control design in time domain sometimes suffers from implementation to actual systems. Meanwhile, the wave equation, which is limitation of number of mass in a multi-mass resonant system, has possibility to implement the controller without approximation because a transfer function of typical wave equation is composed of time-delay elements [60]. Actually, Y. Halevi proposed a transfer function based controller design using a wave equation for suppressing torsional vibration [65]. In addition, H. Iwamoto proposed vibration suppression of a flexible beam using a wave filter [66]. The method constructs a virtual transmission system at boundary of the system, which is equivalent to insert damping with characteristic impedance of the wave system. M. Saigo proposed application to a wave absorbing filter to suppress vibration in a flexible structure [67]. The methods are often applied to vibration suppression of building vibrated by disturbance.

1.1.3 Time-Delay Compensation

Time-delay compensation is also important to control a system with high performance. Time delay has a non-minimum phase lag characteristic which is difficult to control in general [68]. Then, the phase-lag characteristic deceases phase margin of the controlled system. Due to the difficulty, many time-delay compensation methods have been researched actively [69–73]. Examples of time-delay compensation methods are Smith predictor [74, 75], internal model control (IMC) [76], a communication disturbance observer [77]. The most basic method of time delay compensation is a Smith predictor. Smith predictor predicts a future value by using a plant model, and actual response is canceled out by the predicted value multiplied by delay. As a result, time delay existing in a feedback loop will be omitted, controller design can be conducted as if there does not exist time delay in the feedback loop. Although Smith predictor needs to use both plant and time-delay models, a communication disturbance observer [78, 79] proposed by K. Natori does not use a time-delay model but use a plant model. Concept of the communication disturbance observer is that cause of destabilization in a time-delay system is regarded as a network

disturbance. The communication disturbance observer can estimate the network disturbance as well as a typical disturbance observer. Then, the time-delay compensation using estimated network disturbance is performed. Because the communication disturbance observer does not use time-delay model, the control system utilizing the communication disturbance observer has more robust against variation of time delay compared with Smith predictor based control system. However, the communication disturbance observer has disadvantage that suppression performances of disturbance and modeling error in plant model is inferior to those of Smith predictor. To improve the robustness, various methods have been proposed before now [80, 81]. K. Natori proposed combination use of communication disturbance observer and disturbance estimate observer [82] to improve the robustness against disturbance. A. Suzuki proposed a low-frequency model error feedback for improvement in steady-state accuracy [83]. The method is similar to communication disturbance observer using a band-pass filter [84]. However, the conventional researches mainly focus on a typical rigid motor system (i.e. a second-order system). If the plant has some mechanical resonances, implementation of time-delay compensation sometimes faces difficulty due to their low suppression performance of the modeling error and disturbance [85].

1.2 Motivation of This Dissertation

This dissertation focuses on both vibration suppression of mechanical resonance and time-delay compensation for achieving high performance control systems. Remarkable fact of vibration suppression of a resonant system is that, based on the wave equation, the vibration on the mechanical resonant system can be suppressed by reflected wave rejection [86, 87] like time-delay compensation. The reflected wave rejection can estimate and compensate a reflected wave which is cause of vibration in wave system. In addition, a transfer function of the wave equation is quite similar to a feedback control system including input-output time delay [88]. Therefore, it can be guessed that there is a similarity between mechanical resonant and time-delay systems from the wave-transmission point of view. Although, in general, vibration suppression of a mechanical resonant system and time-delay compensation are treated in different fields, there is possibility to construct a unified control law for the two systems by using a wave equation.

Motivation of this dissertation is to construct a generalized framework for control of wave systems which are models for mechanical resonant and time-delay systems. Applying the wave equation to both systems as a system model, it is shown that there is a similarity between the two systems: one is structure which is composed of position-input system and wave transmission system, the other is that

cause of vibration is reflected wave and elimination of reflected waves from wave systems contributes to suppress the vibration. Therefore, this dissertation proposes a control of wave systems based on reflected wave rejection. The advantages of the proposed method are as follows.

- The reflected wave rejection based vibration control considers the infinite number of poles because the system is modeled by a wave equation which is one of distributed parameter models. Hence, spillover problem can be avoided.
- The reflected wave rejection is categorized as the phase stabilization method in vibration control methods.
- The reflected wave rejection is a simple compensator which uses time-delay elements. Hence, it is easy to implement the compensator.
- It is easy to integrate mechanical resonant and time-delay systems because the resonant system modeled by a wave equation can be regarded as a time-delay system.

The framework derived in this dissertation for control of wave systems will play an important role for further improvement of performance of industrial applications.

1.3 Chapter Organization of This Dissertation

Fig. 1-1 shows the chapter organization of this dissertation. First of all, in Chapter 2, modeling of wave systems, which are a mechanical resonant system and a time-delay system, based on a wave equation is explained. Based on the modeling of wave, it is described that there is a similarity between two systems from the wave-transmission point of view [88]. Additionally, it is pointed out that cause of vibration in both two systems is a reflected wave. Then, Chapter 3 shows how to eliminate the reflected wave from the wave system to suppress the vibration, which is called a reflected wave rejection [87]. The reflected wave rejection is a core technique in this dissertation. It is also shown that, if the reflected wave is eliminated from the wave system, a transfer function of the wave system at load side becomes one time-delay element, which implies that there exists only a traveling wave. Based on the basic concept of the reflected wave rejection, Chapters 4 and 5 describe applications and extensions of the reflected wave rejection to various mechanical resonant systems and time-delay system, respectively. Contents of Chapter 4 includes a reflected wave rejections [89, 90] for various resonant systems with different

boundary conditions and wave-transmission characteristics from those in Chapter 3. Chapter 5 explains a reflected wave rejection for a feedback system including input-output time delays [88]. In Chapter 6, a reflected wave rejection for the system including both mechanical resonance and input-output time delay is proposed. Firstly, a basic concept of a reflected wave rejection for an integrated resonant and time-delay system is proposed. Next, the reflected wave rejection for the integrated resonant and time-delay system is extended to the structures which can be implemented at controller side (not remote or plant side) [91–93]. In Chapter 7, a wave-based disturbance observer is proposed for improving robustness against a disturbance acting on a tip side of the wave system. In addition, force control of the wave system by using the wave-based disturbance observer is proposed [94]. Finally, this dissertation is concluded in Chapter 8.

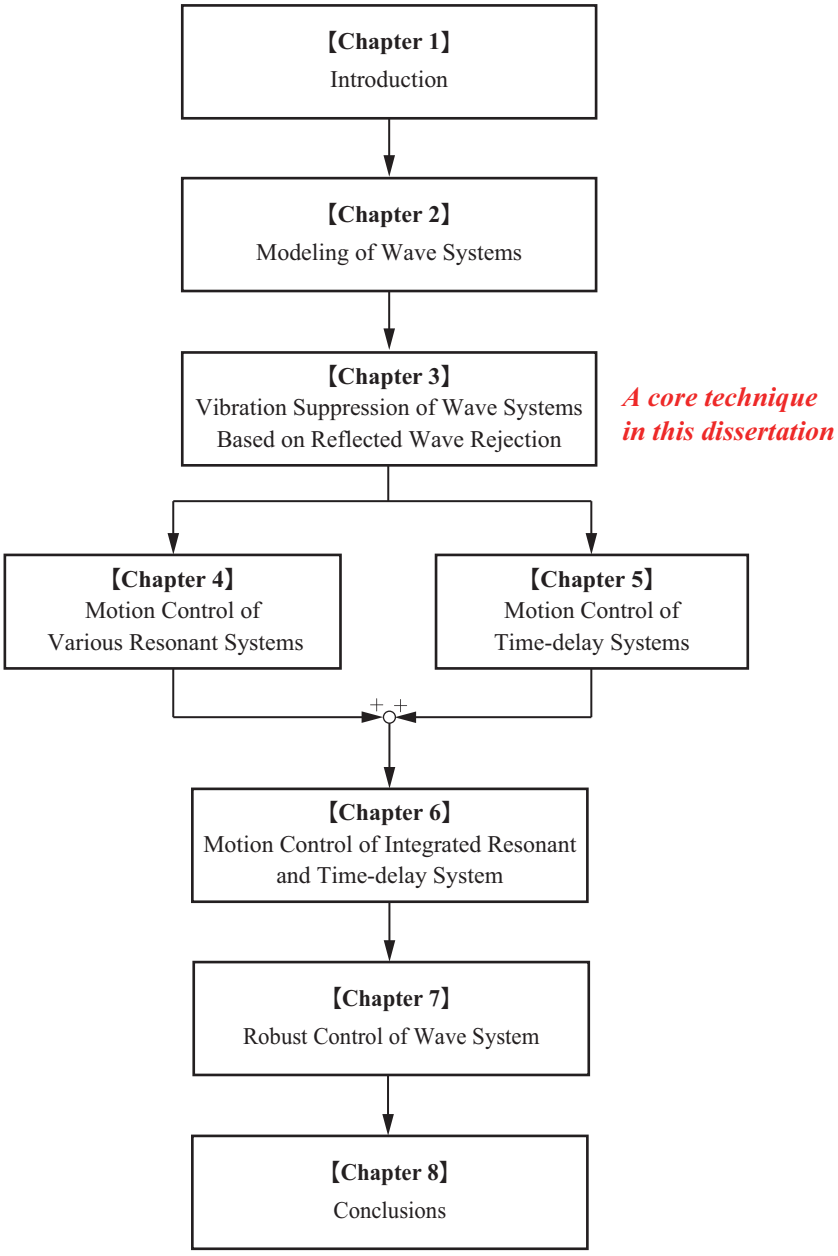

Fig. 1-1: Chapters constructed in this dissertation.

Chapter 2

Modeling of Wave Systems

2.1 Introduction

In this chapter, modeling of wave systems is explained. This dissertation focuses on control of the systems which produce the vibration due to mechanical resonance and time delay. In order to consider high-order vibration, a wave equation is used for modeling of the systems. The wave equation is one of the distributed parameter systems which have infinite numbers of poles.

First of all, in Section 2.2, it is mentioned that limits of a multi-mass resonant system, which is a lumped parameter model, as numbers of mass approaches infinity is a wave equation. Then, the resonant system is modeled by using the wave equation. Section 2.3 explains how a transfer function of the wave equation is expressed [87]. On the other hand, Section 2.4 introduces modeling of a control system including input-output time delay by the wave equation. Additionally, a similarity of the resonant and time-delay systems is analyzed from the wave transmission point of view [88].

2.2 Wave Equation

2.2.1 Derivation of Wave Equation from Multi-mass Resonant System

This part shows that the limits of a multi-mass resonant system as the numbers of mass approaches to infinity is wave equation. The model of a multi-mass resonant system is shown in Fig. 2-1. M, f_m, q, k, m, and f_l^{ext} denote the mass/inertia of motor, the force/torque generated by the motor, the displacement (position), the lumped spring coefficient, and the lumped mass, the external force/torque acting on the tip,

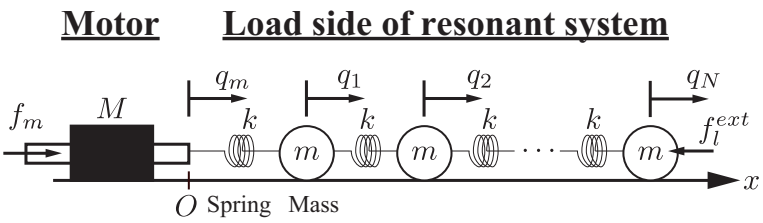

Fig. 2-1: Model of multi-mass resonant system.

respectively. Subscript $_m$ and $_i (1 \leq i \leq N)$ stand for the motor and the number of mass, respectively. The multi-mass resonant system is composed of the motor and the load side of resonant system. The load side is connected with motor by the spring.

The motion equation of each mass is represented as

$$\begin{aligned} M\ddot{q}_m &= f_m - k(q_m - q_1) \\ &\vdots \\ m\ddot{q}_i &= k(q_{i-1} - q_i) - k(q_i - q_{i+1}) \\ &\vdots \\ m\ddot{q}_N &= k(q_{N-1} - q_N) - f_l^{ext}. \end{aligned} \tag{2.1}$$

Eq. (2.1) can be transformed into

$$\begin{aligned} M\ddot{q}_m &= f_m - k(q_m - q_1) \\ &\vdots \\ m\ddot{q}_i &= k(q_{i-1} - 2q_i + q_{i+1}) \\ &\vdots \\ m\ddot{q}_N &= k(q_{N-1} - q_N) - f_l^{ext}. \end{aligned} \tag{2.2}$$

It turns out that motion equations except those at boundary can be represented as same form, which is shown as

$$m\ddot{q}_i = k(q_{i-1} - 2q_i + q_{i+1}). \tag{2.3}$$

Here, the boundary conditions for the system are represented as follow,

$$k(q_1 - q_m) = M\ddot{q}_m - f_m \tag{2.4}$$

$$k(q_N - q_{N+1}) = -f_l^{ext} \tag{2.5}$$

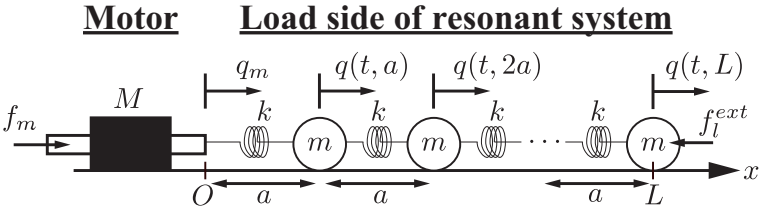

Fig. 2-2: Model of multi-mass resonant system considering spring length.

where q_{N+1} denotes the virtual mass for considering the boundary conditions. By introducing the above boundary conditions, the motion equations at boundaries become same form as (2.3). Hence, the motion equations for all the masses can be expressed as (2.3).

Here, to derive a wave equation from limits of the multi-mass resonant system, the length of spring a is introduced. The model of a multi-mass resonant system considering the spring length is shown in Fig. 2-2. L stands for the entire length of load side of resonant system, which satisfies $L = Na$. It is noted that because L is constant, $N \to \infty$ yields $a \to 0$. By the introduction of the length a, the displacement of i-th mass can be represented as

$$q_i = q(t, ia). \tag{2.6}$$

Considering $a \to 0$, the distributed position is obtained, which is represented as

$$\begin{aligned} q_i &= q(t, ia) \\ &\to q(t, x) \end{aligned} \tag{2.7}$$

where t and x represent the time and the position of the distributed mass, respectively. On the other hand, by using a, (2.3) can be transformed into

$$\frac{m}{a}\ddot{q}_i = ka\frac{(q_{i+1} - 2q_i + q_{i-1})}{a^2}. \tag{2.8}$$

Applying $a \to 0$ to (2.8), the wave equation is derived as

$$\frac{\partial^2 q(t,x)}{\partial t^2} = c^2 \frac{\partial^2 q(t,x)}{\partial x^2} \tag{2.9}$$

where c denotes the propagation velocity of the wave, which is shown as

$$c = \sqrt{\frac{\kappa}{\rho}} \tag{2.10}$$

where $\kappa = \lim_{a\to 0} ka$ and $\rho = \lim_{a\to 0} m/a$ stand for the spring coefficient per unit length and the mass density, respectively. As for the boundary conditions, (2.4) and (2.5) can be also transformed by use of $a \to 0$, which are represented as

$$\frac{\partial q(t,0)}{\partial x} = \frac{1}{\kappa}\left[M\ddot{q}_m - f_m\right] \tag{2.11}$$

$$\frac{\partial q(t,L)}{\partial x} = -\frac{1}{\kappa} f_l^{ext}. \tag{2.12}$$

The proposed control approach is mainly based on the wave equation (2.9) and the boundary conditions (2.11) and (2.12).

In the above modeling, dampers existing between each two masses are neglected. A wave equation including the damper effect can be obtained by the same derivation, and the wave equation is represented as

$$\frac{\partial^2 q(t,x)}{\partial t^2} = c^2 \frac{\partial^2 q(t,x)}{\partial x^2} + c_d^2 \frac{\partial^3 q(t,x)}{\partial t \partial x^2} \tag{2.13}$$

where c_d denotes the propagation velocity of the wave caused by the damper, and it is shown as

$$c_d = \sqrt{\frac{d}{\rho}} \tag{2.14}$$

where d stands for the damper per unit length.

2.2.2 Approximation of Flexible Beam to Wave Equation

This part explains how to approximate a flexible beam to the wave equation. Fig. 2-3 shows a flexible beam dealt with in this dissertation. In Fig. 2-3, $y(t,x)$, $F_s(t,x)$, and $M_b(t,x)$ denote the deflection, the shear force, and the bending momentum, respectively. Governing equations for the flexible arm are represented as

$$\rho A \frac{\partial^2 y(t,x)}{\partial t^2} = \frac{\partial F_s(t,x)}{\partial x} \tag{2.15}$$

$$\rho I \frac{\partial^3 y(t,x)}{\partial x \partial t^2} = \frac{\rho I}{k'GA}\frac{\partial^2 F_s(t,x)}{\partial t^2} + F_s(t,x) + \frac{\partial M_b(t,x)}{\partial x} \tag{2.16}$$

$$\frac{\partial^2 y(t,x)}{\partial x^2} = \frac{M_b(t,x)}{EI} + \frac{\partial}{\partial x}\left(\frac{F_s(t,x)}{k'GA}\right) \tag{2.17}$$

where A, I, G, k', and E stand for the section area, the second moment of area, the modules of rigidity, and the longitudinal elastic modulus, respectively. It is noted that this dissertation does not consider

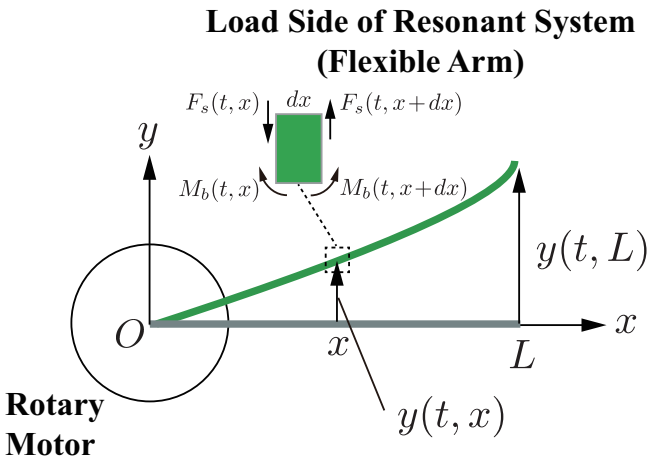

Fig. 2-3: Flexible arm considered in this dissertation.

torsional motion (i.e. cross-section secondary polar moment and torsional stiffness are enough high). Eq. (2.15) denotes the motion equation for the particle at x on y-axis. Eq. (2.16) denotes the motion equation of rotation for the particle at x. Eq. (2.17) represents that the total deflection $y(t,x)$ is superposition of deflection caused by the shear force and the bending momentum. It is assumed that buckling phenomenon and effect of centrifugal force are neglected in the equations. Considering control design based on the governing equations, the control structure becomes complex because transfer functions based on the equations are complex structures. Hence, in this dissertation, the governing equations for the flexible arm is approximated to the wave equation. The approximation of the equation to wave equation can be conducted by introducing following assumptions: the second moment of area I equals to infinity, the deflection caused by the bending momentum is neglected, and the physical parameters are constant value. By using the assumptions, the governing equations represented as (2.15), (2.16) and (2.17) can be approximated as

$$\rho A \frac{\partial^2 y(t,x)}{\partial t^2} = \frac{\partial F_s(t,x)}{\partial x} \tag{2.18}$$

$$\frac{\partial y(t,x)}{\partial x} = \frac{1}{k'GA} F_s(t,x). \tag{2.19}$$

It is noted that, by using the assumptions, (2.16) and (2.17) can be transformed into same form as (2.19). Therefore, by (2.18) and (2.19), the wave equation can be derived as

$$\frac{\partial^2 y(t,x)}{\partial t^2} = c_b^2 \frac{\partial^2 y(t,x)}{\partial x^2} \tag{2.20}$$

where c_b denotes the propagation velocity of the wave in the flexible arm, which is represented as

$$c_b = \sqrt{\frac{k'G}{\rho}}. \tag{2.21}$$

In this dissertation, the rotary motor which drives flexible arm is located at $x = 0$. Because the deflection $y(t, L)$ is a variable in linear direction, the variable is transformed into a variable in rotational direction. By using the length of the flexible arm L, the position $q(t, x)$ and the tip position $q(t, L)$ are represented as

$$\begin{aligned} q(t,x) &= q_m + \tan^{-1}\left(\frac{y(t,x)}{x}\right) \\ &\approx q_m + \frac{y(t,x)}{L}. \end{aligned} \tag{2.22}$$

$$\begin{aligned} q(t,L) &= q_m + \tan^{-1}\left(\frac{y(t,L)}{L}\right) \\ &\approx q_m + \frac{y(t,L)}{L}. \end{aligned} \tag{2.23}$$

In the above equations, it is assumed that $y(t, x)/x$ is enough small value. Because $y(t, x)$ satisfies the wave equation, $q(t, x)$ also satisfies the wave equation under condition $q(t, 0) = q_m$. According to the above, in this dissertation, the flexible arm is modeled as the wave equation. However, modeling error obviously exists due to the introduction of the assumptions for the approximation. The modeling error is compensated by using a wave-based disturbance observer described in Chapter 7.

2.3 Transfer Function of Resonant System based on Wave Equation

In this part, a transfer function of resonant system, which is modeled as the wave equation, is derived. For the sake of simplicity, the effects of damper and the external force are neglected in this part (i.e. $d = 0$ and F_l^{ext}).

First of all, Laplace transformation is applied to the wave equation (2.9), which yields

$$s^2 Q(s,x) = c^2 \frac{\partial^2 Q(s,x)}{\partial x^2}. \tag{2.24}$$

When applying the Laplace transformation, the initial conditions for the resonant system are set as follows,

$$q(0,x) = 0 \tag{2.25}$$

$$\frac{\partial q(0,x)}{\partial t} = 0 \tag{2.26}$$

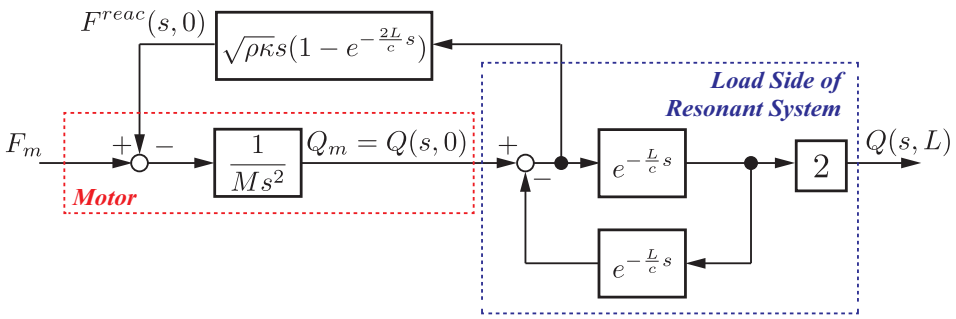

Fig. 2-4: Block diagram of wave system.

where above initial conditions means that position and velocity of each mass at $t = 0$ equal to 0. As for the boundary conditions, (2.11) and (2.12) are transformed into

$$\frac{\partial Q(s,0)}{\partial x} = \frac{1}{\kappa}\left[Ms^2 Q_m - F_m\right] \tag{2.27}$$

$$\frac{\partial Q(s,L)}{\partial x} = 0. \tag{2.28}$$

It is noted that $Q(s,0) = Q_m$ is satisfied. Since the wave equation in Laplace domain (2.24) is a second-order differential equation with respect to x, the general solution of is derived [95] as

$$Q(s,x) = C_1(s)e^{\frac{x}{c}s} + C_2(s)e^{-\frac{x}{c}s} \tag{2.29}$$

where $C_1(s)$ and $C_2(s)$ represent the integral constants which are determined by the boundary conditions. By using the boundary conditions (2.27) and (2.28), the integral constants can be derived as

$$C_1(s) = \frac{e^{-\frac{2L}{c}s}}{Den(s)}F_m \tag{2.30}$$

$$C_2(s) = \frac{1}{Den(s)}F_m \tag{2.31}$$

where

$$Den(s) = Ms^2(1 + e^{-\frac{2L}{c}s}) + \sqrt{\rho\kappa}s(1 - e^{-\frac{2L}{c}s}). \tag{2.32}$$

In this dissertation, the control design is to construct the motion control (i.e. position or force control) for position or force at $x = L$. To construct the control system, the transfer functions from F_m to $Q(s,0)$ and $Q(s,L)$ are derived. The transfer functions are obtained by substituting $x = 0$ and $x = L$ to (2.29)

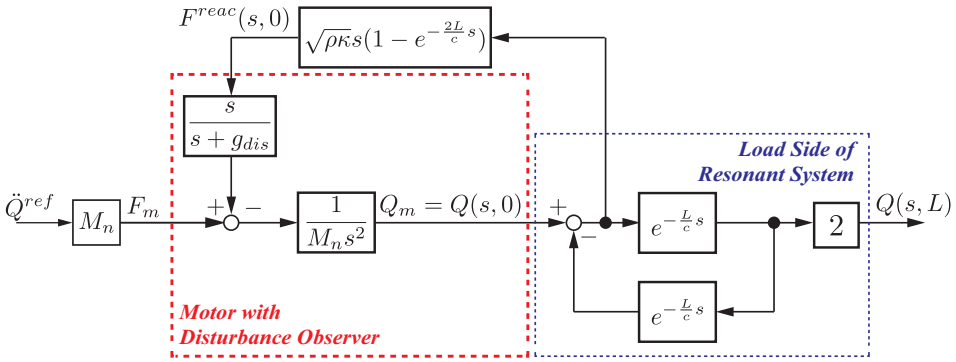

Fig. 2-5: Equivalent block diagram of wave system with disturbance observer.

with (2.30) and (2.31), which is represented as

$$\frac{Q(s,0)}{F_m} = \frac{1+e^{-\frac{2L}{c}s}}{Ms^2(1+e^{-\frac{2L}{c}s})+\sqrt{\rho\kappa}s(1-e^{-\frac{2L}{c}s})}. \tag{2.33}$$

$$\frac{Q(s,L)}{F_m} = \frac{2e^{-\frac{L}{c}s}}{Ms^2(1+e^{-\frac{2L}{c}s})+\sqrt{\rho\kappa}s(1-e^{-\frac{2L}{c}s})}. \tag{2.34}$$

The block diagram of the transfer function represented as (2.34) is shown in Fig. 2-4.

In this dissertation, the robust control of motor is conducted by using a disturbance observer [12] to control tip response accurately. By using the disturbance observer, the reaction force $F^{reac}(s,0)$ from the wave system is canceled out. Fig. 2-5 shows the equivalent block diagram when the disturbance observer is implemented. In this case, the transfer functions represented as (2.33) and (2.34) are changed as

$$\frac{Q(s,0)}{\ddot{Q}^{ref}} = \frac{1+e^{-\frac{2L}{c}s}}{s^2(1+e^{-\frac{2L}{c}s})+\frac{1}{M_n}\frac{s}{s+g_{dis}}\sqrt{\rho\kappa}s(1-e^{-\frac{2L}{c}s})} \tag{2.35}$$

$$\frac{Q(s,L)}{\ddot{Q}^{ref}} = \frac{2e^{-\frac{L}{c}s}}{s^2(1+e^{-\frac{2L}{c}s})+\frac{1}{M_n}\frac{s}{s+g_{dis}}\sqrt{\rho\kappa}s(1-e^{-\frac{2L}{c}s})} \tag{2.36}$$

where g_{dis} denotes the cut-off frequency of the disturbance observer. Under the assumption that cut-off frequency of the disturbance observer g_{dis} equals to ∞, the transfer function from the acceleration reference $\ddot{Q}^{ref}$, which is new input, to $Q(s,x)$ is derived as

$$\frac{Q(s,x)}{\ddot{Q}^{ref}} = \frac{1}{s^2}\frac{e^{-\frac{x}{c}s}+e^{-\frac{2L-x}{c}s}}{1+e^{-\frac{2L}{c}s}}. \tag{2.37}$$

It is noted that $Q_m = \frac{1}{s^2}\ddot{Q}^{ref}$ is realized by the disturbance observer. Block diagram of (2.37) is shown in Fig. 2-6. In Fig. 2-6, it can be seen that there are four waves. The wave A is a wave traveling to x

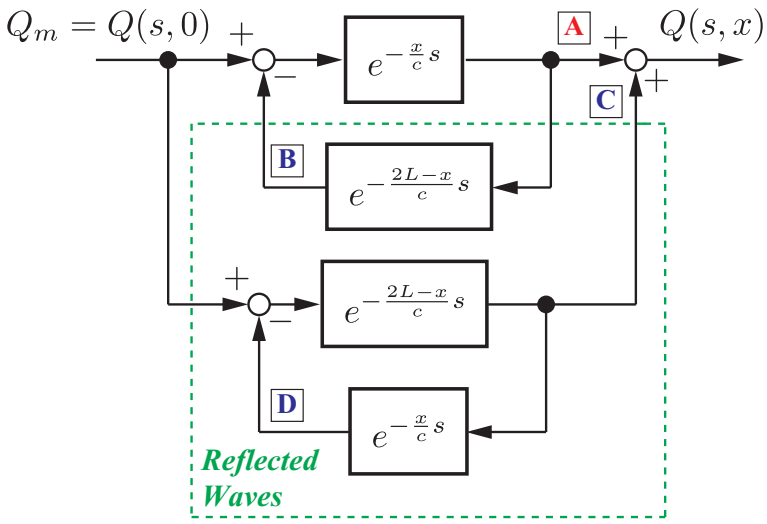

Fig. 2-6: Block diagram of wave system with disturbance-observer-implemented motor with $g_{dis} = \infty$ from Q_m to $Q(s,x)$.

from the left side of x (i.e. motor side). On the other hand, the wave C is approaching to x from the right side of x (i.e. the tip side). The position $Q(s,x)$ is generated by superposition of the waves A and C. The waves A and C are reflected at $x = L$, and they are fedback to $x = 0$ (the motor side). In addition, the transfer function from $\ddot{Q}^{ref}$ to $Q(s,L)$ is derived as

$$\frac{Q(s,L)}{\ddot{Q}^{ref}} = \frac{1}{s^2}\frac{2e^{-\frac{L}{c}s}}{1+e^{-\frac{2L}{c}s}}. \tag{2.38}$$

As shown in the transfer function (2.38), there is time delay in the denominator of the transfer function. In this case, the poles of the wave system can be analytically derived as

$$s = \frac{c}{2L}(2n-1)\pi j \tag{2.39}$$

where n is the integer number. It turns out that the poles of the wave system are located on imaginary axis. In other words, because the poles do not have real-axis component, the response of $Q(s,L)$ vibrates. The block diagram of (2.38) is shown in Fig. 2-7. In Fig. 2-7, the block "2" means the waves A and C corresponding to those shown in Fig. 2-6. In addition, the reflected wave which travels to $x = 0$ is corresponding to the waves B and D. From the control-theoretical point of the view, if the time delay is omitted from the denominator of the transfer function.

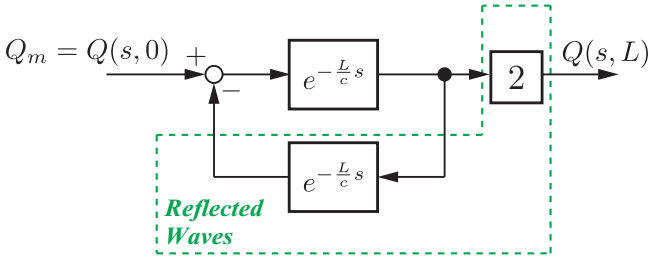

Fig. 2-7: Block diagram of wave system with disturbance-observer-implemented motor with $g_{dis} = \infty$.

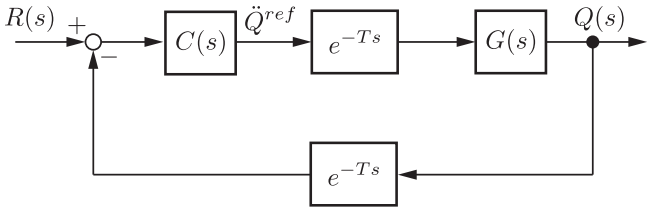

Fig. 2-8: Block diagram of feedback system including input-output time delay.

2.4 Transfer Function of Time-delay System based on Wave Equation

In previous part, the resonant system is modeled as the wave equation, and it is shown that the transfer function of the wave equation comprises the time-delay elements. In addition, the block diagram of the wave equation is obviously similar to that of a typical time-delay system which includes input-output time delay. The block diagram of a time-delay system is shown in Fig. 2-8. In Fig. 2-8, $C(s)$, $G(s)$, and T stand for the feedback controller, the plant, and time delay, respectively. The transfer functions from the command to the position response and from the command to the acceleration reference are represented as

$$\frac{Q(s)}{R(s)} = \frac{C(s)G(s)e^{-Ts}}{1 + C(s)G(s)e^{-2Ts}} \tag{2.40}$$

$$\frac{\ddot{Q}^{ref}}{R(s)} = \frac{C(s)}{1 + C(s)G(s)e^{-2Ts}}. \tag{2.41}$$

It can be guessed that there is an equivalence or similarity between wave and time-delay systems. Considering the above, the wave representation of time-delay system is introduced in this part.

First of all, it is assumed that the time-delay system satisfies the wave equation, which is represented as

$$\frac{\partial^2 \tilde{q}(t,x)}{\partial t^2} = \tilde{c}^2 \frac{\partial^2 \tilde{q}(t,x)}{\partial x^2} \tag{2.42}$$

where $\tilde{c}$ stands for the equivalent propagation velocity of the wave in the time-delay system. $\tilde{\bigcirc}$ means the variable of the wave system corresponding to the time-delay system. The relation between the time delay T, equivalent system length $\tilde{L}$, and equivalent propagation velocity of the wave $\tilde{c}$ is represented as

$$T = \frac{\tilde{L}}{\tilde{c}}. \tag{2.43}$$

The boundary conditions of the time-delay system in the Laplace domain are defined as

$$\begin{aligned} \tilde{Q}(s,0) &= \frac{C(s)G(s)}{1+C(s)G(s)}R(s) && (2.44)\\ \tilde{Q}(s,\tilde{L}) &= Q(s) \\ &= \frac{C(s)G(s)e^{-\frac{\tilde{L}}{\tilde{c}}s}}{1+C(s)G(s)e^{-2\frac{\tilde{L}}{\tilde{c}}s}}R(s). && (2.45) \end{aligned}$$

Eq. (2.44) means that the position input for the time-delay system is represented by using the wave equation. On the other hand, (2.45) is set as the position response $Q(s)$ and is rewritten by using the transfer function (2.40).

Next, the transfer functions from $R(s)$ to $\tilde{Q}(s,x)$ and $\tilde{Q}(s,L)$ are derived. The general solution of (2.42) is derived as

$$\tilde{Q}(s,x) = \tilde{C}_1(s)e^{-\frac{x}{\tilde{c}}s} + \tilde{C}_2(s)e^{\frac{x}{\tilde{c}}s} \tag{2.46}$$

where $\tilde{C}_1$ and $\tilde{C}_2$ stand for the integral constants. $\tilde{C}_1$ and $\tilde{C}_2$ are determined by the boundary conditions (2.44) and (2.45), which are derived as

$$\begin{aligned} C_1(s) &= \frac{1}{1+C(s)G(s)e^{-2\frac{\tilde{L}}{\tilde{c}}s}}\tilde{Q}(s,0) && (2.47)\\ C_2(s) &= \frac{C(s)G(s)e^{-2\frac{\tilde{L}}{\tilde{c}}s}}{1+C(s)G(s)e^{-2\frac{\tilde{L}}{\tilde{c}}s}}\tilde{Q}(s,0). && (2.48) \end{aligned}$$

By substituting the integral constants to the general solution, the transfer function from $\tilde{Q}(s,0)$ to $\tilde{Q}(s,x)$ is derived as

$$\frac{\tilde{Q}(s,x)}{\tilde{Q}(s,0)} = \frac{e^{-\frac{x}{\tilde{c}}s} + C(s)G(s)e^{-\frac{2\tilde{L}-x}{\tilde{c}}s}}{1+C(s)G(s)e^{-2\frac{\tilde{L}}{\tilde{c}}s}}. \tag{2.49}$$

The block diagram of (2.49) is shown in Fig. 2-9. As shown in Fig. 2-9, the block diagram of time-delay system represented by the wave equation is a similar structure as that of resonant system expressed by

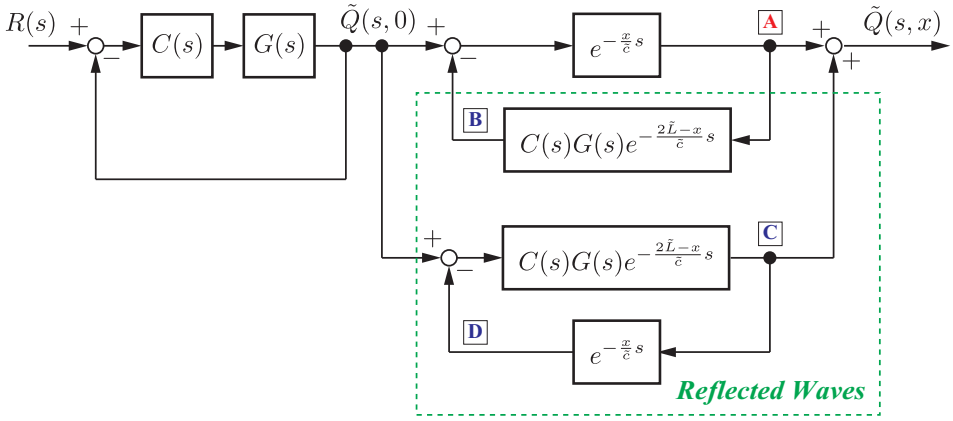

Fig. 2-9: Block diagram of wave representation of time-delay system from $R(s)$ to $\tilde{Q}(s,x)$.

Fig. 2-6. The difference between them is that waves B and C are affected by $C(s)G(s)$. As for the transfer function from $\tilde{Q}(s,0)$ to $\tilde{Q}(s,\tilde{L})$, it can be derived by substituting $x=\tilde{L}$ to (2.49). The transfer function is derived as

$$\frac{\tilde{Q}(s,\tilde{L})}{\tilde{Q}(s,0)}=\frac{e^{-\frac{\tilde{L}}{c}s}\left(1+C(s)G(s)\right)}{1+C(s)G(s)e^{-2\frac{\tilde{L}}{c}s}}. \tag{2.50}$$

It is noted that the transfer function from $R(s)$ to $\tilde{Q}(s,0)$ is represented as (2.44). Hence, the block diagram of time-delay system in Fig. 2-8 can be transformed into an equivalent block diagram based on the wave equation in Fig. 2-10. Fig. 2-10 shows the block diagram for the wave representation of time-delay system. The wave representation of the time-delay system also comprises position-input and wave-transmission systems. This structure implies that the position-input system is not affected by the wave-transmission system which is the same situation as the resonant system with a disturbance observer. In addition, if $C(s)G(s)$ equal to 1 in wave-transmission system, the wave representation of time-delay system is identical with that of resonant system. According to the above, it is clarified that there exists the similarity between resonant and time-delay systems.

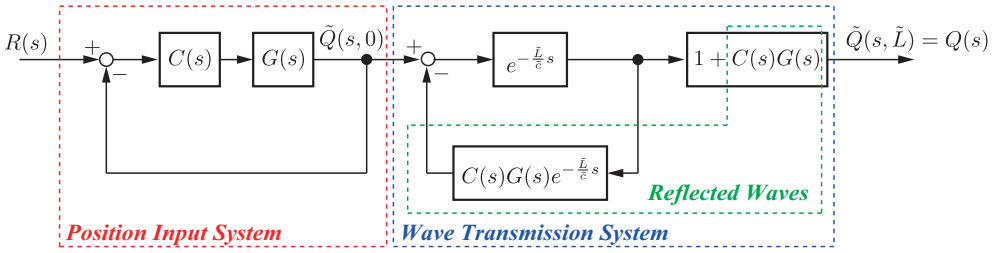

Fig. 2-10: Block diagram of wave representation of time-delay system from $R(s)$ to $\tilde{Q}(s,\tilde{L})$.

2.5 Summary of Chapter 2

In this chapter, the modeling of wave systems, which are a resonant system and a time-delay system, was conducted based on wave equation. In addition, transfer functions for both resonant and time-delay systems are derived for controlling the system. Remarkable fact in these modelings is that both systems are composed of the position-input system and the wave-transmission system. In addition, the wave which is fedback from tip position to position-input system induces vibrations. Therefore, in other words, the cause of vibrations in the wave systems is the reflected wave. Therefore, it is needed to eliminate the reflected wave to suppress the vibrations in both systems.

Chapter 3

Vibration Suppression of Wave Systems Based on Reflected Wave Rejection

---

3.1 Introduction

In this chapter, a reflected wave rejection [86] is proposed to suppress the vibrations for wave systems. From the point of view of the wave transmission, the vibrations occur due to superposition of traveling and reflected waves. Therefore, elimination of the reflected wave contributes to suppress the vibrations. The reflected wave rejection is a core technique in this dissertation.

The contents of this chapter is as follow. Section 3.2 explains a basic concept and structure of reflected wave rejection. In Section 3.3, the reflected wave rejection is applied to the position-control of resonant system. Section 3.4 analyzes the reflected wave rejection based on a open-loop transfer function and sensitivity and complementary-sensitivity functions. Experiments of position control are performed to verify the effect of the proposed method in Section 3.5. Finally, Section 3.6 concludes this chapter.

3.2 Basic Concept of Reflected Wave Rejection

3.2.1 Structure

In this part, vibration suppression based on the reflected wave rejection is proposed. As mentioned in the previous chapter, the cause of vibration in wave system is a reflected wave which is reflected at tip position. Therefore, the vibration suppression is achieved if the reflected wave is eliminated from the wave system. In this dissertation, the reflected wave is estimated and feedforward-compensated by the

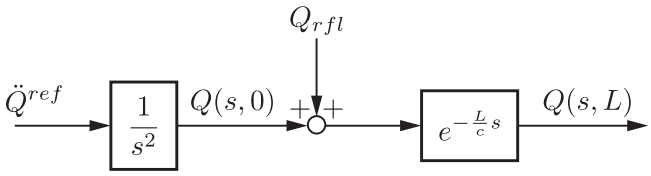

Fig. 3-1: Block diagram of wave system with reflected wave.

proposed reflected wave rejection scheme.

Before explaining the reflected wave rejection, the reflected wave in the wave system shown in Fig. 2-7 is defined. For the sake of simplicity, although the reflected wave rejection for Fig. 2-7 is explained, the reflected wave rejection a for time-delay system can be derived as well as that of resonant system (It is explained in Chapter 5). In addition, it is assumed that the ideal acceleration control is achieved by the disturbance observer (i.e. $g_{dis} = \infty$).

First of all, the reflected wave, which is a cause of vibration, is derived. The transfer function represented as (2.38) is transformed into

$$Q(s,L) = e^{-\frac{Ls}{c}}\left[Q(s,0) + Q(s,0) - e^{-\frac{L}{c}s}Q(s,L)\right]. \tag{3.1}$$

In (3.1), last two terms in right hand side are defined as reflected wave in this dissertation. Therefore, the reflected wave Q_{rfl} is represented as

$$Q_{rfl} = \left[Q(s,0) - e^{-\frac{L}{c}s}\tilde{Q}(s,L)\right]. \tag{3.2}$$

The reflected wave defined in (3.2) includes wave B and D shown in Fig. 2-6. Fig. 3-1 shows the block diagram of the wave system considering the reflected wave. From Fig. 3-1, if the reflected wave is omitted from the wave system, the wave system is obviously stabilized because only one time-delay element, which refers the traveling wave, remains at wave-transmission system.

In this dissertation, the reflected wave rejection is proposed in order to suppress the residual vibrations on the wave system. The reflected wave rejection has a reflected-wave estimator and a feedforward compensator for the reflected wave. The block diagram of the reflected wave rejection is shown in Fig. 3-2. In Fig. 3-2, $\hat{Q}_{rfl}$, Q_{rfl}^{cmp}, and g_r stand for the estimated reflected wave, the compensation value for reflected wave, and the cut-off frequency, respectively. At the reflected-wave estimator, the reflected wave is estimated by using the nominal value of the propagation time of the wave L_n/c_n as follow,

$$\hat{Q}_{rfl} = \left[Q(s,0) - e^{-\frac{L_n}{c_n}s}Q(s,L)\right]. \tag{3.3}$$

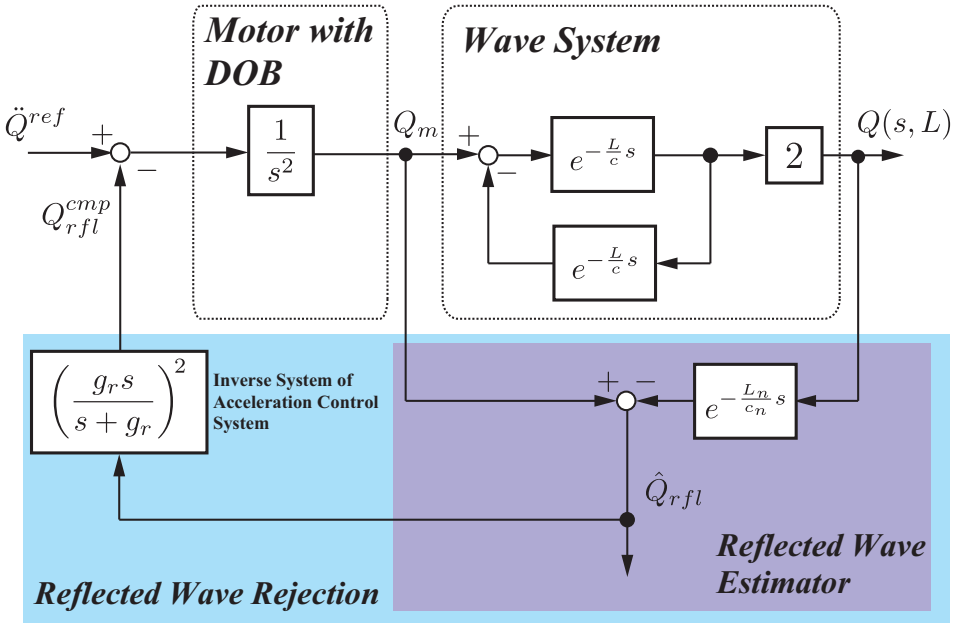

Fig. 3-2: Block diagram of reflected wave rejection.

The estimated reflected wave multiplied by the inverse system of the acceleration control system is fedback to the acceleration reference to eliminate the reflected wave as same manner as disturbance compensation by the disturbance observer. Therefore, the compensation value for the reflected wave is generated as

$$Q^{cmp}_{rfl} = \left(\frac{g_r s}{s+g_r}\right)^2 \hat{Q}_{rfl}. \tag{3.4}$$

In calculation process of (3.4), the low-pass filter with cut-off frequency g_r is used to make the inverse system of acceleration control system $(1/s^2)^{-1}$ be proper transfer function. By utilizing the compensation value, the actual reflected wave is canceled out by feedforward of the estimated reflected wave. Equivalent block diagram of Fig. 3-2 is shown in Fig. 3-3. From Fig. 3-3, it is found that effect of the reflected wave rejection is applying transfer function, which has characteristics of high-pass filter, to the actual reflected wave. Therefore, the actual reflected waves at low-frequency area are suppressed. The transfer function from the acceleration reference to the tip position in Fig. 3-2 is represented as

$$\frac{Q(s,L)}{\ddot{Q}^{ref}} = \frac{1}{s^2} e^{-\frac{L}{c}s} G_r(s) \tag{3.5}$$

where

$$G_r(s) = \frac{2s^2+2g_r s+2g_r^2}{s^2+2g_r s+2g_r^2} \frac{1}{1-\frac{s^2+2g_r s}{s^2+2g_r s+2g_r^2} e^{-\frac{L}{c}s}}. \tag{3.6}$$

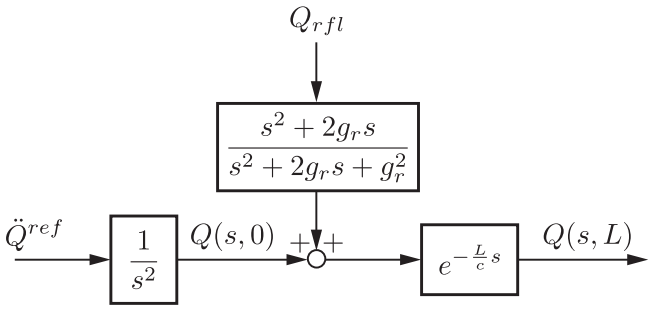

Fig. 3-3: Equivalent block diagram of Fig. 3-2.

Fig. 3-4 shows the bode diagram of the closed-loop transfer function from the acceleration reference $\ddot{Q}^{ref}$ to the tip position $Q(s,L)$ when the cut-off frequency g_r changes from 0 rad/s to 1000 rad/s. From Fig. 3-4, it turns out that the vibrations are suppressed by increasing the cut-off frequency. If the cut-off frequency g_r equals to enough high value (i.e. $g_r \approx \infty$) in (3.5), the transfer function from the acceleration reference to the tip position becomes

$$\frac{Q(s,L)}{\ddot{Q}^{ref}} \approx \frac{1}{s^2} e^{-\frac{L}{c}s}. \tag{3.7}$$

From (3.7), it is found that there is no time-delay in the denominator of the transfer function. In addition, the transfer function expressing the wave-transmission system becomes a simple time delay. Therefore, the wave system without the reflected wave can be regraded as equivalent time-delay system. This regard is useful for integrating the resonant and time-delay systems, and it will be explained in Chapter 6.

3.2.2 Parameter Setting

In order to implement the reflected wave rejection, it is needed to identify the nominal propagation time of the wave $T_{wn} = L_n/c_n$. This part explains how to set the nominal propagation time of the wave T_{wn}. First of all, from theoretical values of the poles of wave system represented as (2.39), the first-order resonant frequency is expressed as

$$\omega_1 = \frac{\pi}{2T_w}. \tag{3.8}$$

By using the above equation and previously-identified value of the first-order resonant frequency, the nominal propagation time of the wave is set as

$$T_{wn} = \frac{\pi}{2\tilde{\omega}_1} \tag{3.9}$$

where $\tilde{\omega}_1$ denotes the identified value of the first-order resonant frequency.

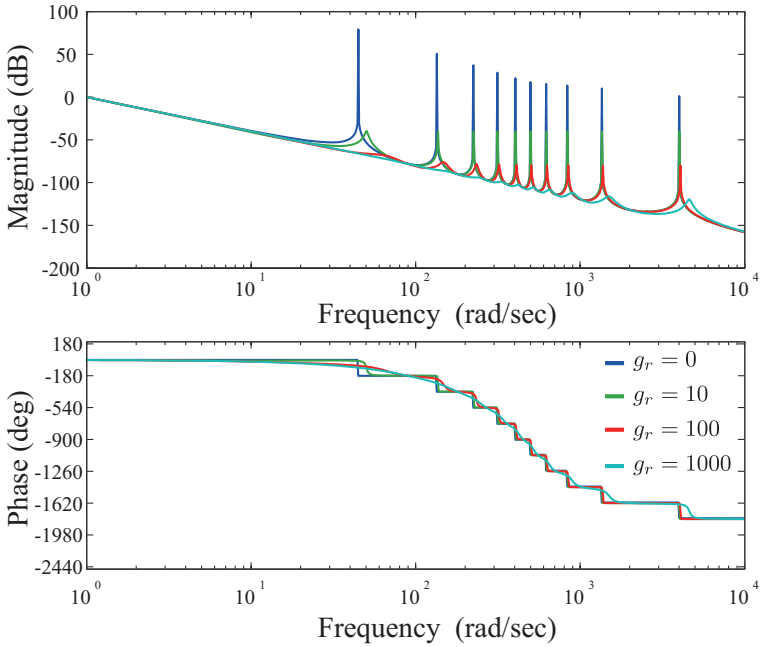

Fig. 3-4: Bode diagram of reflected wave rejection.

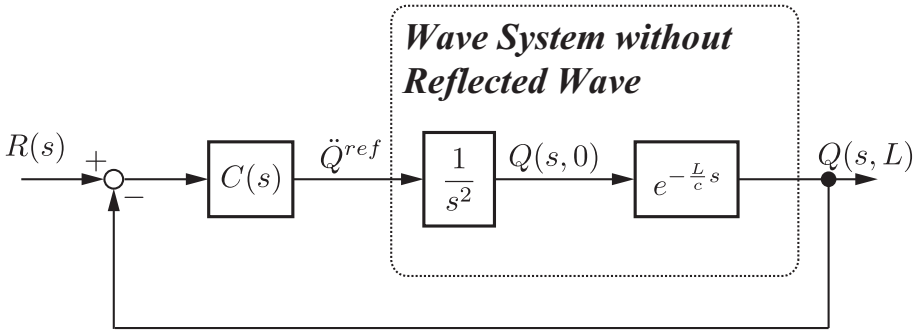

Fig. 3-5: Fully closed-loop control of equivalent time-delay system.

3.3 Application to Position Control

3.3.1 Fully closed-loop Type

In this part, fully closed-loop control of wave system is proposed. The fully closed-loop control system is designed based on the equivalent time-delay system represented as (3.7). Block diagram of the fully closed-loop control system is shown in Fig. 3-5. In Fig. 3-5, $R(s)$ and $C(s)$ denote the command and controller, respectively. From Fig. 3-5, because there exists the time delay in the feedback loop, the stability of the feedback system is affected by the controller bandwidth. If the wide controller bandwidth

is required, time-delay compensation is needed to construct the stable feedback system. In this dissertation, a communication-disturbance observer (CDOB) [77] is used as time-delay-compensation method. The communication-disturbance observer has advantage whose the time-delay model is not needed for the implementation, although a Smith predictor [74], which is the most typical time-delay-compensation method, needs both time-delay and plant models.

Block diagram of the fully closed-loop control of wave system by using the time-delay compensation is shown in Fig. 3-6. In Fig. 3-6, g_{cdob} and Q_{cdob}^{cmp} stand for the cut-off frequency of CDOB and compensation value of CDOB, respectively. In the proposed method, the reflected wave rejection is implemented in the inner loop to suppress the vibration and to make the wave system be the equivalent time-delay system. Then, the CDOB-based time-delay compensation is conducted in the outer loop. The compensation value generated by the CDOB is represented as

$$Q_{cdob}^{cmp} = \frac{g_{cdob}}{s + g_{cdob}} \left[\frac{1}{s^2} \ddot{Q}^{ref} - Q(s, L) \right]. \tag{3.10}$$

According to the above, the acceleration reference is generated as

$$\ddot{Q}^{ref} = C(s) \left[R(s) - (Q(s, L) + Q_{cdob}^{cmp}) \right]. \tag{3.11}$$

By applying the input expressed by (3.11), the transfer function from the command $R(s)$ to the tip position $Q(s, L)$ is derived as

$$\frac{Q(s, L)}{R(s)} = \frac{C(s)e^{-\frac{L}{c}s}}{s^2 + C(s)L(s)} G_r(s) \frac{s^2 + C(s)L_c(s)}{s^2 + C(s)L_c(s) + C(s)G_r(s)e^{-\frac{L}{c}s}(1 - L_c(s))} \tag{3.12}$$

where

$$L_c(s) \quad = \quad \frac{g_{cdob}}{s + g_{cdob}}. \tag{3.13}$$

If the cut-off frequencies g_r and g_{cdob} are enough high values, the transfer function represented as (3.12) becomes

$$\frac{Q(s, L)}{R(s)} = \frac{C(s)}{s^2 + C(s)} e^{-\frac{L}{c}s}. \tag{3.14}$$

As for the controller $C(s)$, since $C(s)$ will be fine if it can allocate two poles, $C(s)$ is set as a PD controller, which is represented as

$$C(s) = K_p + K_d s \tag{3.15}$$

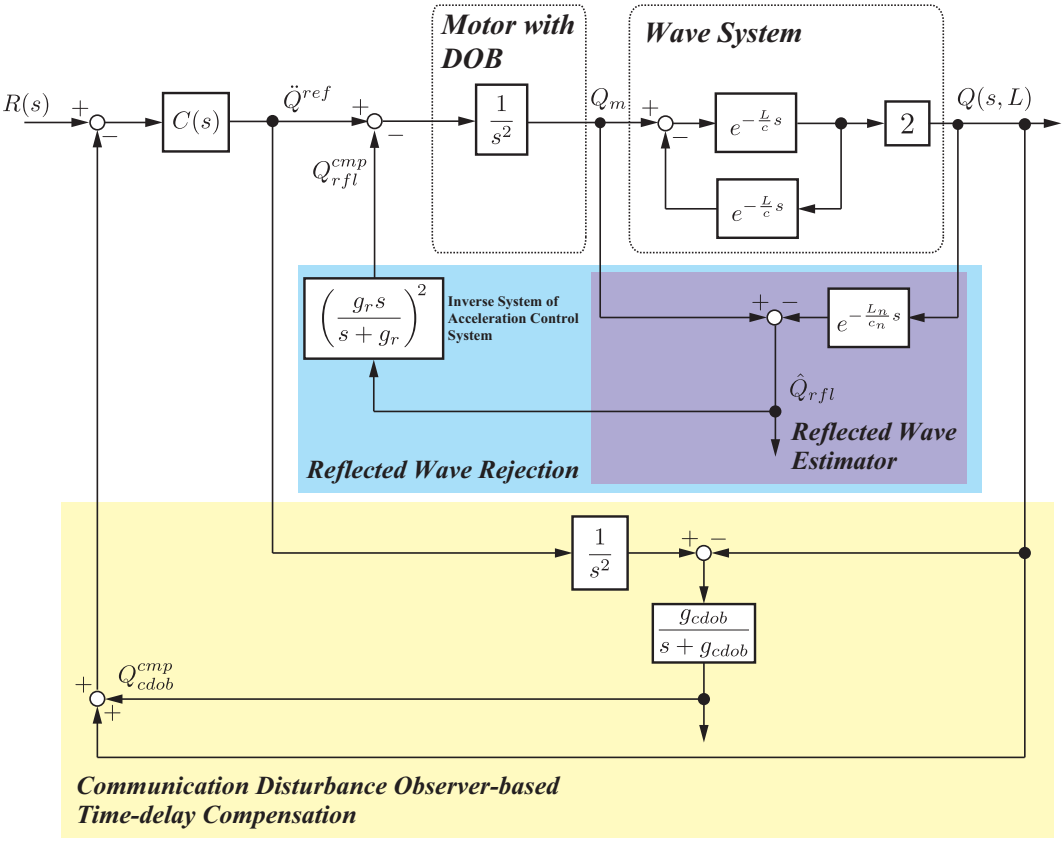

Fig. 3-6: Whole block diagram of fully closed-loop control of equivalent time-delay system with time-delay compensation.

where K_p and K_d denote the proportional gain and differential gain, respectively.

Advantage of the fully closed-loop position control with reflected wave rejection is that it is easy to integrate the time-delay system because the the resonant system becomes the equivalent time-delay system by reflected wave rejection. The detail of the integration of resonant and time-delay systems are explained in Chapter 6. In contrast, disadvantage is low disturbance suppression performance due to implementation of the time-delay compensation. If the disturbance suppression is desired to be improved, the time-delay compensation should be omitted and the controller bandwidth should be set low value to maintain stability, or a wave-based disturbance observer, which is proposed in Chapter 7, should be implemented.

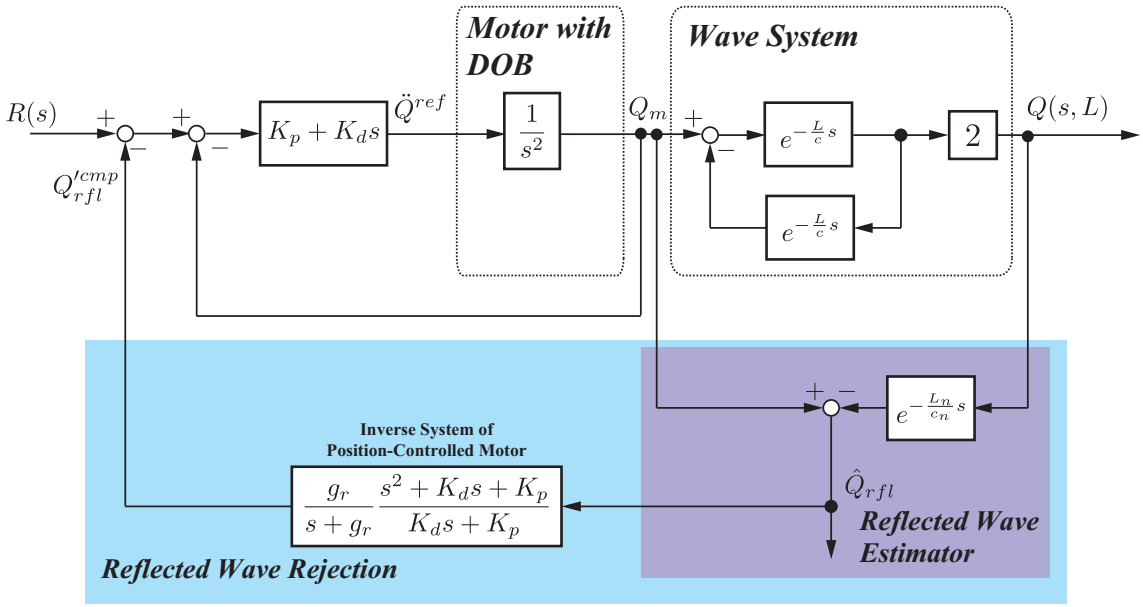

Fig. 3-7: Block diagram of semi-closed-loop type reflected wave rejection.

3.3.2 Semi-closed-loop Type

This part proposes the semi-closed-loop type position control with reflected wave rejection. Compared with fully closed-loop type, the semi-closed-loop type has the advantage that suppression of disturbance acting on the motor is better than that of fully closed-loop type.

The block diagram of the semi-closed-loop type position control with reflected wave rejection is shown in Fig. 3-7. In this case, the motor is position-controlled by a PD controller in inner loop. On the other hand, the reflected wave rejection is implemented at outer loop. Therefore, the compensation value generated by the reflected wave rejection is derived as

$$Q'^{cmp}_{rfl} = \frac{g_r}{s+g_r}\frac{s^2+K_d s+K_p}{K_d s+K_p}\hat{Q}_{rfl}. \tag{3.16}$$

The acceleration reference which is input to the motor is represented as

$$\ddot{Q}^{ref} = (K_p + K_d s)(Q^{cmd} - Q'^{cmp}_{rfl} - Q_m). \tag{3.17}$$

By using the acceleration reference, the closed-loop transfer function from the command $R(s)$ to the tip position $Q(s, L)$ is represented as

$$\frac{Q(s,L)}{R(s)} = \frac{K_d s + K_p}{s^2 + K_d s + K_p}\frac{2e^{-\frac{L}{c}s}}{1 + L(s) + (1 - L(s))e^{-2\frac{L}{c}s}}. \tag{3.18}$$

If the cut-off frequency g_r is enough high value, the transfer function becomes

$$\frac{Q(s,L)}{R(s)} \approx \frac{K_d s + K_p}{s^2 + K_d s + K_p} e^{-\frac{L}{c}s}. \tag{3.19}$$

In the ideal condition ($g_r \to \infty$), the closed-loop transfer function expressed by (3.19) is same as that of the fully closed-loop type represented as (3.14). On the other hand, because the semi-closed-loop position control with reflected wave rejection has position controller implemented in inner loop, the suppression performance of disturbance acting on the motor side is better to that of fully closed-loop type position control with reflected wave rejection. It is noted that, although the fully closed-loop controller has better disturbance suppression performance at tip side in general, time-delay compensation for equivalent time-delay in the fully closed-loop control system explained in previous part degrades the suppression performance of disturbance acting on both motor and tip sides. Therefore, if there is no input-output time delay (e.g. sensor delay, communication delay) in the wave system, the semi-closed-loop control with reflected wave rejection.

3.4 Analyses of Reflected Wave Rejection-based Vibration Control

The previous section explained the basic concept and structure of the reflected wave rejection to suppress the residual vibrations. Physical meaning of reflected wave rejection is obvious, and it is to eliminate reflected wave from the wave system. However, the vibration-suppression performance is not clarified from the control-theoretical point of view. This part analyzes the vibration-suppression performance from the control-theoretical point of view.

3.4.1 Analysis Based on Open-loop Transfer Function

In order to analyze the performance of the reflected wave rejection, the block diagram of reflected wave rejection-based position control shown in Fig. 3-7 is transformed into the equivalent block diagram shown in Fig. 3-8. Here, blue-colored parts in Fig. 3-8 means equivalent structures of the reflected wave rejection. From Fig. 3-8, an open-loop transfer function can be derived as

$$G_o = -\frac{1}{2} F(s) e^{-\frac{L_n}{c_n}s} G_w(s) \tag{3.20}$$

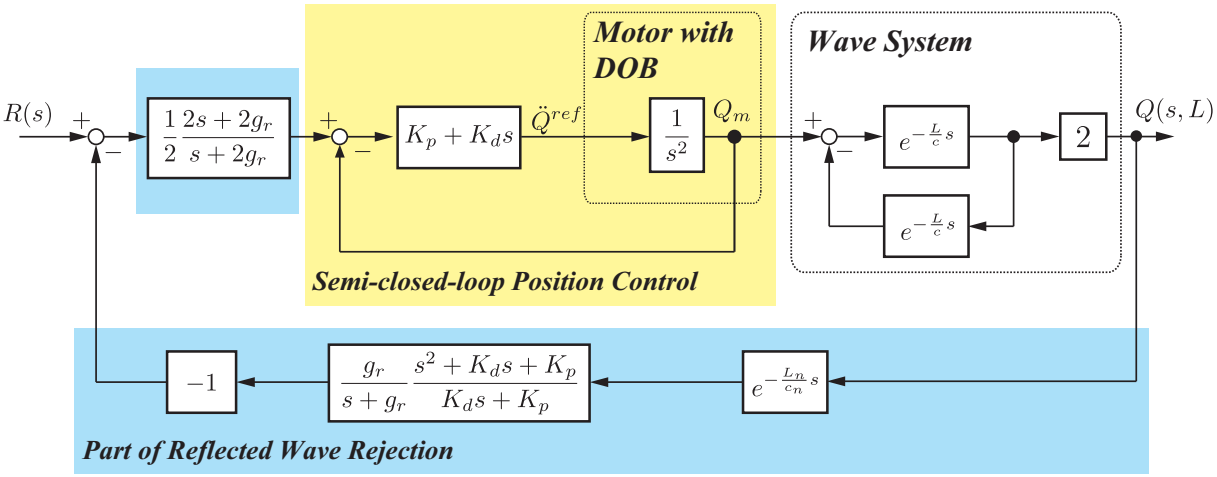

Fig. 3-8: Equivalent block diagram of semi-closed-loop control with reflected wave rejection.

where

$$G_w(s) = \frac{2e^{-\frac{L}{c}s}}{1+e^{-\frac{2L}{c}s}} \tag{3.21}$$

$$F(s) = \frac{2s+2g_r}{s+2g_r}\frac{g_r}{s+g_r} = \frac{2g_r}{s+2g_r}. \tag{3.22}$$

Here, $G_w(s)$ and $F(s)$ denote the transfer function from Q_m to $Q(s,L)$ and the filter caused by the reflected wave rejection, respectively. Fig. 3-9 shows the bode diagram of $G_w(s)$ when $\frac{L}{c} = \frac{\pi}{2}$ (i.e. n-th pole is $\omega_n = (2n-1)$ rad/s). From Fig. 3-9, the resonant peaks can be observed at each resonant frequency. In addition, -180 degree phase delay occurs at each resonant frequency.

If the reflected wave rejection ideally works (i.e. $g_r \to \infty$), $F(s)$ approaches to 1. Therefore, $-\frac{1}{2}e^{-\frac{L_n}{c_n}s}$ intends a main compensator to suppress the resonance by the reflected wave rejection. The frequency response of $-\frac{1}{2}e^{-\frac{L_n}{c_n}s}$ are represented as

$$\left|-\frac{1}{2}e^{-\frac{L_n}{c_n}s}\right| = \frac{1}{2} \tag{3.23}$$

$$\angle -\frac{1}{2}e^{-\frac{L_n}{c_n}s} = \pi - \frac{L_n}{c_n}\omega = \pi - \frac{\pi}{2\tilde{\omega}_1}\omega. \tag{3.24}$$

Bode diagram of $-\frac{1}{2}e^{-\frac{L_n}{c_n}s}$ is shown in Fig. 3-10. From Fig. 3-10, it is found that the gain characteristic is constant over all frequency area. On the other hand, a phase characteristic is varied from 180 degree to

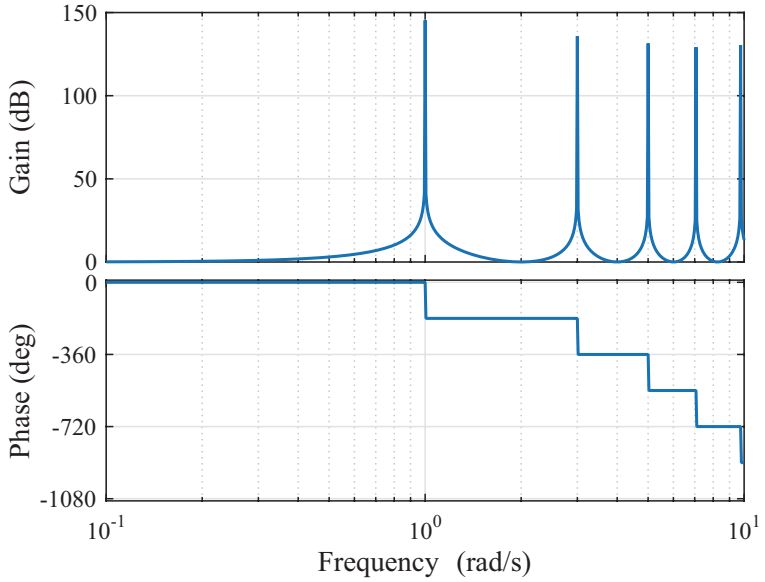

Fig. 3-9: Bode diagram of tip side of wave system G_w.

∞ degree. It is noted that a phase at low-frequency area is 180 degree because of the positive feedback. Therefore, $-\frac{1}{2}e^{-\frac{L_n}{c_n}s}$ has phase lead and lag characteristics alternately as following area,

$$\text{Lead} \quad : \quad 4(n-1)\frac{\pi}{2}\frac{c_n}{L_n} < \omega < 4\left(n-\frac{1}{2}\right)\frac{\pi}{2}\frac{c_n}{L_n} \tag{3.25}$$

$$\text{Lag} \quad : \quad 4\left(n-\frac{1}{2}\right)\frac{\pi}{2}\frac{c_n}{L_n} < \omega < 4n\frac{\pi}{2}\frac{c_n}{L_n} \tag{3.26}$$

where $n = 1,\ 2,\ 3,\ \cdots$. It is noted that, in (3.25) and (3.26), $\frac{\pi}{2}\frac{c_n}{L_n}$ corresponds to the first-order resonant frequency ω_1 as shown in (2.39). The phase compensation by $-\frac{1}{2}e^{-\frac{L_n}{c_n}s}$ at each resonant frequency ($\omega_n = \frac{c}{2L}(2n-1)\pi$) is represented as follow,

$$\text{Phase comp. value} = (-1)^{2n-1}90 \text{ degree}. \tag{3.27}$$

Fig. 3-11 shows the Nyquist diagram of the open-loop transfer function represented as (3.20) when frequency ω is varied from 0 rad/s to ∞ rad/s. For the sake of simplicity, the wave-transmission system

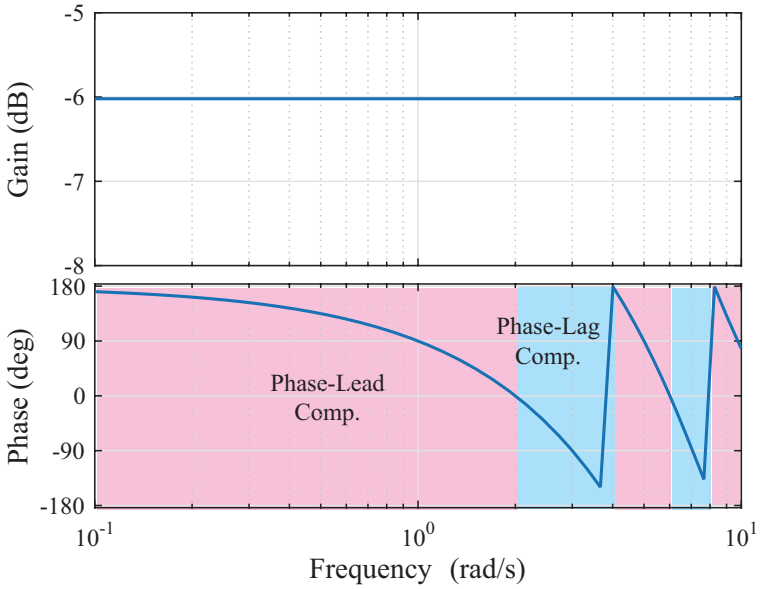

Fig. 3-10: Bode diagram of compensator $-\frac{1}{2}e^{-\frac{L_n}{c_n}s}$ in reflected wave rejection.

G_w is approximated by

$$\begin{aligned} G_w &= \frac{2e^{-\frac{L}{c}s}}{1+e^{-\frac{2L}{c}s}} \\ &= \frac{2}{e^{\frac{L}{c}s}+e^{-\frac{L}{c}s}} \\ &= \frac{1}{\cosh\frac{L}{c}s} \\ &= \frac{1}{\left(1+\frac{1}{\omega_1^2}s^2\right)\left(1+\frac{1}{\omega_2^2}s^2\right)\cdots} \\ &\approx \frac{\omega_1^2\omega_2^2}{\left(s^2+\omega_1^2\right)\left(s^2+\omega_2^2\right)}. \end{aligned} \tag{3.28}$$

The approximated transfer function (3.28) considers the first-order and second-order resonant frequencies. From Fig. 3-11, the resonance is expressed by the circle on Nyquist diagram. It is noted that, if the damping ratio equals to 0, the resonance is expressed by the circle with infinite radius. In Fig. 3-11, very small damping ratio is considered for the simplicity. As seen in trajectory of G_w drawn by blue line in Fig. 3-11(a), it is found that the circle expressed by first-order resonant frequency gets across third and fourth quadrants on complex plane. If the phase delay occurs at the resonant frequency, the system becomes unstable from the point of view of the Nyquist stability criterion because the circle encloses $(-1,\ 0)$. Hence, phase-lead compensation is needed to stabilize the first-order resonance. On the other

hand, the circle drawn by the second-order resonant frequency gets across first and second quadrants on complex plain. In this case, if phase lead occurs at the resonant frequency, the system becomes unstable from the point of view of the Nyquist stability criterion. Therefore, phase-lag compensation is needed to stabilize the second-order resonance. As well as cases of the first-order and second-order resonances, phase-lead compensations are needed for stabilizing $(2n-1)$-th order resonant frequency, and phase-lag compensations are needed for stabilizing $2n$-th order resonant frequency. It is noted that, which compensation is needed for stabilizing the resonances is related to residue of each vibration mode [37].

If the reflected wave rejection is applied to the wave system, the trajectories changes blue line to yellow line in Fig. 3-11. The circles drawn by the first-order and second-order frequencies get across the first and fourth quadrants on complex plain. This location is the farthest from the point $(-1,\ 0)$. At this location, phase margin is 90 degree at each resonance if there is no damper in the wave system. Therefore, it is found that the reflected wave rejection stabilizes all of the wave system.

In the above discussion, it is assumed that the cut-off frequency of the reflected wave rejection is set as enough high value (i.e. $g_r \to \infty$). If the cut-off frequency is finite value, phase compensation represented as (3.27) is not realized at high-frequency area because $F(s)$ itself has phase-lag characteristic whose it is -90 degree at high-frequency area. In the case, the phase compensation value including the effect of $F(s)$ is represented as

$$\text{Phase comp. value} = (-1)^{2n-1}\frac{\pi}{2} - \tan^{-1}\frac{\omega}{2g_r} \text{ rad.} \tag{3.29}$$

Because $\tan^{-1}\omega/2g_r = \pi/2$ under $\omega = \infty$, the phase compensation value at enough-high frequency area becomes 0. At the high-frequency area, the resonances are not stabilized, but they are not destabilized, in other words they are stability limit. Therefore, it is needed to set the cut-off frequency g_r enough high value. Additionally, in practical situation, it is no problem because gain of the plant typically decreases at high-frequency area.

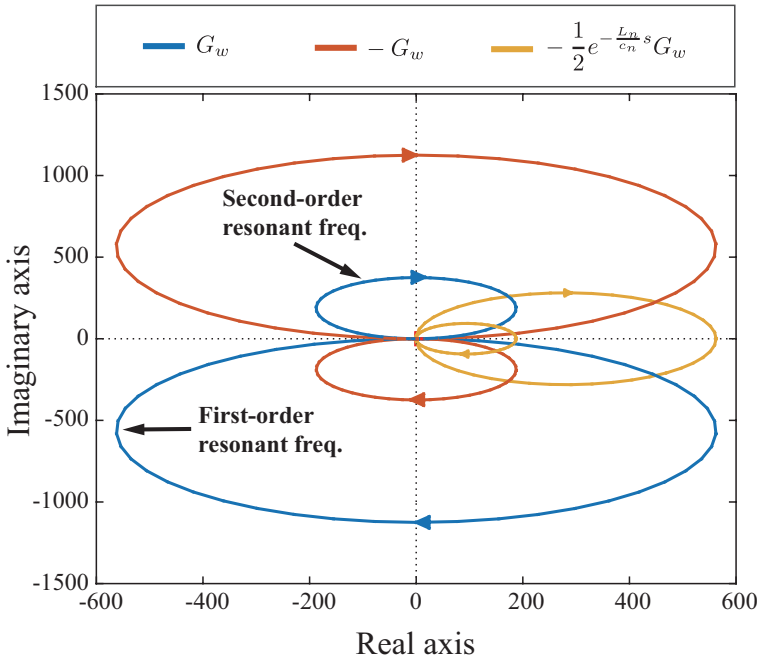

(a) Overview

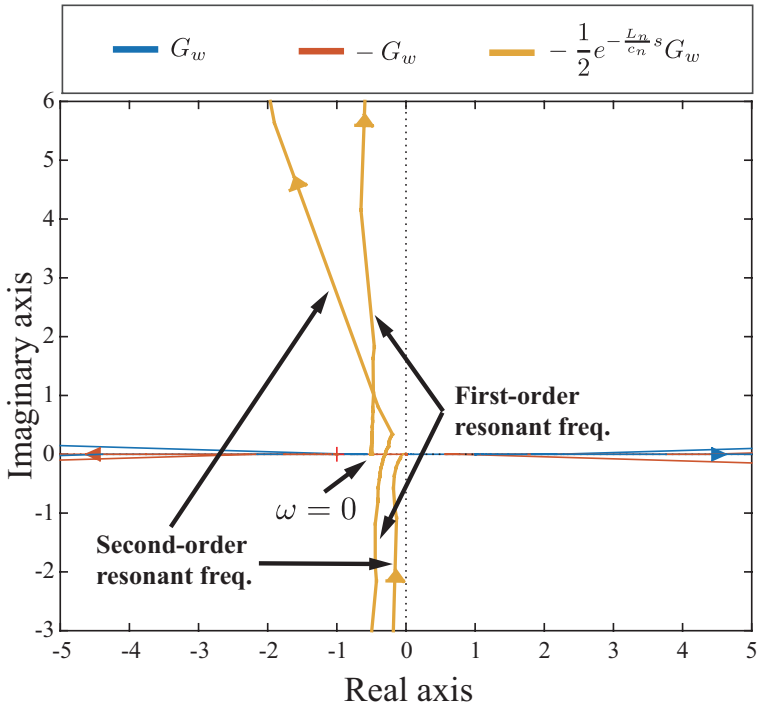

(b) Enlarged view

Fig. 3-11: Nyquist diagram for analyzing performance of reflected wave rejection.

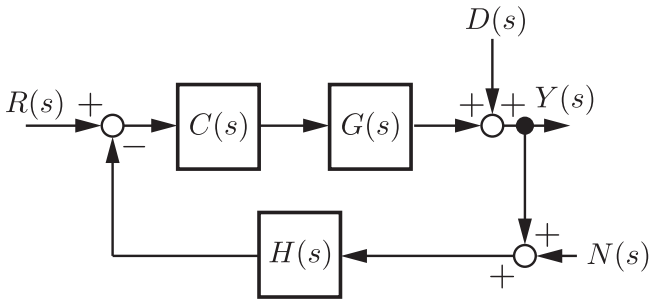

Fig. 3-12: Block diagram of typical feedback system.

3.4.2 Performance Analysis based on Sensitivity and Complementary-Sensitivity Functions

This part analyzes the performance of vibration suppression based on sensitivity and complementary-sensitivity functions.

Preliminary

Fig. 3-12 shows block diagram of a typical feedback system. In Fig. 3-12, $C(s)$, $G(s)$, $H(s)$, $R(s)$, $Y(s)$, $D(s)$, and $N(s)$ denote the controller, the plant, the feedback compensator, the command, the output, the disturbance, and the noise, respectively. The sensitivity function $S(s)$ and complementary-sensitivity function $T(s)$ are defined as

$$S(s) = \frac{1}{1+G_o} \tag{3.30}$$

$$T(s) = \frac{G_o}{1+G_o} \tag{3.31}$$

where G_o stands for the open-loop transfer function, which is represented as

$$G_o = C(s)G(s)H(s). \tag{3.32}$$

The sensitivity function expresses the transfer function from the disturbance $D(s)$ to the output $Y(s)$. Considering the above, the sensitivity function should be set 0. On the other hand, the complementary-sensitivity function is related to the transfer function from $R(s)$ to $Y(s)$ or transfer function from $N(s)$ to $Y(s)$. However, from (3.30) and (3.31), there is trade off between sensitivity and complementary-sensitivity functions as

$$S(s) + T(s) = 1. \tag{3.33}$$

Therefore, in general, the sensitivity function should be set 0 in low-frequency area for suppressing the disturbance. On the other hand, the complementary-sensitivity function should be 0 in high-frequency area for considering noise effect. In addition, because a transfer function from modeling error to output is also represented as a the complementary-sensitivity function, the complementary-sensitivity function should have low-pass characteristic for robust stability.

It is important to maintain the nominal performance under the existence of modeling error, which is called robust performance. Because the nominal performance is represented as a the complementary-sensitivity function, the complementary-sensitivity function is desired not to change under existence of modeling error. Here, the variation rates of plant and complementary-sensitivity function are defined as

$$\Delta_G = \frac{G_n(s) - \tilde{G}(s)}{\tilde{G}(s)} \tag{3.34}$$

$$\Delta_T = \frac{T_n(s) - \tilde{T}(s)}{\tilde{T}(s)} \tag{3.35}$$

where $\tilde{\bigcirc}$ denotes the variation. By using $\tilde{T} = C\tilde{G}/(1 + C\tilde{G})$, the relationship between Δ_G and Δ_T is derived as

$$\Delta_T = S(s)\Delta_G. \tag{3.36}$$

Eq. (3.36) means that sensitivity function decreases the effect of variation of plant model to a complementary-sensitivity function.

Analysis of Reflected Wave Rejection

The sensitivity and complementary-sensitivity functions of the proposed control system shown in Fig. 3-10 are derived as

$$S_w(s) = \frac{1}{1 - \frac{1}{2}F(s)e^{-\frac{L_n}{c_n}s}G_w(s)} \tag{3.37}$$

$$T_w(s) = \frac{-\frac{1}{2}F(s)e^{-\frac{L_n}{c_n}s}G_w(s)}{1 - \frac{1}{2}F(s)e^{-\frac{L_n}{c_n}s}G_w(s)}. \tag{3.38}$$

Fig. 3-13 shows sensitivity and complementary-sensitivity functions represented as (3.37) and (3.38) when the cut-off frequency of the reflected wave rejection equals to infinity (i.e. $F(s) \approx 1$). It is noted that the resonant frequencies set $(2n - 1)$ rad/s ($T_w = \pi/2$) for the sake of simplicity. In this case, the

sensitivity and complementary-sensitivity functions are expressed as

$$S_w^{ideal} = 1 + e^{-2\frac{L_n}{c_n}s} \tag{3.39}$$

$$T_w^{ideal} = -e^{-2\frac{L_n}{c_n}s}. \tag{3.40}$$

According to the above equations and bode diagram, gain of the sensitivity function decreases at resonance frequencies. Therefore, considering (3.36), it is found that effect of variation of resonant frequencies to nominal performance are decreased by sensitivity function generated by the reflected wave rejection. However, since gain of the sensitivity function remains the constant value at low-frequency area, steady state error occurs by the external force acting on the tip. As for the suppression of external force, the wave-based observer, which is described in Chapter 7, is implemented. On the other hand, gain of complementary-sensitivity function equals to 0 dB over all frequency area. It implies the good tracking performance which does not include the vibrations, but robust stability is low because the gain remains constant value at high-frequency area. Therefore, it is needed to set g_r appropriate value considering the robust stability of high-frequency area.

Fig. 3-14 shows the bode diagram of sensitivity and complementary-sensitivity functions when the cut-off frequency g_r is varied from 20 rad/s to 100 rad/s with step of 20 rad/s. From Fig. 3-14(a), the characteristic of the sensitivity function does not change so much by g_r. It is also found that it is impossible to adjust the characteristic of the sensitivity function at low-frequency area by changing g_r. On the other hand, from Fig. 3-14(b), the bandwidth of the complementary-sensitivity function is determined by g_r, which is related to robust stability. From (3.38), because the complementary sensitivity function has $F(s)$ which is a low-pass filter, setting g_r lower value leads to increase robust stability. In contrast, vibration-suppression performance increases by setting g_r higher value. Hence, it can be found that there is a trade-off between vibration suppression performance and robust stability. According to the trade-off, it is better to set g_r higher value unless the system destabilizes.

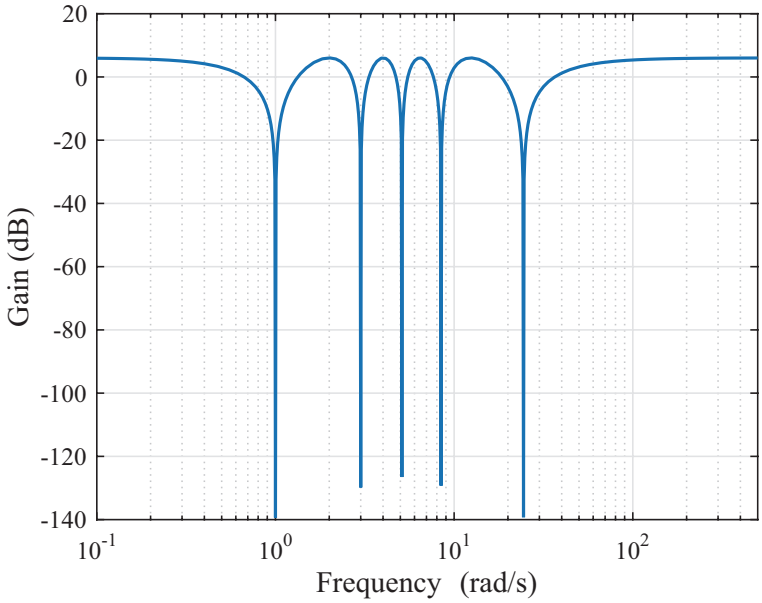

(a) Sensitivity function

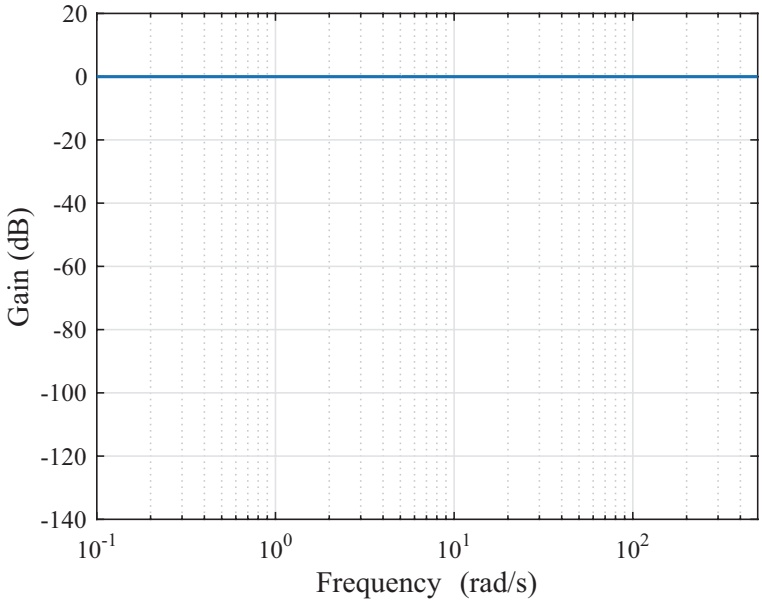

(b) Complementary sensitivity function

Fig. 3-13: Bode diagram of sensitivity and complementary-sensitivity functions of position control with reflected wave rejection when $F(s) = 1$.

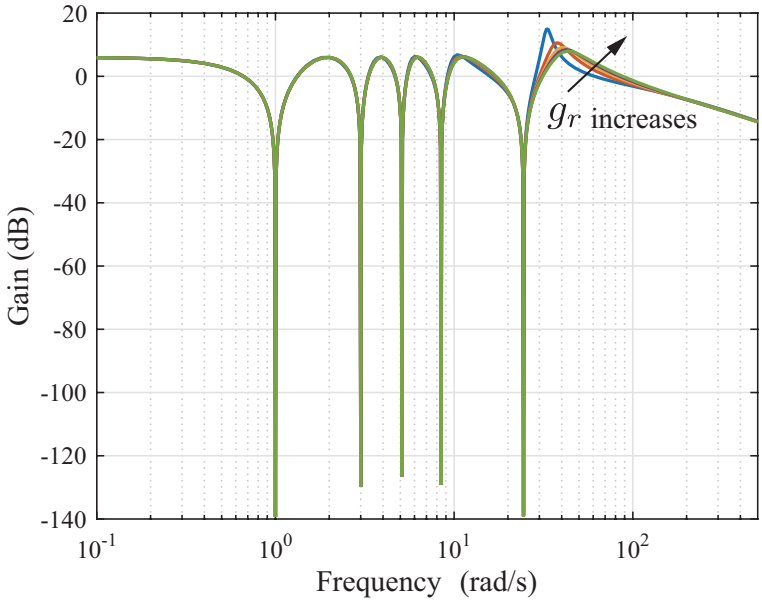

(a) Sensitivity function

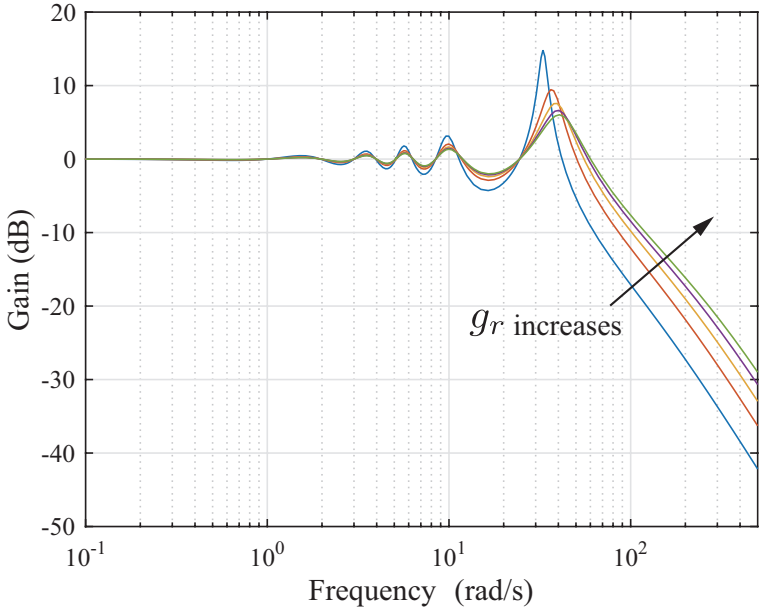

(b) Complementary sensitivity function

Fig. 3-14: Bode diagram of sensitivity and complementary-sensitivity functions when the cut-off frequency g_r is varied from 20 rad/s to 100 rad/s.

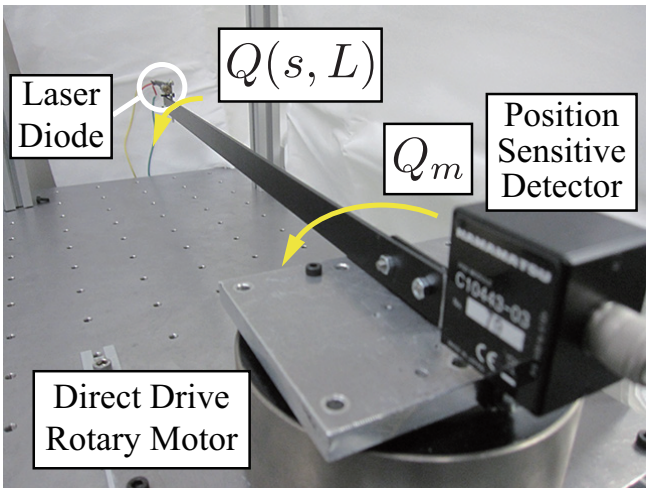

Fig. 3-15: Experimental setup.

3.5 Experiments of Position Control with Reflected Wave Rejection

3.5.1 Experimental Setup

To verify the effectiveness of the proposed method, experiments on position control of flexible arm are performed. Experimental setup is show in Fig. 3-15. The experiments consider propagation of angle defined by deflection which is described in section 2.2.2. The flexible arm is mounted on the direct drive rotary motor with the encoder (resolution: 2^{20} pulse/rev). The load position $q(t, L)$ is obtained by the position sensitive detector (PSD) produced by Hamamatsu Photonics K.K. The PSD detects the position of the irradiation point which is generated by the laser diode mounted on the tip position ($x = L$) and output analog voltage in proportional to the position. The analog voltage is measured by A/D converter board. The above sensing method of tip position is same as the method [96]. The real-time control system is realized by Linux OS with real time application interface (RTAI 3.7).

The experimental parameters are shown in Fig. 3.1. In experiments, a step command ($r(t) = 0.005$ rad) is applied to the system at $t = 2.0$.

In this experiment, the semi-closed-loop type reflected wave rejection is performed. The performance of the proposed method is compared with that of fully closed-loop state feedback control. The block diagram of the compared method is shown in Fig. 3-16. In Fig. 3-16, K_{pm}, K_{vm}, K_{pl}, K_{vl} denote the state feedback gains. K_p, K_i, and K_d stand for the PID controller gain. The control method shown in Fig. 3-16 considers first-order resonant frequency ω_m and anti-resonant frequency ω_a. The characteristic

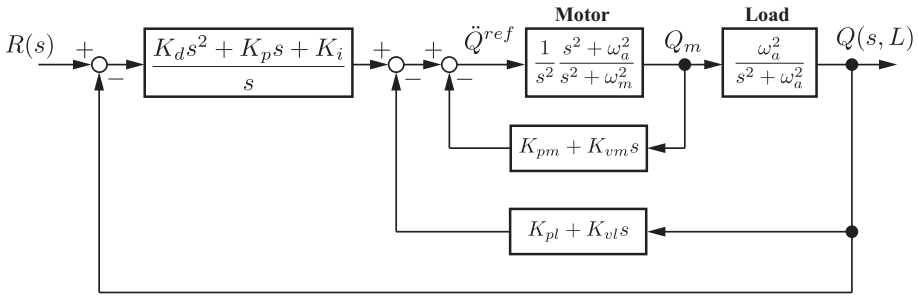

Fig. 3-16: Block diagram of fully closed-loop PID control with state feedback of two-mass resonant system.

equation is represented as

$$\begin{aligned} Den(s) &= s^5 + K_{vm}s^4 + (K_{pm} + \omega_m^2)s^3 + (K_{vm} + K_{vl} + K_d)\omega_a^2 s^2 + \\ &\quad (K_{pm} + K_{pl} + K_p)\omega_a^2 s + K_i\omega_a^2. \end{aligned} \tag{3.41}$$

The gains for pole assignment at 5-multiple roots $s = -\omega_n$ and zero assignment at 2-multiple roots $s = -\omega_z$ are derived as

$$K_i = \frac{\omega_n^5}{\omega_a^2} \tag{3.42}$$

$$K_p = \frac{2K_i}{\omega_z} \tag{3.43}$$

$$K_d = \frac{K_i}{\omega_z^2} \tag{3.44}$$

$$K_{pm} = 10\omega_n^2 - \omega_m^2 \tag{3.45}$$

$$K_{vm} = 5\omega_n \tag{3.46}$$

$$K_{pl} = \frac{5\omega_n^4}{\omega_a^2} - K_{pm} - K_p \tag{3.47}$$

$$K_{vl} = \frac{10\omega_n^3}{\omega_a^2} - K_{vm} - K_d. \tag{3.48}$$

3.5.2 Experimental Results

Experimental results of the compared and proposed methods when $\omega_n = \tilde{\omega}_1$ shown in Figs. 3-17 and 3-18. From Figs. 3-17 and 3-18, it can be found that both methods suppress the vibration well. It can be observed in Fig. 3-18 that steady state error occurs because of sensitivity function of the proposed method

Table 3.1: Experimental parameters for the semi-closed-loop reflected wave rejection.

Parameter	Description	Value
T_s	Sampling time	50 μs
$\tilde{\omega}_1$(=ω_a)	Identified 1st resonant frequency	38 rad/s
T_w	Propagation time of wave	$\pi/(2\tilde{\omega}_1)$ s
K_{tn}	Nominal torque coefficient	1.18 Nm/A
J_n	Nominal inertia of motor	0.0035 kgm^2
K_p	Position gain	ω_n^2
K_v	Velocity gain	4.0ω_n
T_{wn}	Nominal propagation time of wave	$\pi/(2\omega_{1n})$ s
g_{dis}	Cut-off freq. of DOB	2000 rad/s
g_r	Cut-off freq. of reflected wave rejection	65 rad/s

as mentioned in previous part. The steady state error can be eliminated by the wave-based disturbance observer described in Chapter 7.

Figs. 3-19 and 3-20 show the experimental results of both methods when $\omega_n = 1.2\tilde{\omega}_1$. From Fig. 3-19, it is found that first-order resonance is well suppressed. However, the second-order resonance is excited, in other words, the spillover occurs. Hence, it is difficult to improve the control bandwidth by the fully closed-loop state feedback control shown in Fig. 3-16. On the other hand, Fig. 3-20 shows that the reflected wave rejection suppresses both first and second order resonances. Therefore, it is possible to improve the control bandwidth by the proposed method.

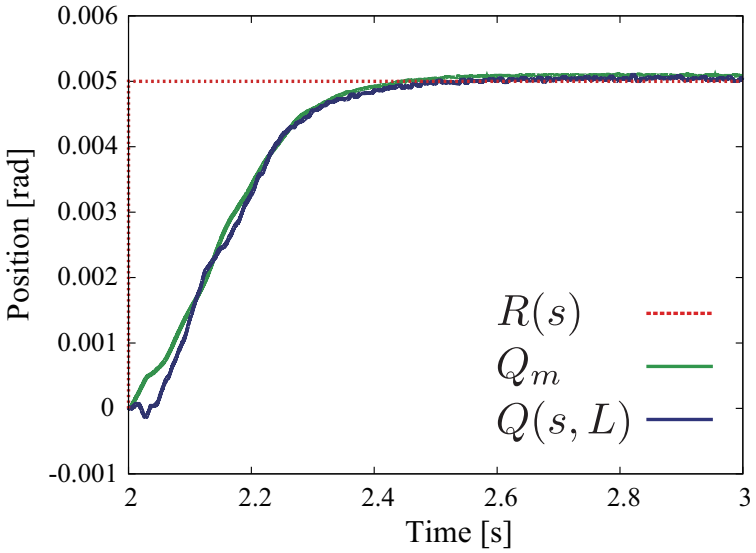

Fig. 3-17: Experimental results of state feedback control with $\omega_n = \tilde{\omega}_1$.

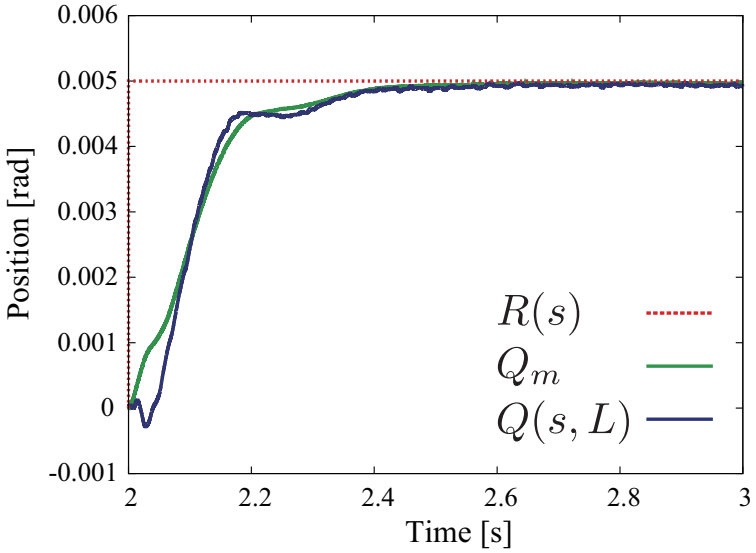

Fig. 3-18: Experimental results of reflected wave rejection with $\omega_n = \tilde{\omega}_1$.

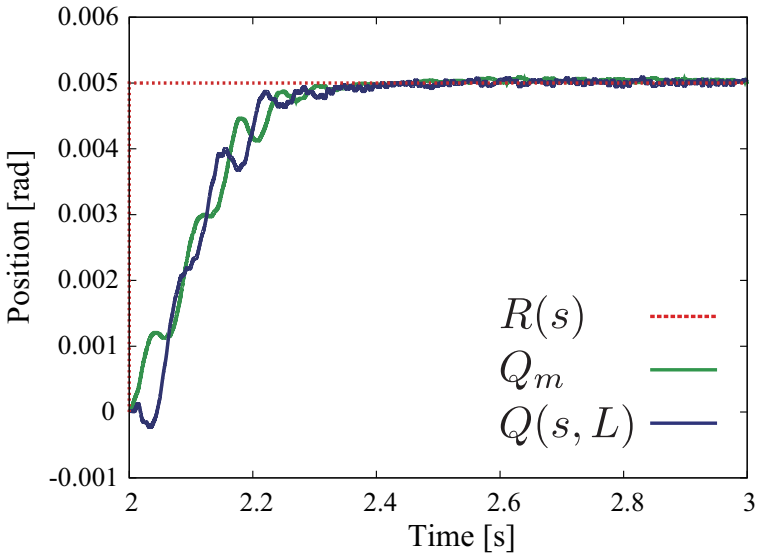

Fig. 3-19: Experimental results of state feedback control with $\omega_n = 1.2\tilde{\omega}_1$.

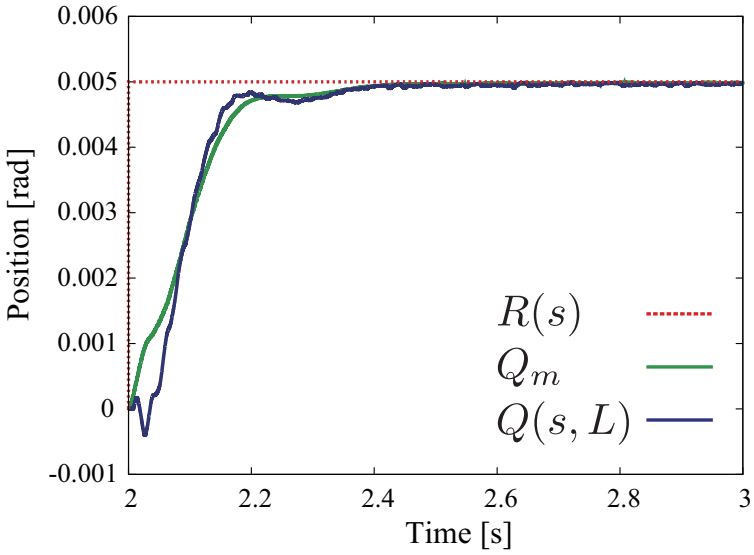

Fig. 3-20: Experimental results of reflected wave rejection with $\omega_n = 1.2\tilde{\omega}_1$.

3.6 Summary of Chapter 3

The basic concept and structure of reflected wave rejection were proposed in this chapter. The reflected wave rejection is composed of reflected wave estimator and feedforward compensator for reflected wave. By the reflected wave rejection, the actual reflected wave is canceled out by the feedforward of the reflected wave. Then, the two types of position control of wave system with reflected wave rejection are proposed: the fully closed-loop type and the semi-closed-loop type.

Next, effect of reflected wave rejection is analyzed by use of open-loop transfer function and Nyquist diagram. By the analysis, effect of the reflected wave rejection is equivalent to infinite-series of phase lag and lead compensators. Under ideal condition ($g_r = \infty$), the reflected wave rejection gives 90 degree phase margin to each vibration mode. In addition, the reflected wave rejection is categorized to phase stabilization method in vibration control methods.

Moreover, the sensitivity function and complementary-sensitivity function are derived for investigating the robust stability and robust performance. From the sensitivity function, because the gain is low near the resonant frequencies, the reflected wave rejection has some robustness against the variation of the resonant frequency. However, because the gain at low-frequency area is constant value, it means that steady state error occurs when disturbance acts on the tip position. Hence, an additional disturbance compensator is needed to be implemented, which will be explained in Chapter 6.

Finally, the validity of the proposed method was confirmed by the experiments of position control of flexible arm. Additionally, the performance of the proposed method was compared by that of fully closed-loop state feedback control.

Chapter 4

Motion Control of Various Resonant Systems

4.1 Introduction of Chapter 4

This chapter describes the reflected wave rejections for various resonant systems. First of all, the reflected wave rejection considering damper in wave system [89] is proposed. The transfer function of wave equation including damper is shown, and it is shown that the transfer function is composed of time-delay-like element. Due to difficulty in implementation of the time-delay-like element, the reaction-force-based-reflected wave rejection [90] with fractional low-pass filter is constructed. Then, the reflected wave rejection considering mass on tip is proposed. In many industrial application, some load is mounted at tip position. It is explained that the effect of the mass on tip position equals to all pass filter [97]. Finally, Section 4.4 summarizes this chapter.

4.2 Reflected Wave Rejection Considering Damper Effect

4.2.1 Wave Equation Considering Damper Effect

This part explains reflected wave rejection considering damper effect. The typical wave equation which considers only distributed spring has restriction that the resonant poles are located on the imaginary axis at regular intervals. Consideration of damper effect is able to alleviate the restriction, which leads to extend the range of application for the reflected-wave-rejection-based vibration control. Wave

equation considering damper is represented as

$$\frac{\partial^2 q(t,x)}{\partial t^2} = c_k^2 \frac{\partial^2 q(t,x)}{\partial x^2} + c_d^2 \frac{\partial}{\partial t} \frac{\partial^2 q(t,x)}{\partial x^2} \tag{4.1}$$

where c_k and c_d are propagation velocities of the wave, which are represented as

$$c_k = \sqrt{\frac{\kappa}{\rho}} \tag{4.2}$$

$$c_d = \sqrt{\frac{d}{\rho}} \tag{4.3}$$

where ρ, κ and d denote the density of mass, the density of the spring, and the density of damping coefficient, respectively. Furthermore, boundary conditions are represented as

$$q(t,0) = q_m(t) \tag{4.4}$$

$$\frac{\partial q(t,L)}{\partial x} = 0. \tag{4.5}$$

(4.4) means applying position input by the motor at $x = 0$, and (4.5) means free end at $x = L$. Moreover, initial conditions are represented as

$$q(0,x) = 0 \tag{4.6}$$

$$\frac{\partial q(0,x)}{\partial t} = 0. \tag{4.7}$$

Using (4.4)–(4.7), a transfer function from $Q(s,0)$ to $Q(s,x)$ is derived as

$$\begin{aligned} G(s,x) &= \frac{Q(s,x)}{Q(s,0)} \\ &= \frac{e^{-\frac{x}{c(s)}s} + e^{-\frac{(2L-x)}{c(s)}s}}{1 + e^{-2\frac{L}{c(s)}s}} \end{aligned} \tag{4.8}$$

where $c(s)$ denotes the propagation velocity of the wave, and it is represented as

$$\begin{aligned} c(s) &= \sqrt{c_k^2 + c_d^2 s} \\ &= c_k\sqrt{1 + \alpha s}. \end{aligned} \tag{4.9}$$

In (4.9), α denotes the ratio of c_k and c_d. From (4.9), it is found that the propagation velocity depends on frequency due to the damper elements. Finally, a transfer function from the position input $Q(s,0) = Q_m$ to the tip position $Q(s,L)$ is derived as

$$\frac{Q(s,L)}{Q_m} = \frac{2e^{-\frac{Ls}{c(s)}}}{1 + e^{-\frac{2Ls}{c(s)}}}. \tag{4.10}$$

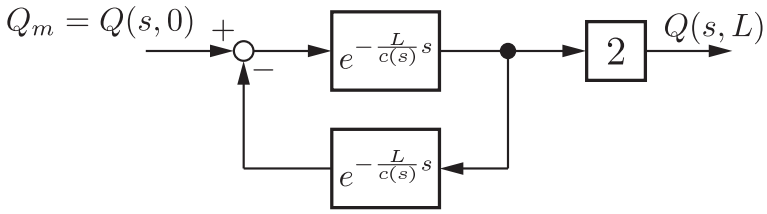

Fig. 4-1: Block diagram of resonant system based on wave equation.

The transfer function has infinite number of poles which are located near the imaginary axis. Therefore, vibrations occur on response of the tip position. The block diagram of the transfer function is shown in Fig. 4-1. In Fig. 4-1, the negative feedback represents a reflected wave. In a concept of the wave, the vibration is caused by superposition of traveling and reflected waves. If the reflected wave is eliminated, vibrations caused by the resonances are suppressed.

4.2.2 Reflected Wave Rejection with Fractional-Order Low-Pass Filter

In this part, a vibration control of the resonant system by using a reflected wave rejection with a fractional-order low-pass filter is proposed. By using the fractional-order low-pass filter, the reflected wave including the damper effect is eliminated and vibration caused by the reflected wave is suppressed.

Reflected Wave Rejection Considering Damper Effect

A basic structure of reflected wave rejection has already been shown in Chapter 3. It is possible to construct the reflected wave rejection for the wave system considering damper by replacing a time-delay element $e^{-\frac{L}{c}s}$ in Fig. 3-2 a time-delay-like element $e^{-\frac{L}{c(s)}s}$. Under assumption that such element can be implemented, the reflected wave is estimated according to

$$\begin{aligned} \hat{Q}_{rfl} &= F(s)(Q_m - Q(s,L)e^{-\frac{L}{c(s)}s}) \\ &= F(s)\frac{1-e^{-2\frac{L}{c(s)}s}}{1+e^{-2\frac{L}{c(s)}s}}Q_m \end{aligned} \tag{4.11}$$

where $F(s)$ denotes the low-pass filter. In the derivation of (4.11), the transfer function shown in (4.10) is used. Now, it is assumed that $F(s) = 1$ for the sake of simplicity of explanation. Then, the transfer function from position input Q_m to the tip position $Q(s,L)$ is derived as

$$\frac{Q(s,L)}{Q_m} = e^{-\frac{L}{c(s)}s}. \tag{4.12}$$

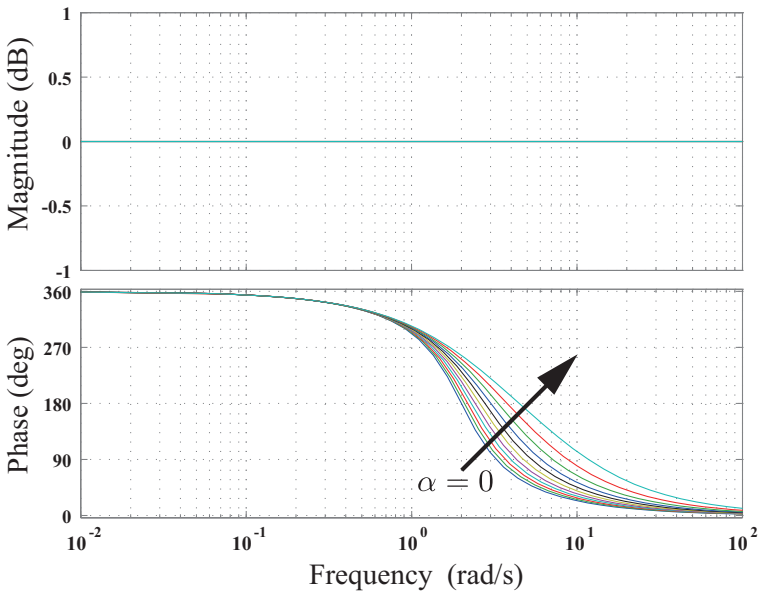

Fig. 4-2: Bode diagram of element like time delay expressed as (4.12).

In (4.12), there is no $e^{-\frac{L}{c(s)}s}$ in the denominator of the transfer function. Bode diagram of transfer function (4.12) is shown in Fig. 4-2. From Fig. 4-2, it turns out that vibrations caused by the resonances are suppressed. When the parameter α in $c(s)$ equals to 0, (4.12) becomes a time delay. If α becomes higher value, phase delay is reduced.

However, in the actual implementation, it is difficult to implement the time-delay-like element $e^{-\frac{L}{c(s)}s}$ in the digital computer because it is not a pure time-delay element. Therefore, for obtaining the effect of the reflected wave rejection, (4.11) is transformed by using a reaction force $F^{reac}(s,0)$ so that the calculation process in estimation of the reflected wave for the reflected wave does not include the time-delay-like element.

Firstly, by applying partial differentiation of (4.8) with respect to x, the torsion at $x = 0$ is derived as

$$\frac{\partial Q(s,0)}{\partial x} = -\frac{s}{c(s)} \frac{1 - e^{-2\frac{L}{c(s)}s}}{1 + e^{-2\frac{L}{c(s)}s}} Q_m. \tag{4.13}$$

The reaction force at $x = 0$ is represented as

$$\begin{aligned} F^{reac}(s,0) &= (\kappa + ds) \frac{\partial Q(s,0)}{\partial x} \\ &= -(\kappa + ds) \frac{s}{c(s)} \frac{1 - e^{-2\frac{L}{c(s)}s}}{1 + e^{-2\frac{L}{c(s)}s}} Q_m. \end{aligned} \tag{4.14}$$

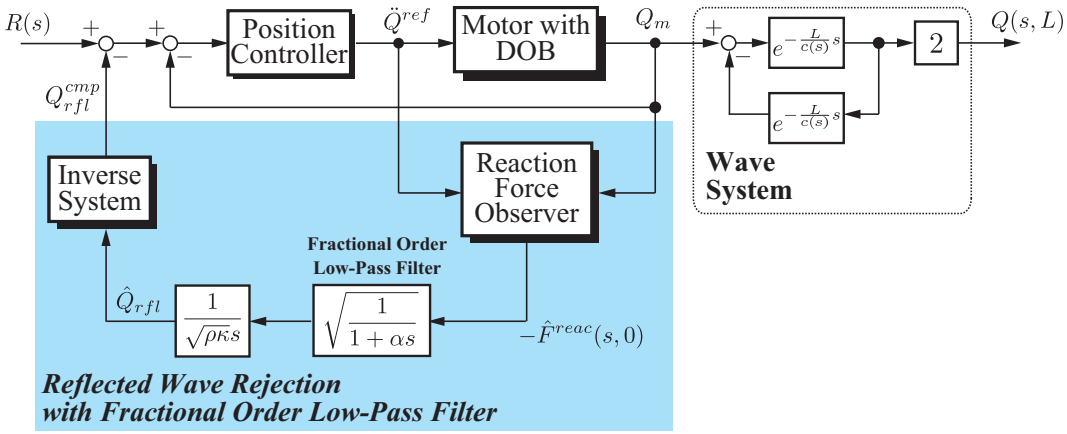

Fig. 4-3: Block diagram of reflected wave rejection with fractional order low-pass filter.

It can be seen that there exists a same part which is composed of time-delay elements in the right side of (4.12) and (4.14). Hence, the estimated reflected wave can be expressed by using the reaction force. By using (4.14), the estimated reflected wave (4.11) is transformed into

$$\begin{aligned}\hat{Q}_{rfl} &= \frac{1-e^{-2\frac{L}{c(s)}s}}{1+e^{-2\frac{L}{c(s)}s}}Q_m \\ &= -\frac{c(s)}{s}\frac{\partial Q(s,0)}{\partial x} \\ &= -\frac{c(s)}{s}\frac{1}{\kappa+ds}(\kappa+ds)\frac{\partial Q(s,0)}{\partial x} \\ &= -\frac{1}{s}\frac{1}{\sqrt{\rho\kappa}}\sqrt{\frac{1}{1+\alpha s}}F^{reac}(s,0). \end{aligned} \tag{4.15}$$

In (4.15), the reaction force $F^{reac}(s,0)$ is estimated by a reaction-force observer [15]. Additionally, $\sqrt{\frac{1}{1+\alpha s}}$ denotes a fractional-order low-pass filter, and how to implement it is explained in a next part.

The block diagram of whole control system is shown in Fig. 4-3. As well as the reflected wave rejection shown in Chapter 3, the estimated reflected wave multiplied by the inverse system is fedback to the position command. Hence, the compensation value for the reflected wave is represented as

$$Q_{rfl}^{cmp} = \frac{g_r}{s+g_r}\frac{s^2+K_ds+K_p}{K_p+K_ds}\hat{Q}_{rfl}. \tag{4.16}$$

Finally, the transfer function from the position command $R(s)$ to the tip position $Q(s,L)$ is represented as

$$\frac{Q(s,L)}{R(s)} = \frac{K_p+K_ds}{s^2+K_ds+K_p}e^{-\frac{L}{c(s)}s}. \tag{4.17}$$

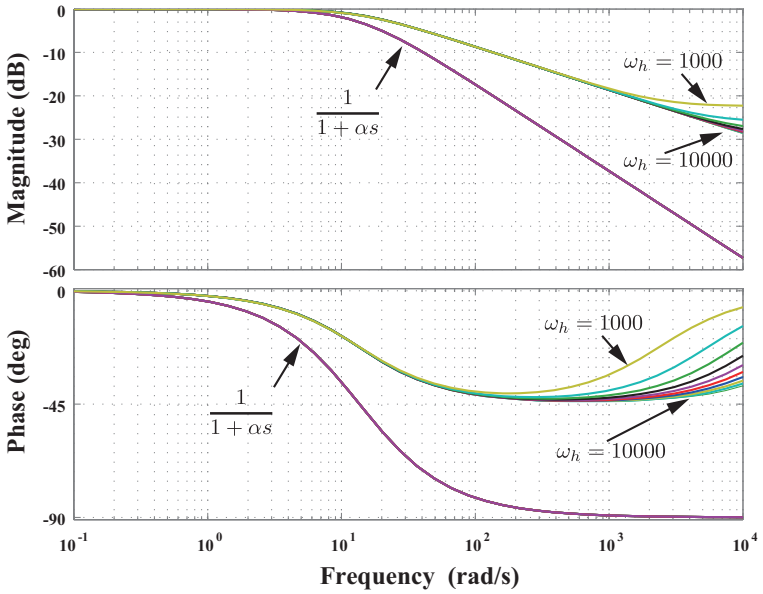

Fig. 4-4: Bode diagram of fractional order low-pass filter.

According to the above equation, the wave system including damper effect can be stabilized by the reflected wave rejection shown in Fig. 4-3.

Implementation of Fractional-Order Low-Pass Filter

In this part, implementation of the fractional-order low-pass filter is explained. The conventional research of fractional-order calculus proposed implementation of the fractional order lead-lag compensator by using a broken-line approximation [64]. In this dissertation, based on the above method, the fractional order low-pass filter is approximated by the fractional order lead-lag compensator,

$$\sqrt{\frac{1}{1+\alpha s}} \approx \left(\frac{\frac{s}{\omega_h}+1}{\frac{s}{\omega_b}+1} \right)^{0.5} \tag{4.18}$$

where $\omega_b = \frac{1}{\alpha}$. If the parameter ω_h equals to enough high value, this approximation is realized. (4.18) is realized by using the broken-line approximation, which is represented as

$$\left(\frac{\frac{s}{\omega_h}+1}{\frac{s}{\omega_b}+1} \right)^{0.5} = \prod_{i=0}^{N-1} \frac{\frac{s}{\omega_i'}+1}{\frac{s}{\omega_i}+1} \tag{4.19}$$

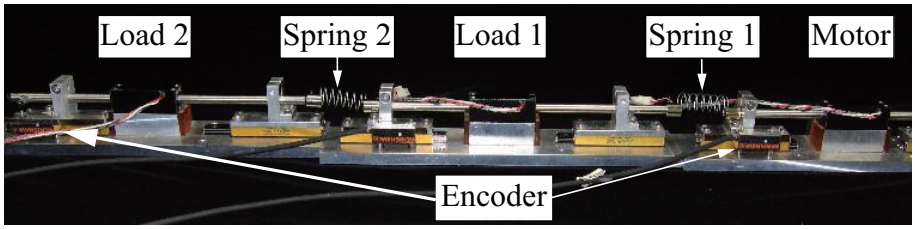

Fig. 4-5: Experimental setup.

where N denotes the number of approximation order. ω_i and ω_i' are represented as

$$\begin{aligned} \omega_i &= \left(\frac{\omega_h}{\omega_b}\right)^{\frac{i+\frac{1}{4}}{N}} \omega_b, \\ \omega_i' &= \left(\frac{\omega_h}{\omega_b}\right)^{\frac{i+\frac{3}{4}}{N}} \omega_b. \end{aligned} \tag{4.20}$$

Needless to say, if N is large value, (4.19) approaches the real one, but calculation cost becomes higher. In this dissertation, considering the calculation cost, N is set as 6. Fig. 4-4 shows the bode diagram when ω_h changes from 1000 rad/s to 10000 rad/s every 1000 rad/s. It turns out that gain characteristic matches the real one from 0 rad/s to ω_h. On the other hand, phase characteristic matches the real one form 0 rad/s to $\frac{\omega_h}{2}$ Therefore, bandwidth of the reflected wave rejection is limited form 0 rad/s to $\frac{\omega_h}{2}$. The parameter ω_h should be set by considering the resonances which should be suppressed.

Next, how to set the parameter α is explained. Theoretical value of the parameter α is represented as

$$\alpha = \frac{d}{\kappa}. \tag{4.21}$$

In this dissertation, the parameter α is set by first and second order resonant frequencies. By using those resonant frequencies, the parameter α is derived as

$$\alpha = \frac{x_1 x_2 (x_2 - x_1)}{x_2^2 \omega_1^2 - x_1^2 \omega_2^2} \sqrt{\frac{x_2 \omega_1^2 - x_1 \omega_2^2}{x_1 x_2 (x_2 - x_1)}} \tag{4.22}$$

where ω_1 and ω_2 denote the first and second order resonant frequencies, and x_i $(i = 1,\ 2)$ is represented as

$$x_i = \left(\frac{(2i+1)\pi}{4L}\right)^2. \tag{4.23}$$

Table 4.1: Experimental parameters for control with reflected wave rejection considering damper.

Parameter	Description	Value
T_s	Sampling time	0.1 ms
K_{tn}	Nominal torque coefficient	3.33 N/A
M_n	Nominal mass	0.245 kg
K_p	Proportional gain	2250
K_d	Differential gain	190
$\frac{1}{\alpha}$	Cut-off frequency of fractional-order low-pass filter	14.1 rad/s
g_r	Cut-off frequency of reflected wave rejection	300 rad/s
g_{dis}	Cut-off frequency of disturbance observer	1000 rad/s
g_{reac}	Cut-off frequency of reaction force observer	500 rad/s
ω_1	First-order resonance	47 rad/s
ω_2	Second-order resonance	110 rad/s
L	Length of a system	0.05 m

4.2.3 Experiments

Experimental Setup

In order to verify the effectiveness of the proposed method, experiments of position control are conducted in a three-mass resonant system. The control software is written in C language under RTAI 3.7. The experimental setup is shown in Fig. 4-5. In the experiments, three linear motors connected by springs are used. The experiments consider linear motion as shown in Fig. 2-1. The right motor is controlled. On the other hand, the left and central motors are used as load and not controlled. Position information of each motor is obtained by linear encoders (resolution capability: 0.1 μm).

The experimental parameters are shown in Table 4.1. The resonant frequencies are obtained by conducting the preliminary frequency identification. The parameter α is calculated by the first and second resonant frequencies. For decreasing noise effect caused by derivation, pseudo derivations are used for calculating the motor velocity and compensation value of the reflected wave.

In these experiments, the proposed method is compared with a method with a PD controller with the disturbance observer. Moreover, the proposal is compared with a method with the reaction-force-based

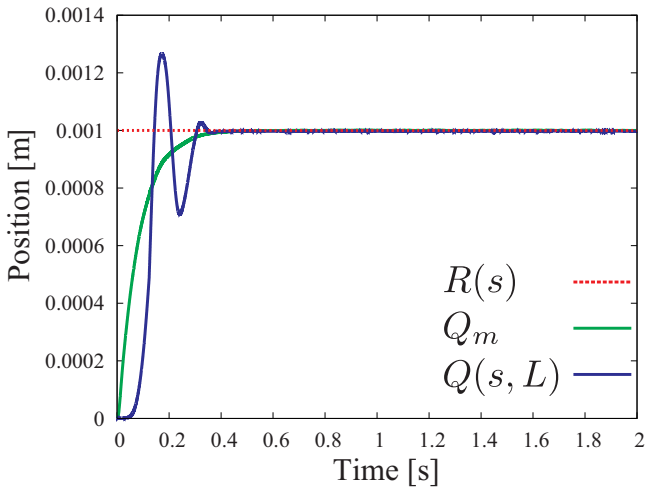

Fig. 4-6: Experimental results by PD controller with disturbance observer.

reflected wave rejection [90] which is in the case that $\alpha = 0$.

Experimental Results

Experimental results of the proposed and conventional methods are shown in Figs. 4-6–4-8. From Fig. 4-6, it is found that the vibration occurs on the response of the tip position because anti-resonance zero is canceled out by the disturbance observer. On the other hand, from Fig. 4-7, it can be seen that the vibration is suppressed by the reflected wave rejection. However, the overshoot occurs because the conventional reflected wave rejection is based on assumption that poles of the resonant system are located on the imaginary axis at regular intervals. From the results of the proposed method shown in Fig. 4-7, not only the first-order resonance but also second resonance are well suppressed. However, in experimental results of the proposed method, a little vibration like chattering effect occurs at motor side. It is not caused by the resonance but caused by a friction included in the estimated reaction force by the reaction-force observer. Therefore, it is necessary to identify the friction more accurately and the accurate identification of the friction reduces the chattering effect. In addition, steady state errors occur in all the results shown in Figs. 4-6–4-8. Steady state errors are caused by disturbance acting on the tip position such as frictions included in linear slider. The steady state errors can be compensated by using a disturbance obsever proposed in Chapter 7.

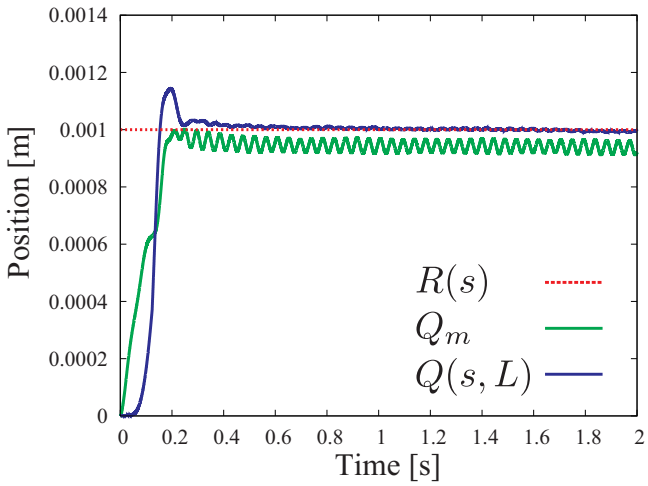

Fig. 4-7: Experimental results of by conventional reflected wave rejection ($\alpha = 0$).

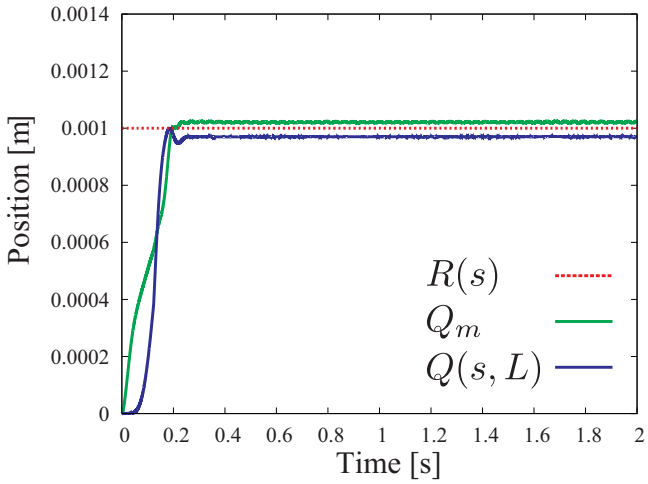

Fig. 4-8: Experimental results of by reflected wave rejection with fractional order low-pass filter.

4.3 Reflected Wave Rejection Considering Mass on Tip Position

4.3.1 Modeling of Resonant System Considering Mass on Tip Position

This part describes the modeling of the resonant system considering mass on tip position. The resonant system dealt with in this part is shown in Fig. 4-9. In Fig. 4-9, q_m, $q(t, x)$, L, M, and M_l stand for the motor position (angle), the position at $x = L$, the length of the flexible arm, the motor mass, and the tip mass, respectively. The resonant system shown in Fig. 4-9 represents the flexible arm mounted on the

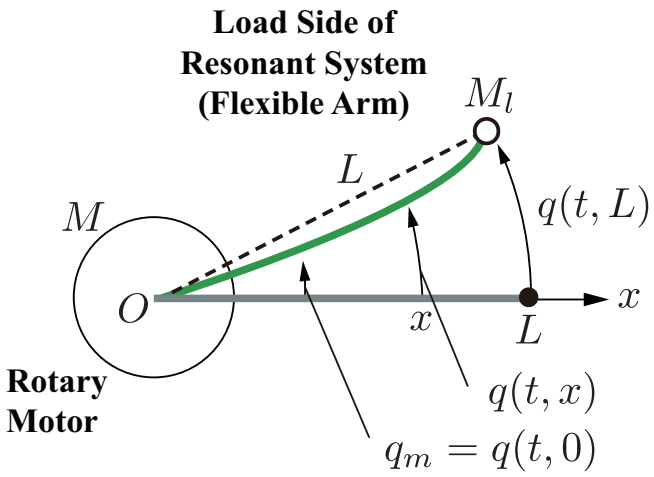

Fig. 4-9: Resonant system modeled as wave equation considering tip mass.

rotary motor. The motor position q_m and the tip position $q(t, L)$ are measurable variables. The control objective is a position control of tip angle $q(t, L)$ without the residual vibrations caused by its flexible mechanism.

The wave equation for the system dealt with in this part is same as (2.24), but the boundary conditions for Fig. 4-9 are different. The boundary conditions for the resonant system considering mass are represented as follows,

$$Q(s, 0) = Q_m \tag{4.24}$$

$$\frac{\partial Q(s, L)}{\partial x} = -\frac{M_l}{\kappa} s^2 Q(s, L) \tag{4.25}$$

where M_l and κ represent the tip mass and the stiffness per unit length, respectively. Eq. (4.24) represents that the motor implementing the DOB is mounted on $x = 0$. On the other hand, (4.25) means that the tip mass is mounted on $x = L$. The general solution of wave equation is derived as

$$Q(s, x) = C_1 e^{\frac{xs}{c}} + C_2 e^{-\frac{xs}{c}} \tag{4.26}$$

where C_1 and C_2 stand for the integral constants which are determined by the boundary conditions. By using the boundary conditions (4.24) and (4.25), the transfer function from Q_m to $Q(s, x)$ can be derived as follow,

$$\frac{Q(s, x)}{Q_m} = \frac{e^{-\frac{x}{c}s} + H(s) e^{-\frac{2L-x}{c}s}}{1 + H(s) e^{-\frac{2L}{c}s}} \tag{4.27}$$

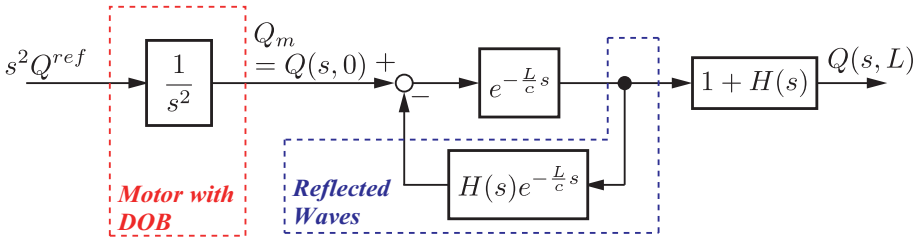

Fig. 4-10: Block diagram of wave system considering tip mass.

where

$$H(s) = \frac{1 - \frac{M_l c}{\kappa}s}{1 + \frac{M_l c}{\kappa}s}. \tag{4.28}$$

By substituting $x = L$ to (4.28), a transfer function is derived as

$$\frac{Q(s,L)}{Q_m} = \frac{(1 + H(s))e^{-\frac{L}{c}s}}{1 + H(s)e^{-\frac{2L}{c}s}}. \tag{4.29}$$

From (4.29), it turns out that the denominator of transfer function includes the time-delay elements. Therefore, the residual vibrations on the response of $Q(s,L)$ occur due to phase lag induced by time delays. The block diagram of the resonant system is shown in Fig. 4-10. In Fig. 4-10, the enclosed part denotes the wave reflected at $x = L$. $1 + H(s)$ means that the superposition of the wave traveling from $x = 0$ and the wave reflected at $x = L$. Then, the reflected wave moves to $x = 0$, which is described by a negative feedback in Fig. 4-10. Because the negative feedback makes the system vibrate, vibrations are suppressed by eliminating the reflected wave.

The typical reflected wave rejection described in Chapter 3 deals with the wave equation without considering the tip mass, which is equivalent to (4.29) with $M_l = 0$ (i.e. $H(s) = 1.0$). In that case, because the characteristic equation represents $1 + e^{-2\frac{L}{c}s} = 0$, the poles of the wave equation are derived as $s = \frac{c}{2L}(2n-1)\pi j$. Therefore, the conventional method can be only applied for the plant whose the poles are located on imaginary axis at regular intervals. In the proposed approach, the restriction can be removed by considering the effect of tip mass $H(s)$.

4.3.2 Vibration Control Based on Reflected Wave Rejection Considering Mass on Tip

Reflected Wave Rejection Considering Mass on Tip

In this part, a novel reflected wave rejection for the plant shown in Fig. 4-10 which includes the effect of tip mass. Firstly, the transfer function (4.29) from the motor position Q_m to the tip position $Q(s,L)$

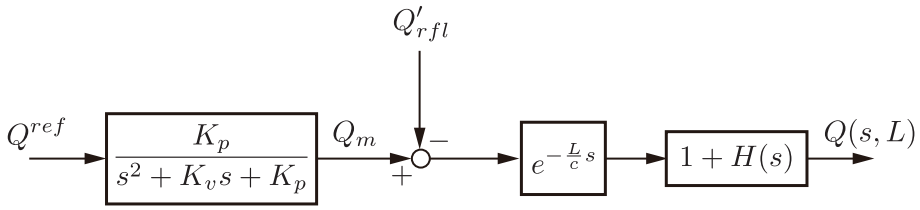

Fig. 4-11: Block diagram of resonant system with reflected wave.

is transformed into

$$(1+H(s)e^{-\frac{2L}{c}s})Q(s,L) = (1+H(s))e^{-\frac{L}{c}s}Q_m. \tag{4.30}$$

Then, (4.30) is transformed into

$$\begin{aligned} Q(s,L) &= e^{-\frac{L}{c}s}\left[(1+H(s))Q_m - H(s)e^{-\frac{L}{c}s}Q(s,L)\right] \\ &= e^{-\frac{L}{c}s}\left[(1+H(s))Q_m - Q'_{rfl}\right] \end{aligned} \tag{4.31}$$

where Q'_{rfl} denotes the reflect wave going back to $x = L$, which is defined as

$$Q'_{rfl} = H(s)e^{-\frac{L}{c}s}Q(s,L). \tag{4.32}$$

The block diagram of the resonant system with the reflected wave Q'_{rfl} is shown in Fig. 4-11. In this dissertation, to reject the reflected wave, the positive feedback of reflected wave, which is equivalent to feedforward compensation, is conducted. In order to conduct the compensation, the reflected wave is obtained as follows,

$$\hat{Q}'_{rfl} = H_n(s)e^{-\frac{L_n}{c_n}s}Q(s,L) \tag{4.33}$$

where subscript $_n$ denotes the nominal value preliminarily identified. By using the above reflected wave, the feedforward compensation of reflected wave is conducted as shown in Fig. 4-12. In Fig. 4-12, g_r and $R(s)$ stand for cut-off frequency of the low-pass filter and the position command, respectively. $F_1(s)$ and $F_2(s)$ denote the filters which make $1/(1+H(s))$ and an inverse system of position controlled-motor be proper transfer function. Because $1+H(s)$ and the inverse system are first-order and second-order transfer functions respectively, $F_1(s)$ and $F_2(s)$ are selected as first-order and second-order low-pass filters which are represented as

$$F_1(s) = \frac{g_f}{s+g_f} \tag{4.34}$$

$$F_2(s) = \frac{g_r^2}{s^2+2g_rs+g_r^2} \tag{4.35}$$

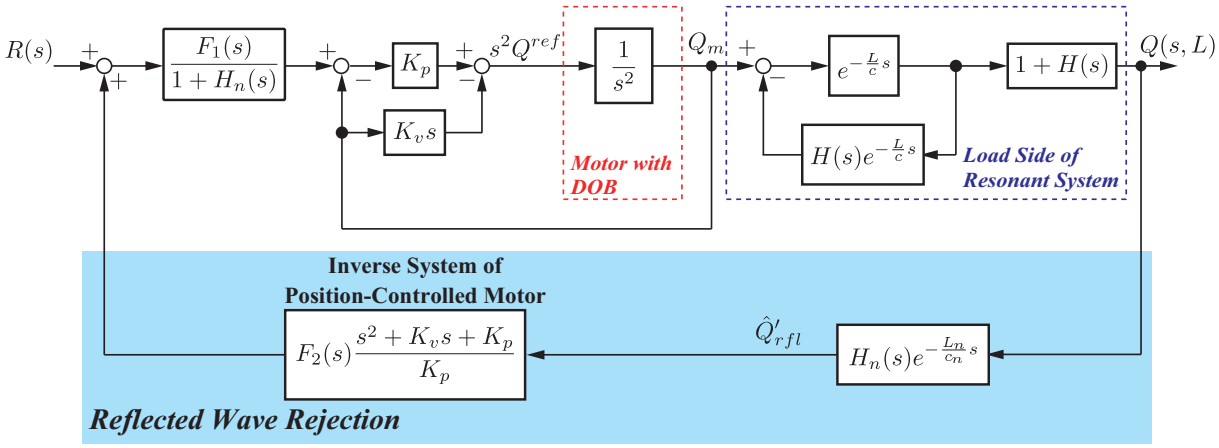

Fig. 4-12: Whole block diagram of semi-closed-loop control with reflected wave rejection considering mass on tip.

where g_f and g_r denote the cut-off frequencies. The compensation value Q_{rfl}^{comp} for the reflected wave rejection is calculated as

$$Q_{rfl}^{comp} = F_2(s)\frac{s^2+K_vs+K_p}{K_p}\hat{Q}'_{rfl}. \tag{4.36}$$

Finally, the acceleration reference which is input to the motor with DOB is represented as

$$s^2Q^{ref} = K_p\left[\frac{F_1(s)}{1+H_n(s)}(R(s)+Q_{rfl}^{comp})-Q_m\right]-K_vQ_m. \tag{4.37}$$

In Fig. 4-12, transfer function from the position command $R(s)$ to the tip position $Q(s,L)$ is derived as

$$\frac{Q(s,L)}{R(s)} = \frac{K_pe^{-\frac{L}{c}s}}{s^2+K_vs+K_p}\frac{F_1(s)}{1+H(s)e^{-\frac{2L}{c}s}(1-F_1(s)F_2(s))}. \tag{4.38}$$

If the cut-off frequencies of the low-pass filters equal to enough high value (i.e. $F_1(s),\ F_2(s)\to 1$), the transfer function represented as (4.38) becomes as follows,

$$\frac{Q(s,L)}{R(s)} = \frac{K_pe^{-\frac{L}{c}s}}{s^2+K_vs+K_p}. \tag{4.39}$$

From (4.39), it is found that, because there is no time delay in denominator of the transfer function, the residual vibrations caused by the mechanical resonances are suppressed if gains K_p and K_v are set so as to be stable.

Fig. 4-13 shows a bode diagram of closed-loop transfer function represented as (4.38) when the cut-off frequency g_r in $F_2(s)$ is varied. In calculation of the bode diagram, K_p, K_v, g_f, M_l, and L/c set

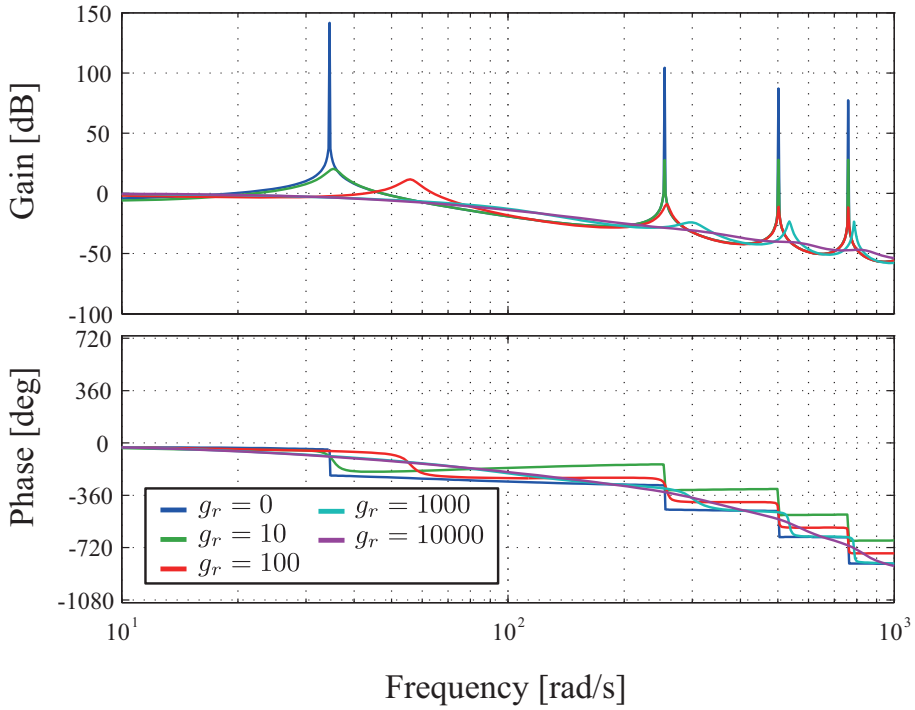

Fig. 4-13: Bode diagram of transfer function from position command $R(s)$ to tip position $Q(s, L)$ when the cut-off frequency g_r in $F_2(s)$ is changed.

2500 1/s^2, 100 1/s, 10000π rad/s, 0.0181 kgm^2, and 0.0126 s, respectively. In this case, the first, second, third resonant frequencies are 34.5, 254.0, and 502.0, respectively. If the cut-off frequency g_r equals to 0, in other words, the reflected wave is not compensated at all, it can be observed that there are some resonances. On the other hand, if the g_r set higher value, the resonance peak is gradually suppressed.

Here, the effect of the reflected wave rejection is analyzed from a control-theory point of view as well as that in Chapter 3. A main compensator of the reflected wave rejection considering mass on tip is represented as

$$\text{Main Comp.} = \frac{H_n(s)}{1 + H_n(s)} e^{-\frac{L_n}{c_n} s}. \tag{4.40}$$

It is noted that, in the derivation of (4.40), the filters $F_1(s)$ and $F_2(s)$ equal to 1 for the sake of simplicity. Bode diagram of the main compensator (4.40) is shown in Fig. 4-14. In Fig. 4-14, a nominal propagation of wave in the reflected wave rejection without considering effect of mass is determined according to (3.9) (i.e. $T_{wn} = \pi/(2\tilde{\omega}_1)$). As for the proposed reflected wave rejection, the nominal parameter is determined by a identification method described in a next part. From Fig. 4-14, phase-lead effect with 90 degree is realized for the first-order resonance by both methods. However, phase-lag effect with 90 degree

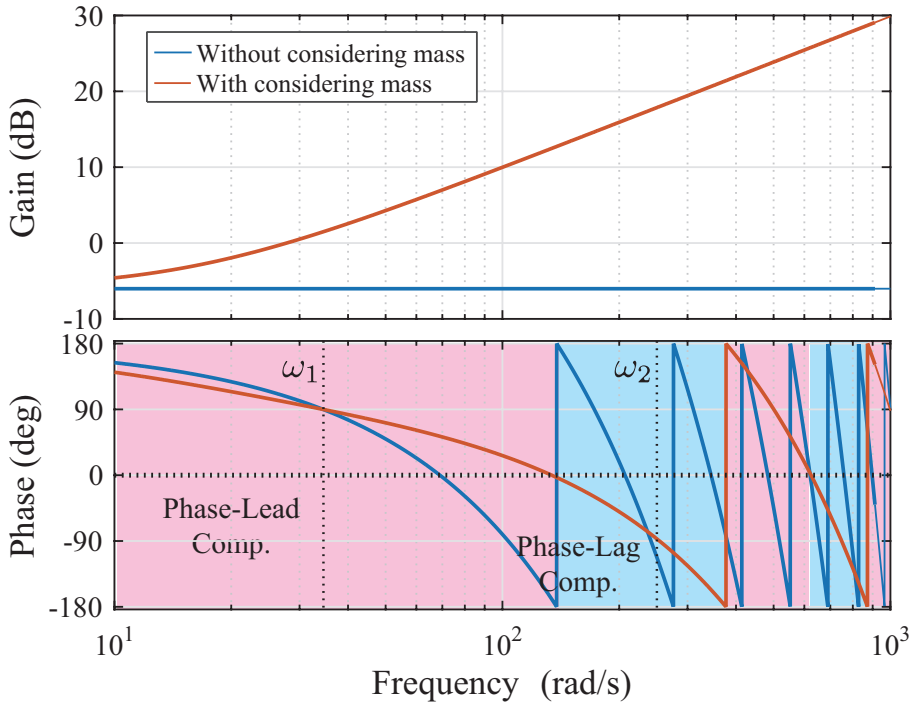

Fig. 4-14: Bode diagram of the main compensator of reflected wave rejection considering mass on tip.

is not achieved for the second-order resonance by the typical reflected wave rejection because the typical reflected wave rejection has a restriction of location of resonant frequencies: the resonant frequencies are located on imaginary axis at a regular intervals. In contrast, the reflected wave rejection considering mass on tip can realize phase-lag effect with 90 degree for the second-order resonant frequency. In addition, frequency region having phase-lag effect becomes wider than that of typical reflected wave rejection. Hence, the robustness against variation of the resonant frequency improves.

Identification of Plant Parameters

For the implementation of the proposed method shown in Fig. 4-12, it is needed to set some nominal values: the transfer function related to the tip mass $H_n(s)$, the propagation time of the wave L_n/c_n. In this part, a simple identification method of those parameters is introduced.

In this dissertation, the open-loop transfer function of wave system is used for the identification. The

open-loop transfer function is represented as

$$\begin{aligned} G_o &= H(s)e^{-\frac{2L}{c}s} \\ &= \frac{1-T_l s}{1+T_l s}e^{-2T_w s} \end{aligned} \tag{4.41}$$

where $T_l = cM/\kappa$ and $T_w = L/c$ are set for the sake of simplicity. If T_l and T_w are identified, the proposed method can be implemented. Frequency response of the open-loop transfer function G_o is described as

$$|G_o| = 1 \tag{4.42}$$

$$\angle G_o = -\left[2\tan^{-1}(T_l\omega) + 2T_w\omega\right]. \tag{4.43}$$

Focusing on the phase characteristics (4.43), because the phases when first-resonance and second-resonance occur equal to $-\pi$ and -3π rad, the following equations can be obtained as

$$-\left[2\tan^{-1}(T_l\omega_1) + 2T_w\omega_1\right] = -\pi \tag{4.44}$$

$$-\left[2\tan^{-1}(T_l\omega_2) + 2T_w\omega_2\right] = -3\pi \tag{4.45}$$

where ω_1 and ω_2 are first- and second-resonant frequencies which are preliminary identified. By numerically solving (4.44) and (4.45) with respect to T_l and T_w, the nominal values of T_{ln} and T_{wn} can be obtained. Finally, the identification is summarized as following steps.

(1) Identifying first- and second-resonant frequencies ω_1 and ω_2

(2) Numerically solving (4.44) and (4.45) with respect to T_l and T_w

4.3.3 Experiments

Experimental Setup

To verify the effectiveness of the proposed method, the experiments on position control of flexible arm are performed. Experimental setup is same system as shown in Fig. 3-15. The flexible arm is mounted on the direct drive rotary motor with the encoder (resolution: 2^{20} pulse/rev). The tip position $q(t, L)$ is obtained by the position sensitive detector (PSD) produced by Hamamatsu Photonics K.K. The PSD detects the position of the irradiation point which is generated by the laser diode mounted on the tip position ($x = L$) and output analog voltage in proportional to the position. The analog voltage is measured by A/D converter board. The real-time control system is realized by Linux OS with RTAI 3.7.

Table 4.2: Experimental parameters for control with reflected wave rejection considering mass.

Parameter	Description	Value
T_s	Sampling time	50 μs
K_{tn}	Nominal torque coefficient	1.18 N/A
M_n	Nominal motor mass	0.245 kgm^2
$\tilde{\omega}_1$	First-order resonant frequency	35.3 rad/s
$\tilde{\omega}_2$	Second-order resonant frequency	250.0 rad/s
K_p	Proportional gain	ω_n^2
K_d	Differential gain	$4\omega_n$
g_{pd}	Cut-off frequency of pseudo derivation	2000.0 rad/s
g_{dis}	Cut-off frequency of disturbance estimation observer	1000.0 rad/s
g_f	Cut-off frequency of filter $F_1(s)$	62832.0 rad/s
g_r	Cut-off frequency of filter $F_2(s)$	200.0 rad/s
T_{wn}	Nominal propagation time	0.0128 s
T_{ln}	Time constant of $H(s)$	0.02 s

The experimental parameters are shown in Table 4.2. The first- and second-order resonant frequencies are identified by sweep test. According to the resonant frequencies ω_1 and ω_2, the control parameters T_{ln} and T_{wn} are derived as 0.0582 s and 0.0128 s. However, considering the phase lag of the filter $F_2(s)$ (cut-off frequency is g_r), the parameter T_{ln} is modified from 0.0582 s to 0.02 s.

In the experiments, performance of the proposed method is compared with that of the typical reflected wave rejection described in Chapter 3. The nominal propagation time of the wave is set $T_{wn} = \pi/(2\omega_1)$. The gains in the PD controller are same value as those of the proposed method.

Experimental Results

Figs. 4-15 and 4-16 show the experimental results of position responses when $\omega_n = \omega_1$. In this case, both the proposed method and resonance ratio control suppress the vibrations effectively. In both results, steady state errors are observed due to disturbance such as friction, cable stiffness for power suppy to the laser diode.

Figs. 4-17 and 4-18 show the experimental results of the position responses when the bandwidth of the

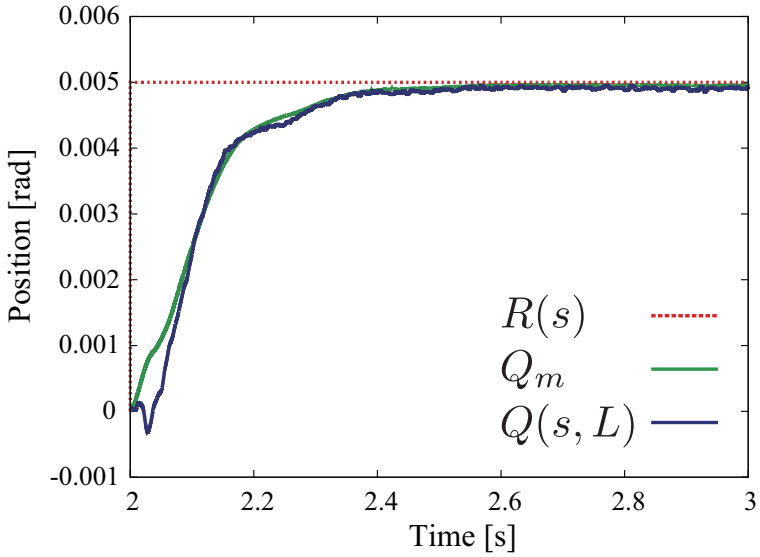

Fig. 4-15: Experimental results of the conventional reflected wave rejection ($\omega_n = \omega_1$).

controller is higher than that in Figs. 4-15 and 4-16 ($\omega_n = 2.0\omega_1$). It is found that vibrations, which is caused by second-order resonant frequency, occurs on the responses of the typical reflected wave rejction because of the restriction of the pole locations. On the other hand, Fig. 4-18 shows that the proposed method can suppress both first- and second-order resonances.

Finally, Fig. 4-19 shows the experimental results of the position responses when $\omega_n = 5\omega_1$. It turns out that both the first- and second-order resonance are well suppressed by the proposed method. In theory, the bandwidth of the position controller can increase higher value in ideal case. However, in actual case, the bandwidth of the position controller is limited by the cut-off frequencies g_r, g_f, and g_{dis}. In future work, the limitation by those cut-off frequencies will be analyzed. In addition, undershoot phenomenon can be observed in the reponses of the proposed method. The usndershoot is caused by the modeling error of the $H_n(s)$, and it can be observed cleary when the higher-bandwidth controller is used. The analysis on the undershoot will be also conducted in the future work.

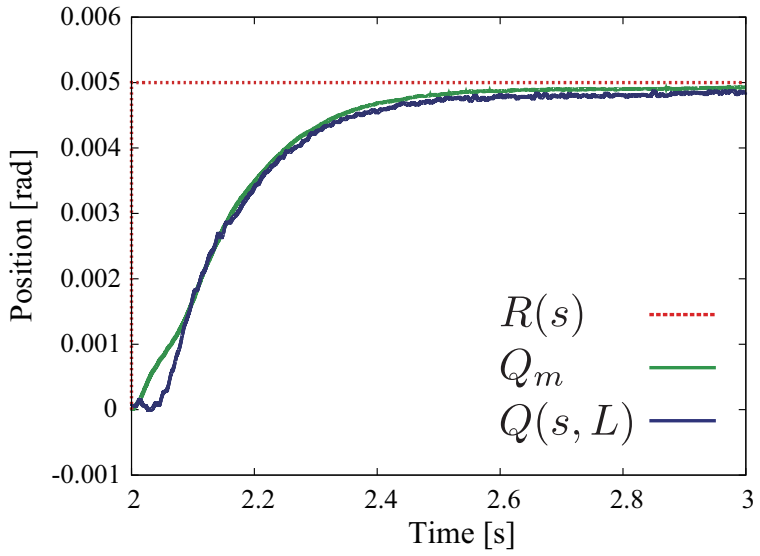

Fig. 4-16: Experimental results of the proposed reflected wave rejection ($\omega_n = \omega_1$).

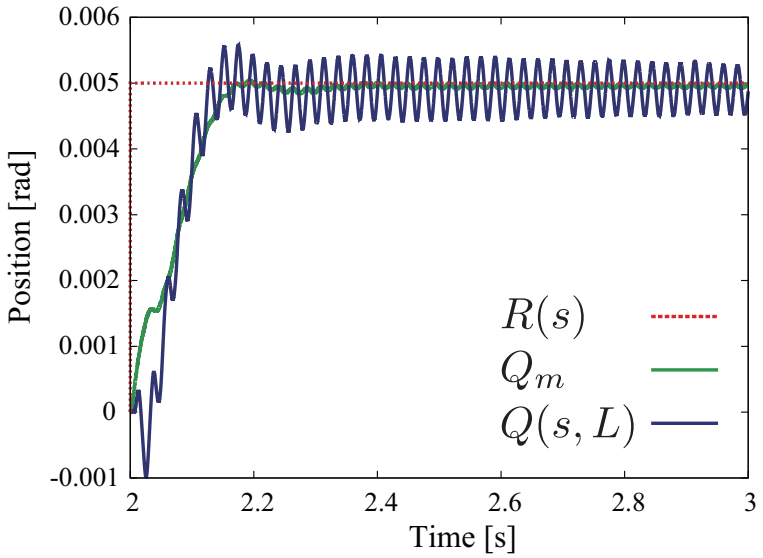

Fig. 4-17: Experimental results of the conventional reflected wave rejection ($\omega_n = 2.0\omega_1$).

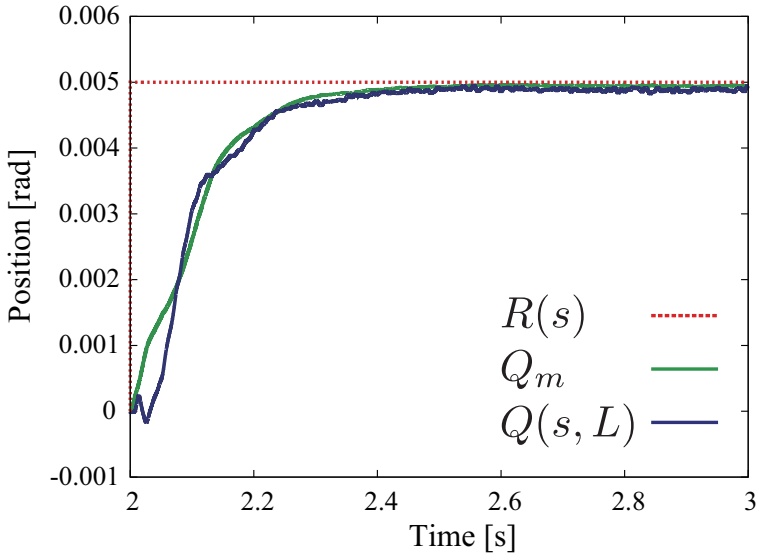

Fig. 4-18: Experimental results of the proposed reflected wave rejection ($\omega_n = 2.0\omega_1$).

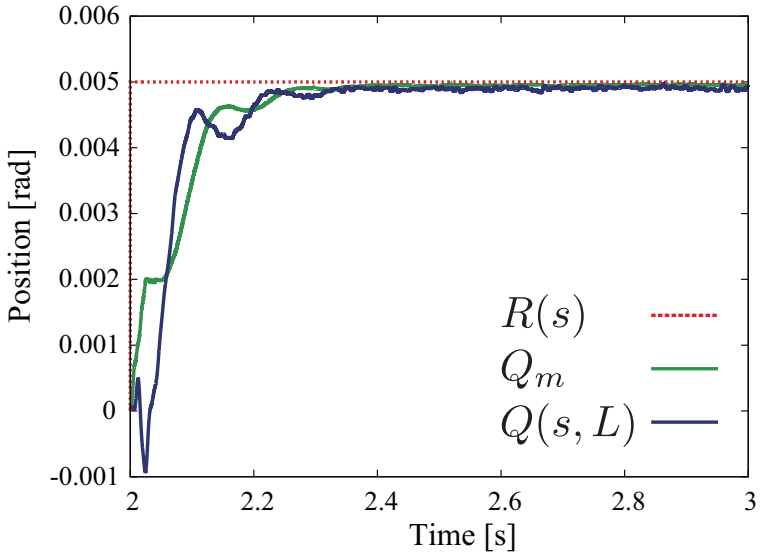

Fig. 4-19: Experimental results of the proposed reflected wave rejection ($\omega_n = 5.0\omega_1$).

4.4 Summary of Chapter 4

In this chapter, reflected wave rejections for various resonant systems based on basic concept described in previous chapter was proposed. First of all, the reflected wave rejection considering the damper effect was proposed. Transfer function of typical wave equation has restriction regarding the location of resonant poles. Consideration of damper effect alleviates the restriction, and the range of application of reflected wave rejection can be extended. It was shown how the transfer function of wave equation considering damper is expressed, which is composed of time-delay-like elements. Due to difficulty in implementation of the time-delay-like element, the reaction-force-based reflected wave rejection with fractional-order low-pass filter was proposed. Finally, the reflected wave rejection considering mass on tip was proposed. In many industrial applications, some loads are often attached to tip position. It was shown that effect of mass on tip position appears as all pass filter. The reflected wave rejection is transformed to avoid amplifying noise effect by the equivalent transfer function of reflected wave rejection including all-pass filter. As a result, the positive delay-feedback type reflected wave rejection was derived.

Chapter 5

Motion Control of Time-delay System

5.1 Introduction of Chapter 5

This chapter describes the reflected wave rejection for time-delay system. In Chapter 2, the time-delay system which includes the input-output time delay was modeled by using a wave equation. It was shown that there was a similarity between mechanical resonant system and time-delay system from the wave-transmission point of view. Chapter 3 explained how to construct the reflected wave for stabilizing the wave system. Based on the similarity between them, vibration control of resonant system based on the reflected wave rejection can be applied to time-delay system. According to the above aspect, Section 5.2 explains the reflected wave rejection for time-delay system [88]. Next, Section 5.2 describes a time-delay compensation method by an equivalent elastic force feedback [99]. Finally, Section 5.3 summarizes this chapter.

5.2 Time-delay Compensation by Reflected Wave Rejection

This part proposes a time-delay compensation based on reflected wave rejection as well as the case of resonant systems. The system dealt with in this chapter is shown in Fig. 2-8.

5.2.1 Reflected Wave Rejection in Time-delay System

In Chapter 2, the wave representation of time-delay system was derived and it was explained that Fig. 2-10 is an generalized structure of the wave system. Therefore, it is possible to suppress the vibra-

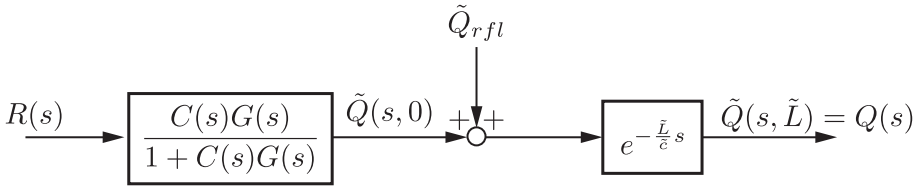

Fig. 5-1: Equivalent transformed block diagram of Fig. 2-9 by using reflected wave.

tions or to make the system stable by using reflected wave rejection as well as that in the resonant system as shown in Chapters 3 and 4.

Before explaining how to eliminate a reflected wave, the reflected wave in the time-delay system is derived. The reflected wave is shown in the enclosed part by green-dashed line in Fig. 2-10. It is possible to derive the reflected wave in time-delay system. The transfer function (2.50) is transformed into a following equation,

$$\tilde{Q}(s,\tilde{L}) = e^{-\frac{\tilde{L}}{\tilde{c}}s}\left(\tilde{Q}(s,0) + \tilde{Q}_{rfl}\right) \tag{5.1}$$

where $\tilde{Q}_{rfl}$ denotes the reflected wave defined in time-delay system, and it is represented as

$$\tilde{Q}_{rfl} \;=\; C(s)G(s)\tilde{Q}(s,0) - C(s)G(s)e^{-\frac{\tilde{L}}{\tilde{c}}s}\tilde{Q}(s,\tilde{L}) \tag{5.2}$$

Fig. 5-1 shows the equivalent block diagram of time-delay system by using the reflected wave. If the reflected wave is eliminated, the transfer function from $R(s)$ to $\tilde{Q}(s,L)$ is represented as

$$\frac{\tilde{Q}(s,\tilde{L})}{R(s)} = \frac{C(s)G(s)e^{-\frac{\tilde{L}}{\tilde{c}}}}{1+C(s)G(s)}. \tag{5.3}$$

From (5.3), the system is stable because there is no time delay in the denominator of transfer function. Therefore, it is found that the reflected wave rejection achieves time-delay compensation as well as the case of the resonant system described in Chapter 3.

In order to eliminate the reflected wave, a feedforward compensation of reflected wave is conducted in this dissertation, and it is shown in Fig. 5-2. In Fig. 5-2, $\tilde{Q}_{rfl}^{cmp}$ denotes the compensation value for eliminating reflected wave. The compensation value is calculated as

$$\tilde{Q}_{rfl}^{cmp} \;=\; \frac{1+C(s)G_n(s)}{C(s)G_n(s)}\tilde{Q}_{rfl}. \tag{5.4}$$

In this dissertation, it is assumed that there is no modeling error in the plant model $G_n(s)$. In this case, by using (2.40) and (2.41), the compensation value of the reflected wave is simplified as

$$\tilde{Q}_{rfl}^{cmp} \;=\; C(s)G_n(s)R(s) - \left(1+C(s)G_n(s)\right)e^{-Ts}Q(s) \tag{5.5}$$

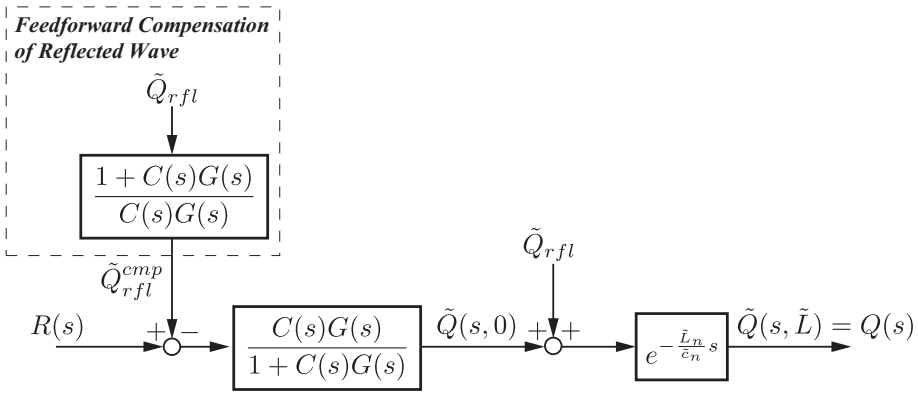

Fig. 5-2: Feedforward compensation of reflected wave in time-delay system.

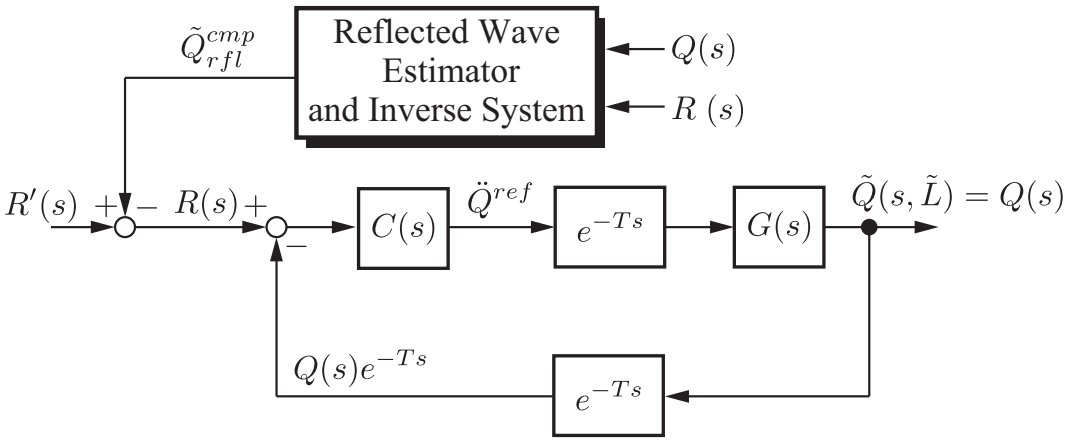

Fig. 5-3: Block diagram of the proposed time-delay compensation method by using reflected wave rejection.

where $T = \tilde{L}/\tilde{c}$. The acceleration reference which is sent to the remote side is calculated as

$$\ddot{Q}^{ref} = C(s)\left(R'(s) + \tilde{Q}^{cmp}_{rfl} - e^{-Ts}Q(s)\right). \tag{5.6}$$

The block diagram of time-delay compensation based on the reflected wave rejection is shown in Fig. 5-3. In Fig. 5-3, $R'(s)$ denotes the position command and the block of "reflected wave estimator and inverse system" means (5.5). It is noted that the reflected wave rejection for the time-delay system considers only input-output time delays, but it does not consider packet loss and jitter appearing in a communication system. Hence, under existence of these phenomena, performance of the proposed method degrades.

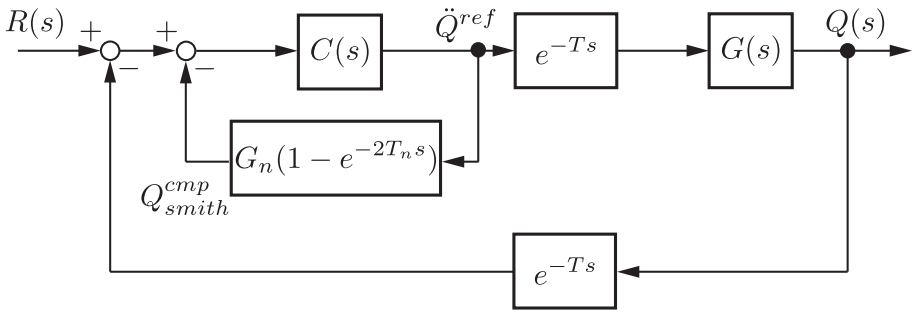

Fig. 5-4: Block diagram of Smith predictor.

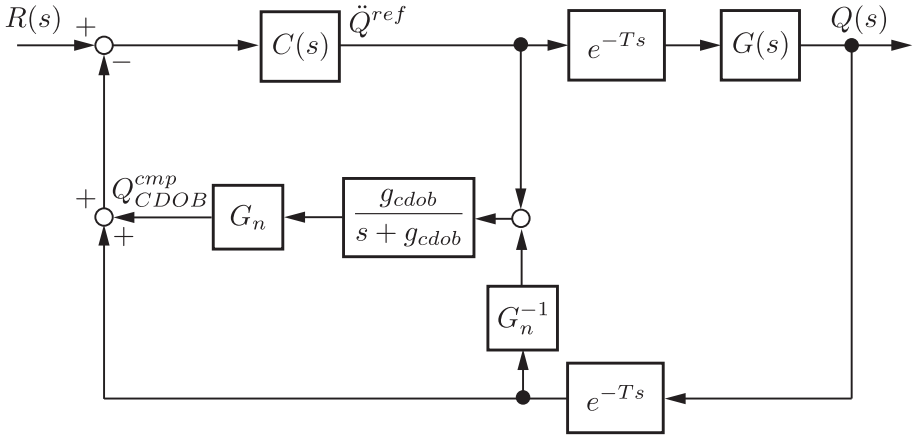

Fig. 5-5: Block diagram of communication disturbance observer.

5.2.2 Relation between the Proposal and Typical Time-delay Compensation

Lastly, relation between the proposed method and typical time-delay compensation methods, such as Smith predictor and a communication disturbance observer, is explained. The block diagrams of Smith predictor and a communication disturbance observer are shown in Figs. 5-4 and 5-5, respectively. The compensation value generated by the Smith predictor is represented as

$$\begin{aligned} Q^{cmp}_{smith} &= G_n(s)(1-e^{-2T_n s})\ddot{Q}^{ref} \\ &= C(s)G_n(s)R(s) - (1+C(s)G_n(s))\,e^{-Ts}Q(s) \\ &= \tilde{Q}^{cmp}_{rfl}. \end{aligned} \tag{5.7}$$

In the above transformation, the transfer function represented as (2.40) and $\ddot{Q}^{ref} = C(s)(R(s) - e^{-Ts}Q(s))$ are used. On the other hand, the compensation value generated by the communication dis-

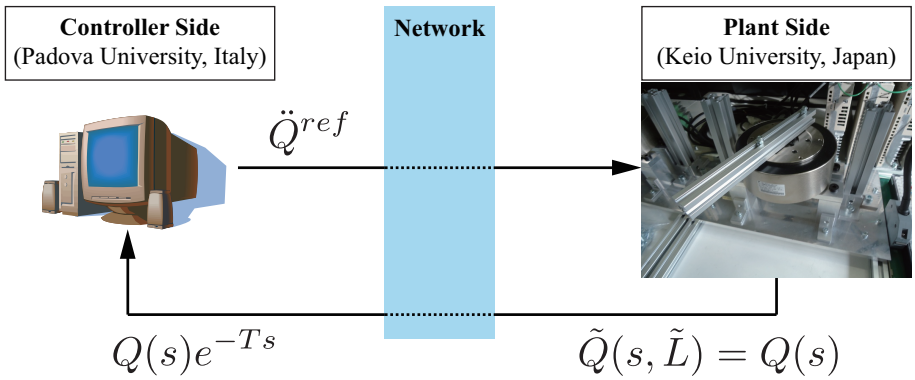

Fig. 5-6: Experimental setup.

turbance observer is represented as

$$\begin{aligned} Q_{CDOB}^{cmp} &= \frac{g_{cdob}}{s+g_{cdob}} G_n(s)(\ddot{Q}^{ref} - G_n^{-1}(s)Q(s)e^{-Ts}) \\ &= \frac{g_{cdob}}{s+g_{cdob}} \left[C(s)G_n(s)R(s) - (1+C(s)G_n(s))\, e^{-Ts}Q(s)\right] \\ &\approx \tilde{Q}_{rfl}^{cmp}. \end{aligned} \tag{5.8}$$

In the above transformation, $\ddot{Q}^{ref} = C(s)(R(s) - e^{-Ts}Q(s))$ is used. Additionally, the cut-off frequency of the communication disturbance observer assumes enough high value. It is noted that, in the transformations, the modeling error is neglected (i.e. $T = T_n$ and $G(s) = G_n(s)$) and a disturbance is also neglected. From (5.7) and (5.8), it turns out that the compensation value of the proposed method (5.5) are same as those of (5.7) and (5.8). Therefore, it implies that physical meanings of Smith predictor and communication disturbance observer are elimination of reflected wave from the time-delay system as well as the reflected wave rejection. It is noted that the above mention is correct under no existence of disturbance and modeling error. The difference among those methods is models and variables used in generation of the compensation values. The fact is related to trade off between disturbance suppression performance and sensitivity of jitter effect. For example, the communication disturbance observer has low-sensitivity against jitter because time-delay model is not used. However, the disturbance suppression performance is the worst in three methods.

Table 5.1: Experimental parameters for control with reflected wave rejection for time-delay system.

Parameter	Description	Value
T_s	Sampling time	1.0 ms
K_{tn}	Nominal torque coefficient	1.18 N/A
J_n	Nominal inertia	0.0028 kg
K_p	Proportional gain	2500
K_d	Differential gain	100
g_{pd}	Cut-off frequency of pseudo derivation	500 rad/s

5.2.3 Experiment

Experimental Setup

In order to confirm the validity of the proposed method, experiment of position control with communication delay is conducted. The experimental setup is shown in Fig. 5-6. The position controller implemented in the real-time computer is located at Italy, and generates the acceleration reference $\ddot{Q}^{ref}$. On the other hand, the plant is located at Japan, which is a one-link serial manipulator which is composed of a direct drive motor with an encoder and a link. The position of the motor is obtained by the encoder (resolution capability: 260000 pulse/rev). This manipulator is controlled via a communication system which is constructed by User Datagram Protocol (UDP). The sending period of data is set as 1.0 ms as same as the sampling period. As result of using $ping$ command, packet loss rate is 0.05 % when 10000 packet is sent to remote side. Moreover, a real-time control is realized by Linux 2.6.32.11 with real-time application interface (RTAI 3.8.1).

The experimental parameters used in this experiment are shown in Table 5.1. Each gain is set so that characteristic equation $1 + C(s)G(s)$ has multiple roots which are located on a real axis. For decreasing noise effect, the pseudo differential which has the cut-off frequency g_{pd} is used for calculating the acceleration reference in the PD controller. The position command is set as a step command and it is applied at $t = 5.0$.

Experimental Results

First of all, Fig. 5-7 shows the response of round-trip time delay ($2T$) measured by using time stamp. The time delay means the total time delay which includes the communication, sensing, and processing

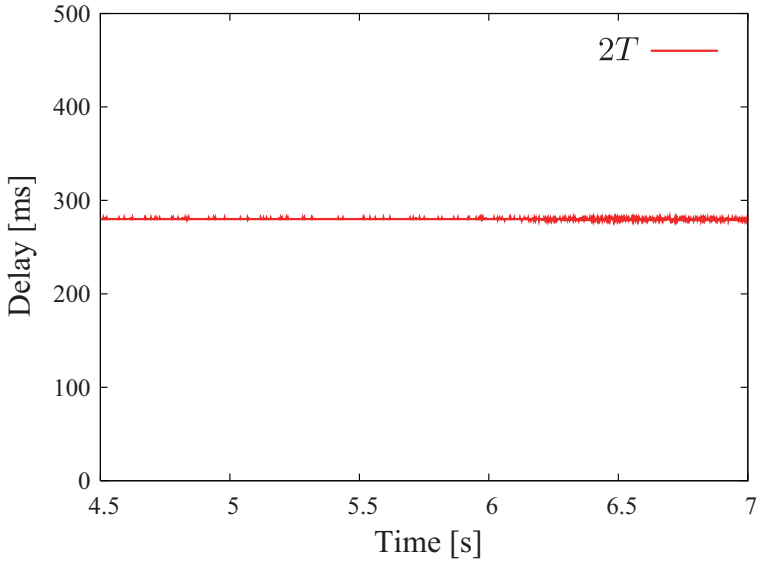

Fig. 5-7: Measured round trip delay by using time stamp.

delays. As a result, it is found that the mean value and standard deviation of round-trip time delay are 291 ms and 0.5 ms, respectively. Hence, in this experiment, the time delay can be regarded as constant time delay.

Experimental results of position response by using the reflected wave rejection are shown in Fig. 5-8. From Fig. 5-8, it turns out that the controlled system is kept stable by the reflected wave rejection. Steady state error is observed because the plant includes the Coulomb and viscous frictions. To improve the steady state characteristic, it is possible to use the disturbance observer for time-delay system [82].

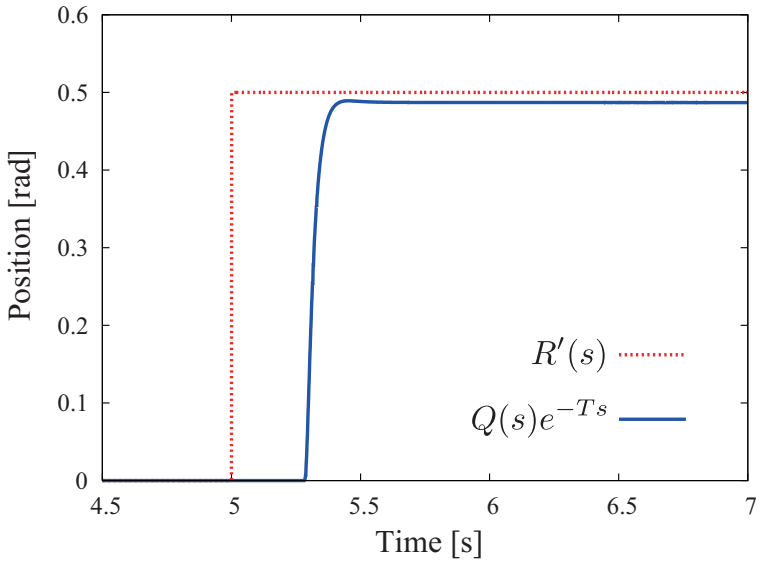

Fig. 5-8: Experimental results of position control with reflected wave rejection.

5.3 Equivalent Elastic Force Feedback in Time-delay System

5.3.1 Feedback of Equivalent Elastic Force

According to the wave representation of the time-delay system shown in Fig. 2-10, it is found that the position-transmission system is not affected by the wave-transmission system at all. Hence, it is interpreted that vibration or destabilization are caused by the robustness of the position-input system against the wave-transmission system. This aspect comes from vibration control of the resonant system. In general, the load position of a two-mass resonant system becomes vibrating when the mass of the motor is greater than the mass of the load [54]. In particular, if the motor implements a disturbance observer, the vibration occurs heavily on the load side because the equivalent mass against the reaction force becomes infinity. Resonance ratio control [49], which is a vibration-control method for a two-mass resonant system, introduces reaction-force feedback to reduce the equivalent mass of the motor against the reaction force from the resonant system. As a result, the vibration is suppressed effectively by the velocity feedback. Here, this concept of resonance ratio control is applied to the time-delay system.

Firstly, the deformation in the wave system is derived to define the elastic force in time-delay system. The deformation is represented as the partial differentiation of the position $\tilde{Q}(s,x)$ with respect to x:

$$\frac{\partial \tilde{Q}(s,x)}{\partial x} = \frac{-s}{\tilde{c}} \frac{e^{-\frac{x}{\tilde{c}}s} - C(s)G(s)e^{-\frac{2\tilde{L}-x}{\tilde{c}}s}}{1 + C(s)G(s)e^{-2\frac{\tilde{L}}{\tilde{c}}s}} \tilde{Q}(s,0). \tag{5.9}$$

By using the above equation and the equivalent stiffness $\tilde{\kappa}$, the elastic force at x is derived as

$$\tilde{F}^{reac}(s,x) = -\tilde{\kappa}\frac{\partial \tilde{Q}(s,x)}{\partial x}. \tag{5.10}$$

It is noted that the reason why "-1" exists in right hand of (5.10) is that the definition in sign of torsion in the wave equation, which is $\lim_{\Delta x \to 0}(Q(s,x+\Delta x) - Q(s,x))/\Delta x$, is opposite to the definition of two-mass resonant system used in [49, 50, 55–57, 59], which is motor position minus the load position. Because the position-input system is located at $x = 0$, the elastic force acting on the position-input system is derived as

$$\begin{aligned} \tilde{F}^{reac}(s,0) &= -\tilde{\kappa}\frac{\partial \tilde{Q}(s,0)}{\partial x} \\ &= \frac{s\tilde{\kappa}}{\tilde{c}} \frac{1 - C(s)G(s)e^{-\frac{2\tilde{L}}{\tilde{c}}s}}{1 + C(s)G(s)e^{-2\frac{\tilde{L}}{\tilde{c}}s}} \tilde{Q}(s,0). \end{aligned} \tag{5.11}$$

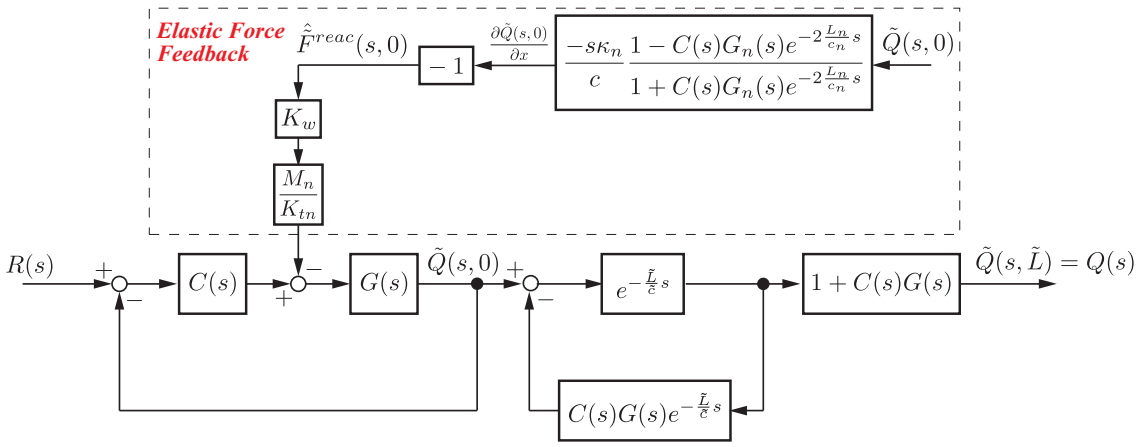

Fig. 5-9: Block diagram of elastic force feedback in time-delay system expressed as wave.

The concept diagram of the elastic force feedback for vibration suppression on time-delay system is shown in Fig. 5-9. In Fig. 5-9, K_w denotes the elastic force gain. By the feedback of the equivalent elastic force, motion equation of the input system is changed as follow,

$$s^2\tilde{Q}(s,0) = \frac{K_t}{M}\left[C(s)(R(s)-\tilde{Q}(s,0)) - \frac{M_n}{K_{tn}}K_w\tilde{F}^{reac}(s,0)\right]. \tag{5.12}$$

Therefore, an equivalent mass $\tilde{M}^{eq}$ in Fig. 5-9, which means the influence on the acceleration which is given by elastic force $\hat{\tilde{F}}^{reac}(s,0)$, is represented as

$$\tilde{M}^{eq} = \frac{1}{K_w}. \tag{5.13}$$

It can be seen that the equivalent mass equals to infinity when there is no feedback of the elastic force (K_w=0). In this case, the position-input system is robust against wave-transmission system, which results to induce the vibration. It is also found that the elastic force feedback can reduce the equivalent mass of the position-input system. Therefore, it is expected to suppress the vibration due to the time delay because robustness of the position-input system against elastic force is reduced.

There is a problem with implementing the control system shown in Fig. 5-9: it is needed to know the equivalent velocity of the wave $\tilde{c}$ and stiffness $\tilde{\kappa}$. Here, the elastic force gain is redefined as follow,

$$K_w' = K_w\frac{\tilde{\kappa}}{\tilde{c}}. \tag{5.14}$$

The gain is determined by cut and try in this dissertation. By using the above redefined elastic force gain,

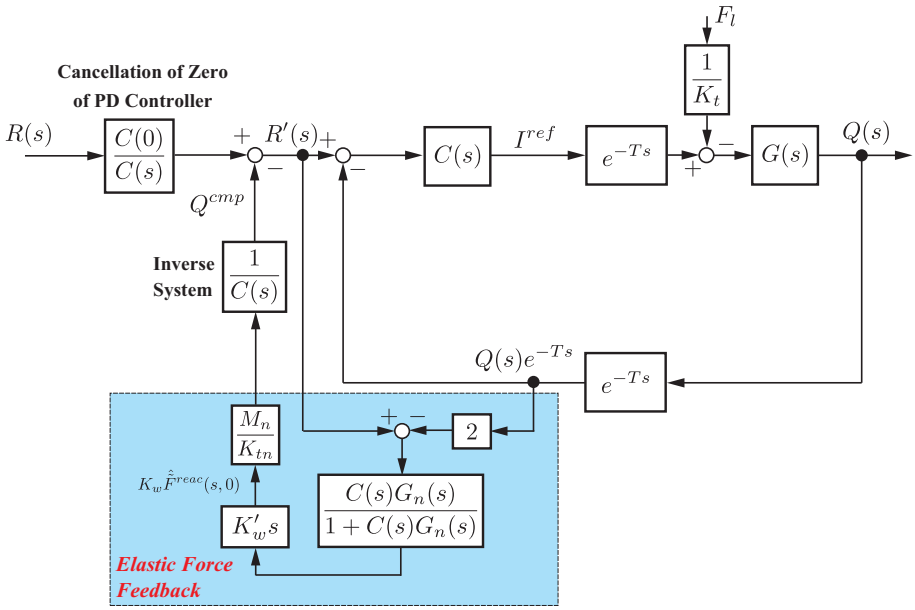

Fig. 5-10: Equivalent block diagram of elastic force feedback in time-delay system for implementation (the proposed method).

the reaction force feedback can be conducted as follows,

$$\begin{aligned} K_w\hat{\tilde{F}}^{reac}(s,0) &= K_w\frac{s\tilde{\kappa}_n}{\tilde{c}_n}\frac{1-C(s)G_n(s)e^{-\frac{2\tilde{L}_n}{\tilde{c}_n}s}}{1+C(s)G_n(s)e^{-2\frac{\tilde{L}_n}{\tilde{c}_n}s}}\tilde{Q}(s,0) \\ &= K'_w s\frac{1-C(s)G_n(s)e^{-\frac{2\tilde{L}_n}{\tilde{c}_n}s}}{1+C(s)G_n(s)e^{-2\frac{\tilde{L}_n}{\tilde{c}_n}s}}\tilde{Q}(s,0) \end{aligned} \tag{5.15}$$

where $\hat{\tilde{F}}^{reac}(s,0)$ denotes an estimated equivalent elastic force. Since $e^{-Ts}Q(s)$ can be observed at controller side, the above equation can be transformed into the following equation not including the time-delay model,

$$K_w\hat{\tilde{F}}^{reac}(s,0) = K'_w s\frac{C(s)G_n(s)}{1+C(s)G_n(s)}\left(R'(s)-2e^{-Ts}Q(s)\right) \tag{5.16}$$

where $R'(s)$ is the command including the compensation value. The block diagram of time-delay compensation based on elastic force feedback for actual implementation is shown in Fig. 5-10. In Fig. 5-10, Q^{cmp} means the compensation value including the equivalent elastic force. The compensation value Q^{cmp} for time delay is calculated as

$$Q^{cmp} = \frac{1}{C(s)}\frac{M_n}{K_{tn}}K_w\hat{\tilde{F}}^{reac}(s,0). \tag{5.17}$$

Feedback of Q^{cmp} to the position command makes a same effect as shown in Fig. 5-9. The acceleration reference which is transmitted to plant side is represented as

$$\ddot{Q}^{ref} = C(s)\left(\frac{C(0)}{C(s)}R(s) - Q^{cmp} - e^{-Ts}Q(s)\right). \tag{5.18}$$

It is noted that, in this dissertation, the zero of PD controller is canceled out by the feedforward compensator in order to improve the performance of the vibration suppression; it has the same effect as a P controller with velocity minor loop. In addition, the control gains ($K_p,\ K_d,\ K'_w$) in the proposed method have clear physical meanings. Therefore, it is expected to set those gains easily by cut and try.

5.3.2 Disturbance Suppression Performance of Proposed Method

This part explains the better point of proposed method compared with the other time-delay compensation methods. In contrast to the well-known Smith predictor [74] and communication disturbance observer (CDOB) [77], the proposed method maintains the feedback characteristics. If the nominal parameters equal to actual plant parameters, the transfer function from the disturbance F_l to position response $Q(s)$ is represented as

$$G_{FQ} = \frac{-1}{M_n}\frac{s^2 + (K_d + K'_w)s + K_p}{Den(s)} \tag{5.19}$$

where

$$\begin{aligned} Den(s) &= s^4 + (K_d + K_w)s^3 + K_p s^2 + \\ &\quad \left[K_d s^3 + (K_p + K_d^2 - K_d K_w)s^2 + (2K_p K_d - K_p K_w)s + K_p^2\right] e^{-2Ts}. \end{aligned} \tag{5.20}$$

From (5.19), it turns out that the direct-current (DC) gain of (5.19) equals to $1/(M_n K_p)$, which means that it is same disturbance suppression performance as a typical PD controller. On the other hand, with the CDOB and Smith predictor, instead of the control design that does not require to consider time delay, the feedback characteristic is removed or reduced. In other words, the DC component is removed or reduced from feedback signals by the time-delay compensation. Thus, these methods are easily affected by the disturbance such as a friction, external forces. In contrast, the proposed method does not remove the DC component of the feedback signals. Fig. 5-11 shows the bode diagram of each method regarding the closed-loop transfer function from disturbance to position. From the bode diagram, DC gains of the Smith predictor and the CDOB with low-frequency model error feedback [83] are infinite with 20 dB/dec (one pole is located at the imaginary axis), which means that steady state error does not occur

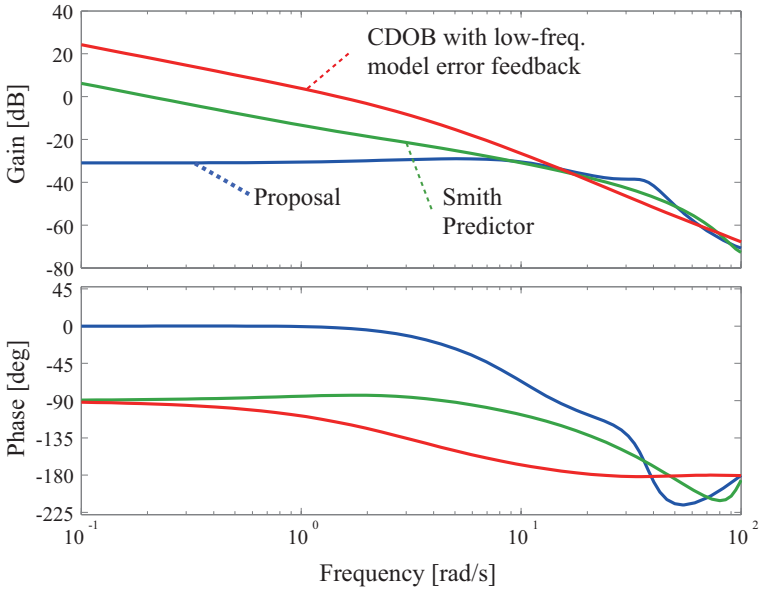

Fig. 5-11: Bode diagram of the closed-loop transfer function from disturbance to position.

Table 5.2: Simulation parameters of motor.

Parameter	Description	Value
T_s	Sampling time	0.2 ms
K_{tn}	Thrust force coefficient	2.7/0.81 N/A
M_n	Mass of motor	0.245 kg

by the impulse disturbance. On the other hand, DC gain of the proposed method equals to finite value, which means that steady state error does not occur by the impulse disturbance. It is noted that if some kinds of the disturbance observer can be implemented, steady state error does not occur by the step disturbance. Therefore, the disturbance response becomes better than that of CDOB and Smith predictor and the response at steady state is improved.

5.3.3 Simulations

To confirm the effectiveness of the proposed method, simulations of position control are conducted. Simulation parameters are shown in Table 5.2. In all the simulations, step input ($R(s) = 5.0$ mm) is applied to the control system.

Firstly, effect of elastic force feedback are confirmed. Fig. 5-12 shows the simulation results when

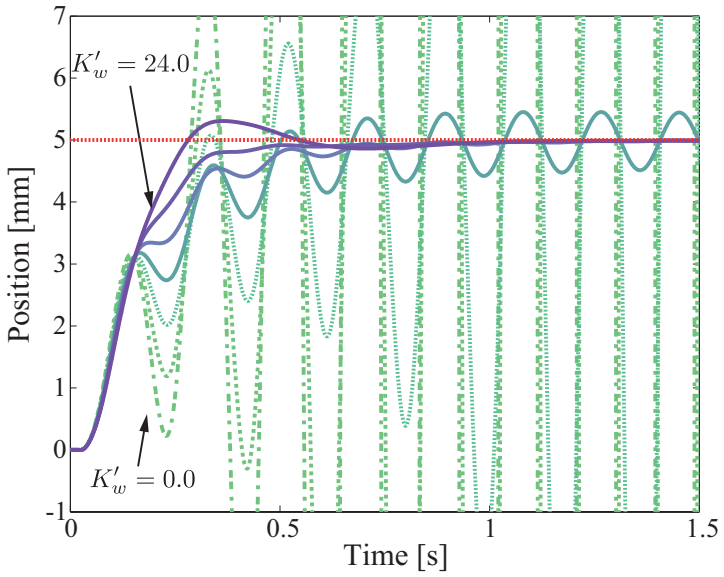

Fig. 5-12: Simulation results when K'_w changes from 0.0 to 24.0 ($2T = 50$ ms, $K_p = 144,\ K_d = 48$).

$K_p = 144$, $K_d = 48$, and K_w is varied from 0.0 to 24.0 with the step of 4.0. In this simulation, the round-trip time delay $2T$ is equal to 50 ms. When $K'_w = 0$, the response of the motor position is unstable. On the other hand, when K'_w is gradually increased, the control system is stabilized and the vibration is gradually decreased. It is confirmed that the equivalent elastic force feedback is confirmed to be effective at suppressing the vibration due to time delay. However, too much increasing K'_w makes the system unstable again. Hence, adjustment of the appropriate value of K'_w is needed.

Fig. 5-13 shows the simulation results in the case of large round-trip time delay ($2T = 200.0$ ms). In this simulation, $K_p = 16$, $K_d = 16$, and K'_w is varied from 0.0 to 9.0 with the step of 1.5. As well as Fig. 5-12, the feedback of elastic force can stabilize the system. Fig. 5-14 shows the simulation results in the case of $2T = 200.0$ ms with large controller gains ($K_p = 25$, $K_d = 20$). From Fig. 5-14, the feedback of elastic force can stabilize the system. In the case of Fig. 5-14, K'_w is varied from 9.0 to 12.0 with the step of 0.5. However, vibration still remains on the response with optimal gain. Therefore, stability region by using the elastic force feedback depends on the value of gains in the position controller.

Figs. 5-13 and 5-14 imply that the proposed method has weak points which is the variation of time delay (i.e. jitter). From the point of view of robustness against the jitter, performance of the proposed method is inferior to performance of the smith predictor and communication disturbance observer based methods. Therefore, if there exists large variation of time delay, it is needed to use some kinds of jitter

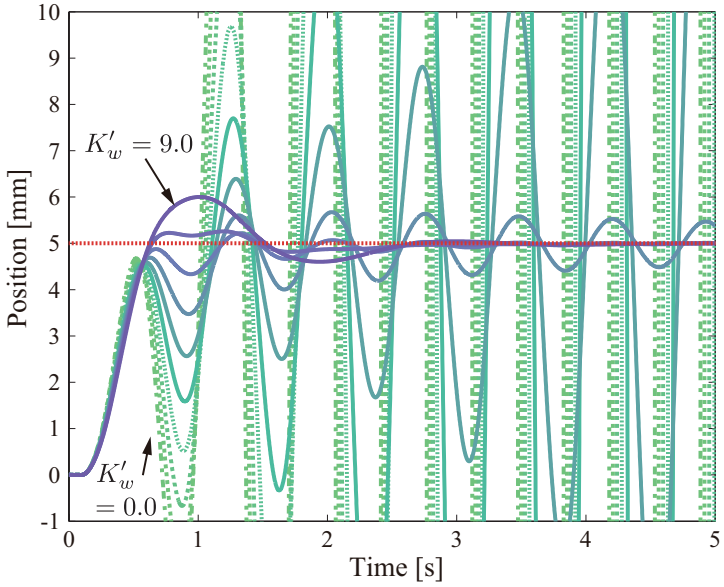

Fig. 5-13: Simulation results when K'_w changes from 0.0 to 9.0 ($2T = 200.0$ ms, $K_p = 16,\ K_d = 16$).

compensator (e.g. jitter buffer) for implementation of the proposed method.

In addition, the parameter variation in K_t and M also degrades both the control performance and the stability because the elastic force feedback gain is equivalently changed. Fig. 5-15 shows Simulation results when parameter variations $\alpha = (K_t M_n)/(K_{tn} M)$, change from 0.5 to 3.0 ($2T = 50.0$ ms, $K_p = 148,\ K_d = 48,\ K'_w$=20). Interpreting the results shown in Fig. 5-15 roughly, if α decreases, the damping ratio provided by the PD controller also decreases. On the other hand, if α increases, the damping ratio increases. However, if α increases too much, the system becomes unstable because increasing K_p and K'_w destabilizes the system. If there exists large variation in K_t and M, a compensator should be designed to maintain robust stability.

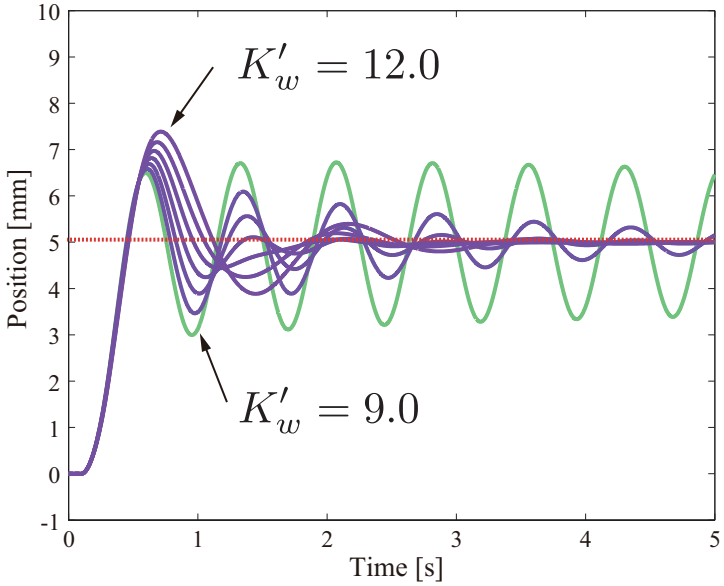

Fig. 5-14: Simulation results when K'_w changes from 9.0 to 12.0 ($2T = 200.0$ ms, $K_p = 25,\ K_d = 20$).

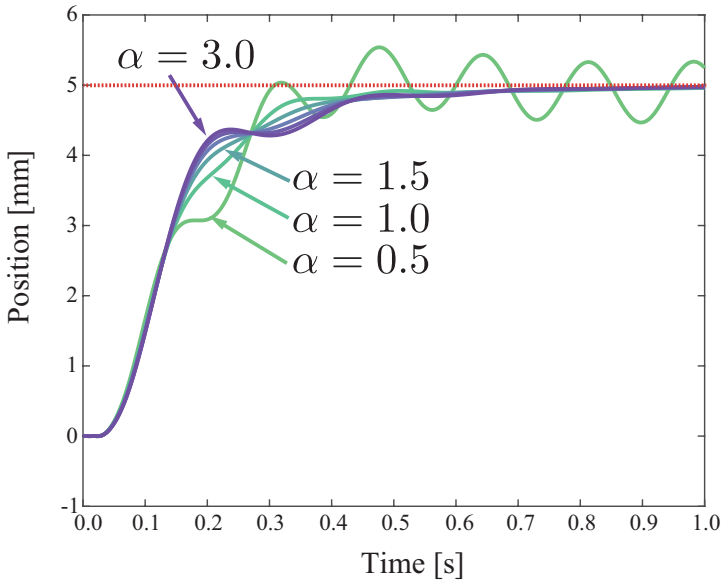

Fig. 5-15: Simulation results when parameter variations α change from 0.5 to 3.0 ($2T = 50.0$ ms, $K_p = 144,\ K_d = 48,\ K'_w$=20).

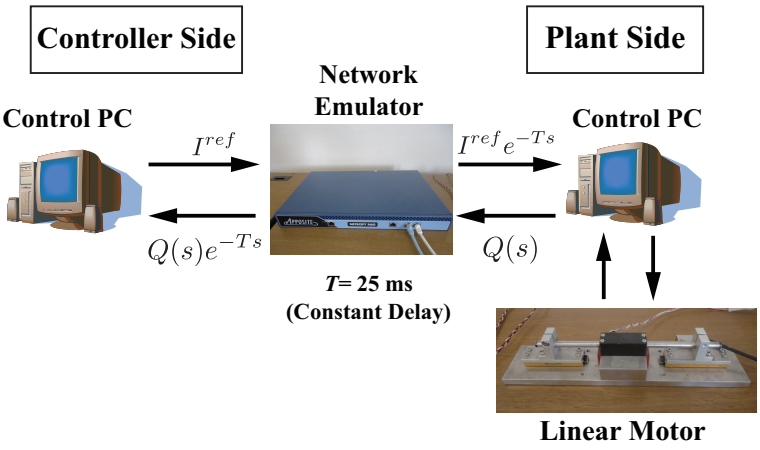

Fig. 5-16: Experimental setup for elastic force feedback in time-delay system.

Table 5.3: Experimental parameters for control with elastic force feedback in time-delay system.

Parameter	Description	Value
T_s	Sampling time	0.2 ms
K_{tn}	Nominal thrust force coefficient	2.7/0.81 N/A
M_n	Nominal mass of motor	0.245 kg
K_p	Proportional gain	144
K_d	Differential gain	48
K'_w	Elastic force gain	21.0
g_{pd}	Cut-off frequency of pseudo derivation	2000 rad/s
g_{dis}	Cut-off frequency of disturbance estimation observer	250 rad/s
$2T = \frac{2\tilde{L}}{\tilde{c}}$	Time delay	50 ms

5.3.4 Experiments

Experimental Setup

In order to verify the effectiveness of the proposed method, the position control experiments are performed. The schematic diagram of experimental system is shown in Fig. 5-16. A linear motor with a optical encoder (resolution capability: 100 nm) is used as the controlled plant. A constant time delay is artificially generated by a network emulator. Jitter of the communication delay is not considered in the experiments. Communication system is realized by using the UDP, and the sending period is the same

Table 5.4: Experimental parameters for CDOB and Smith predictor.

Parameter	Description	Value
K_p	Proportional gain in Smith Predictor	324
K_d	Differential gain in Smith Predictor	36
K_p	Proportional gain in CDOB	225
K_d	Differential gain in CDOB	60
g_c	Cut-off freq. of CDOB	1000.0
g_e	Cut-off freq. of low-freq. model error feedback	2.5
g_{pd}	Cut-off frequency of pseudo derivation	2000 rad/s
g_{dis}	Cut-off frequency of disturbance estimation observer	250 rad/s

as the control period. Real-time control system is realized by using RTAI 3.7 on Linux, and the control program is written in C language.

The performance of the proposed method is compared with that of the typical Smith predictor and a communication disturbance observer with low-frequency model error feedback [83] when a step position command is applied. The disturbance estimation observer [82], which is a disturbance observer for time-delay system, is implemented in all methods for reducing the effect of the disturbance such as static friction. The compensation current generated by the disturbance estimation observer is represented as

$$I_{dis}^{cmp} = \frac{g_{dis}^2}{s^2 + 2g_{dis}s + g_{dis}^2}\left[K_{tn}I^{ref}e^{-Ts} - M_n s^2 Q(s)e^{-Ts}\right]. \tag{5.21}$$

The experimental parameters are listed in Table 5.3. In this dissertation, the derivation in the PD controller is implemented by using the pseudo derivation with cut-off frequency g_{pd}. The parameters of the compared methods is adjusted to coincide with the time constant of the proposed method. As a result, the parameters of the compared methods are obtained by the cut and try as shown in Table 5.4.

Experimental Results

Figs. 5-17–5-19 compare the experimental results of the three methods. Fig. 5-17 shows that the communication disturbance observer stabilizes the control system. However, the communication disturbance observer based method is not able to eliminate the steady state error even if the low-frequency model error feedback is implemented. Low-frequency model error feedback is effective for suppress the mod-

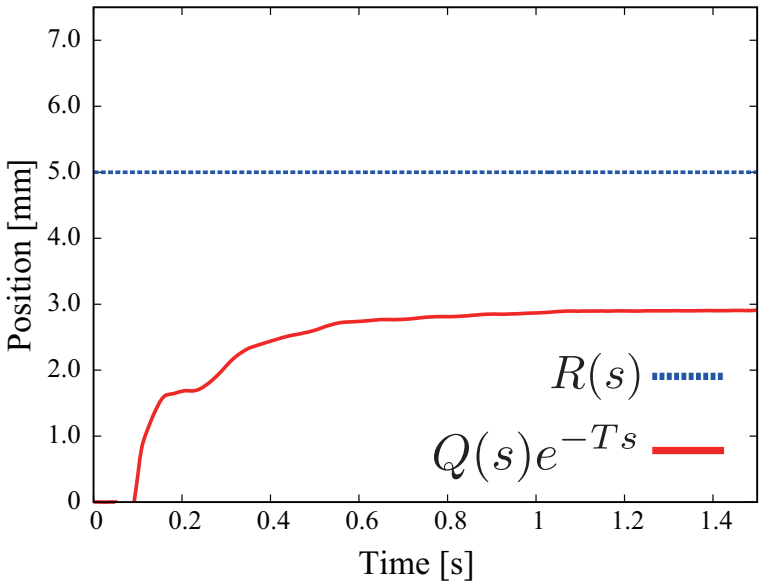

Fig. 5-17: Experimental result of communication disturbance observer with low-frequency model error feedback.

eling error, but is not effective for eliminate the disturbance such as static friction. Fig. 5-18 shows that Smith predictor also stabilizes the control system. However, steady state error is observed due to the disturbance. It is because Smith predictor based method also loses the feedback characteristic as same as the communication disturbance observer based method. On the other hand, Fig. 5-19 shows the proposed method can also stabilize the control system. In addition, it is found that the proposed method can eliminate the steady state error because feedback characteristic is maintained. Validity of the proposed method is confirmed by these experimental results.

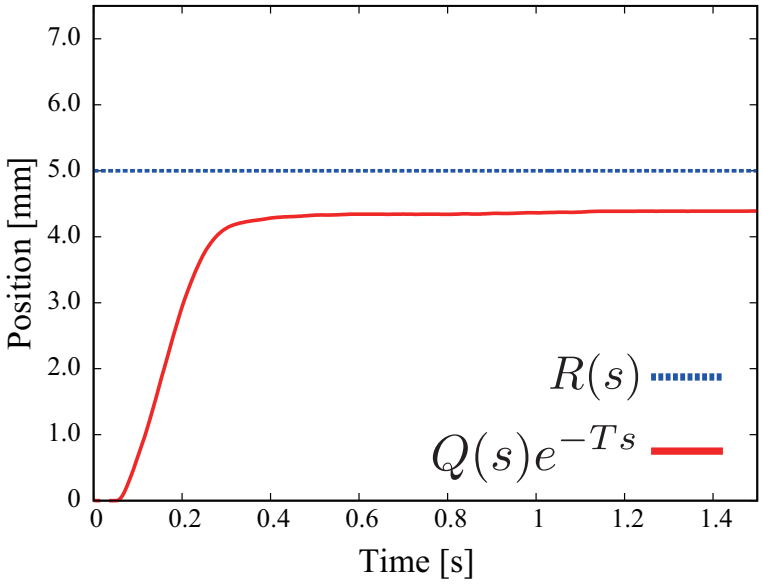

Fig. 5-18: Experimental result of Smith predictor.

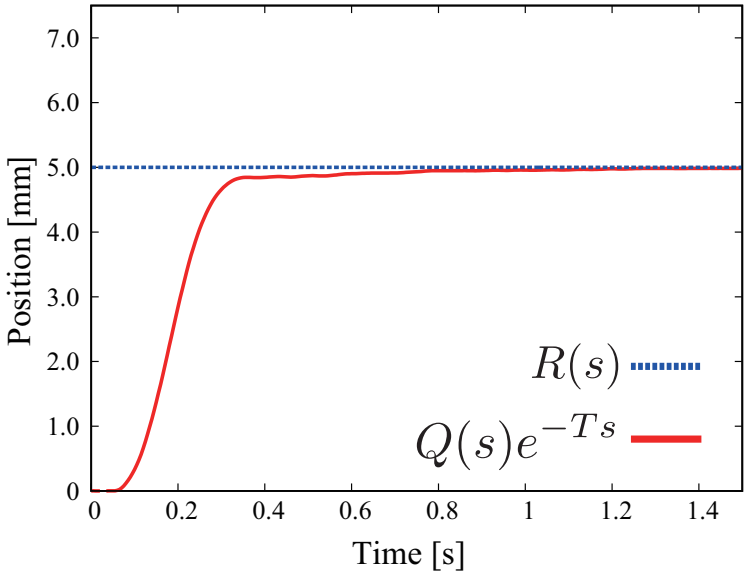

Fig. 5-19: Experimental result of the proposed method.

5.4 Summary of Chapter 5

In this chapter, a reflected wave rejection for time-delay system was proposed. Based on similarity between mechanical resonant and time-delay system described in Chapter 2, the reflected wave rejection is constructed. The reflected wave rejection for the time-delay system has same effect as that of Smith predictor and a communication disturbance observer. In addition, based on the similarity and concept of resonance ratio control, a time-delay compensation by equivalent elastic force feedback was proposed. The time-delay compensation by equivalent elastic force feedback has advantage of disturbance suppression performance compared with that of typical time-delay compensation methods. In contrast, the time-delay compensation by the equivalent elastic force feedback has disadvantage of robust stability against variation of time delay (jitter) and plant dynamics.

Chapter 6

Motion Control of Integrated Resonant and Time-delay System

6.1 Introduction of Chapter 6

This chapter explains reflected wave rejection for an integrated resonant and time-delay systems. Although Chapters 4 and 5 deal with reflected wave rejection for mechanical resonant system and time-delay system, respectively, this chapter treats the mechanical resonant system with input-output time delay. As mentioned in Chapter 1, in the case of the integrated system, simple integration of vibration suppression and time-delay compensation does not work well because typical time-delay compensation methods are weak against the variation of the plant. On the other hand, because the reflected wave rejection is based on the transfer function of wave equation which is composed of time-delay elements, it is easy to integrate the two systems.

Section 6.2 explains a basic concept of integration scheme based on reflected wave rejection. Next, Section 6.3 explains that reflected wave rejection form the integrated system is extended to the structure whose all the compensator and controller are implemented at local (controller) side. Finally, Section 6.4 describes that reflected wave rejection explained in Section 6.3 is extended to a reaction-force-based reflected wave rejection for the integrated system.

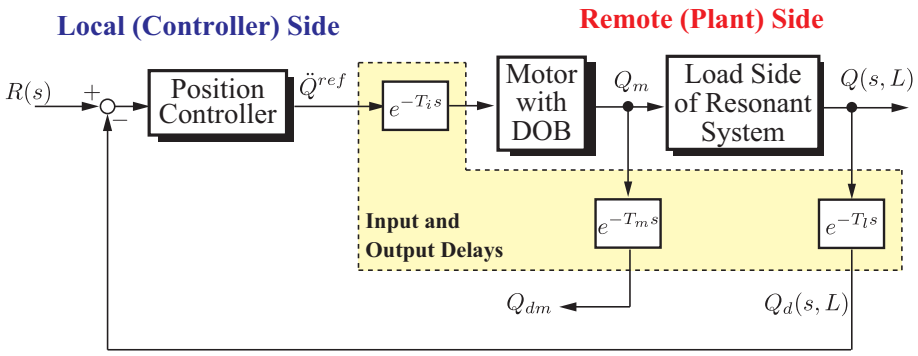

Fig. 6-1: Block diagram of integrated resonant and time-delay system.

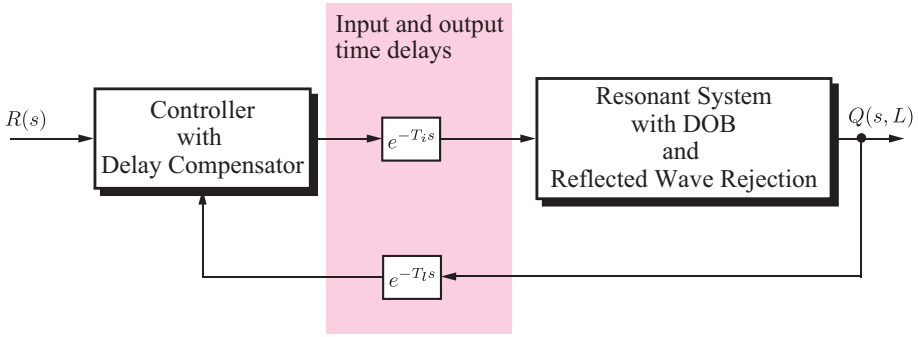

Fig. 6-2: Overview of the proposed structure for control of integrated system.

6.2 System Integration by Using Reflected Wave Rejection

The block diagram of integrated resonant and time-delay system is shown in Fig. 6-1 where T_i, T_m, T_l, Q_{dm}, and $Q_d(s, L)$ are the input delay, the output delay at motor side, the output delay at load side, the delayed motor position, and the delayed tip position, respectively. In this section, basic concept of integration of two systems by reflected wave rejection is explained. Overview of the proposed method is shown in Fig. 6-2. In the proposal, a controller and a time-delay compensator which is the proposed method are implemented at the local side. On the other hand, at the remote side, a DOB and a reflected wave rejection are implemented. By using the reflected wave rejection shown in Fig. 3-2 under the ideal condition ($g_r = \infty$), the transfer function from the acceleration reference $\ddot{Q}^{ref}$ to tip position $Q(s, L)$ is represented as

$$\frac{Q(s, L)}{\ddot{Q}^{ref}} = \frac{1}{s^2} e^{-\frac{L}{c}s}. \tag{6.1}$$

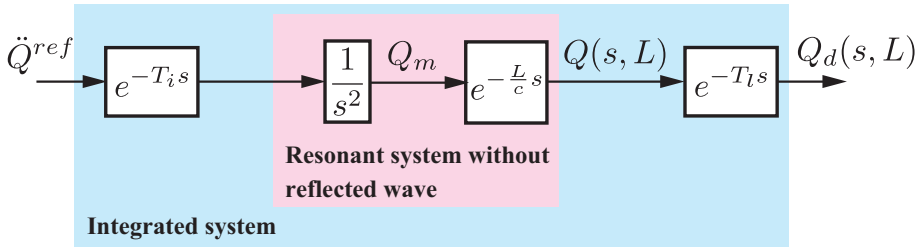

Fig. 6-3: Block diagram of integrated time-delay system.

From (6.1), the resonant system without reflected wave can be regarded as equivalent time-delay system. The block diagram of open-loop of the plant is shown in Fig. 6-3. Therefore, equivalent system of the integrated system is represented as

$$\frac{Q_d(s,L)}{\ddot{Q}^{ref}} = \frac{1}{s^2} e^{-(\frac{L}{c}+T_i+T_l)s}. \tag{6.2}$$

As shown in (6.2), owing two the reflected wave rejection, the plant becomes a simple time-delay system which is second order dynamics with sum of input-output and equivalent time delays. Hence, it is easy to design the control system by using the typical time-delay compensation methods. Total block diagram of control of integrated resonant and time-delay system based on the reflected wave rejection is shown in Fig. 6-4. Structure of Fig. 6-4 is equivalent to fully closed-loop type control with reflected wave rejection introduced in Chapter 3. In addition, a CDOB is used as a time-delay compensation method. If the cut-off frequency of a CDOB is enough high value and a PD controller is used for the position controller, the transfer function from position command to tip position is represented as

$$\frac{Q(s,L)}{R(s)} = \frac{K_d s + K_p}{s^2 + K_d s + K_p} e^{-(\frac{L}{c}+T_i)s}. \tag{6.3}$$

In (6.3), there is no time delay in the denominator of the transfer function. Therefore, it is possible to suppress the vibration of integrated resonant and time-delay systems.

6.2.1 Numerical Analysis

In this section, in order to analyze the validity of the proposal, numerical simulations and analyses are conducted. First, for confirming the performance of the proposed method, a position control of a three-mass resonant system with input-output time delay is conducted. Next, we analyze variation of delay of a resonant system and time-delay system.

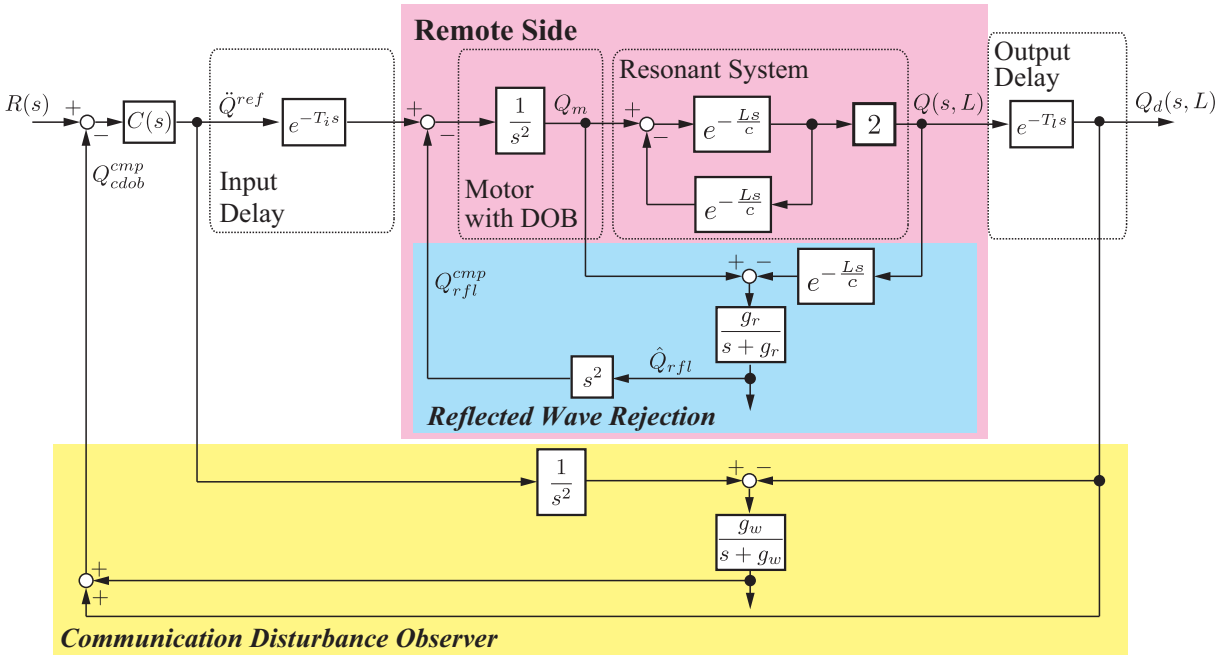

Fig. 6-4: Block diagram of the proposed control system.

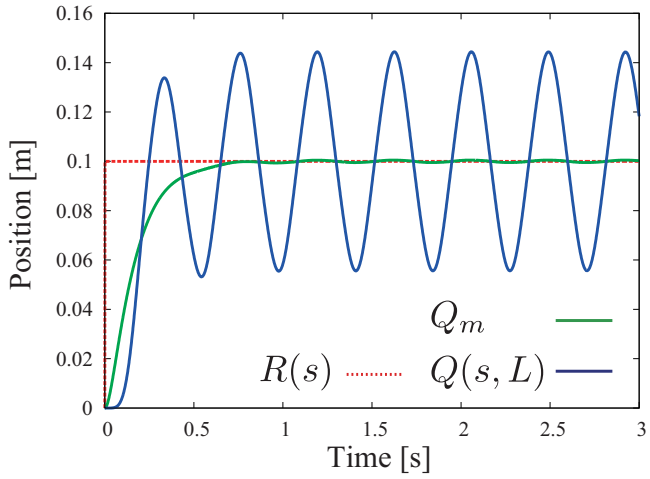

Fig. 6-5: Simulation results by DOB (without input-output time delay).

Position Control

In this part, position control of a three-mass resonant system with input-output time delay is conducted. The simulation parameters are shown in Table 6.1. In this simulation, step input is used as the position

Table 6.1: Simulation parameters for reflected wave rejection for integrated system.

Parameter	Description	Value
T_s	Sampling time	0.1 ms
K_{tn}	Nominal force coefficient	3.33 N/A
M_n	Nominal mass	0.245 kg
$\frac{L}{c}$	Propagation time of wave	107 ms
$T_i + T_l$	input-output time delays (Round trip delay)	200 ms
ω_1	First-order resonance	14 rad/s
ω_2	Second-order resonance	42 rad/s
K_p	Proportional gain	200
K_d	Differential gain	30
g_{pd}	Cut-off frequency of pseudo derivation	3000 rad/s
g_{dis}	Cut-off frequency of DOB	2000 rad/s
g_r	Cut-off frequency of reflected wave rejection	1000 rad/s
g_w	Cut-off frequency of CDOB	2000 rad/s

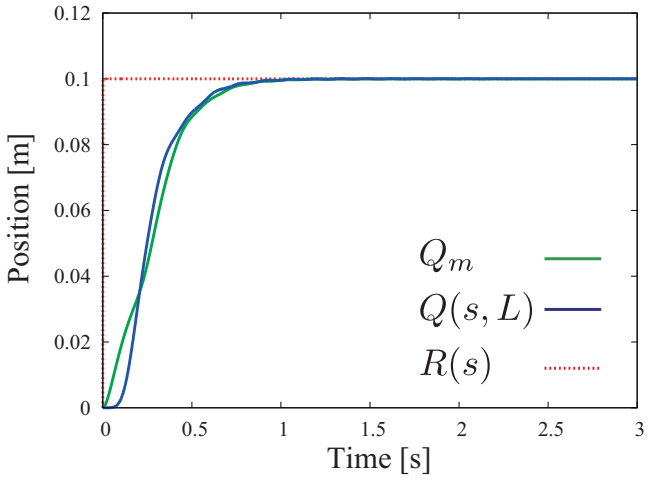

Fig. 6-6: Simulation results by the proposed method (without input-output time delay).

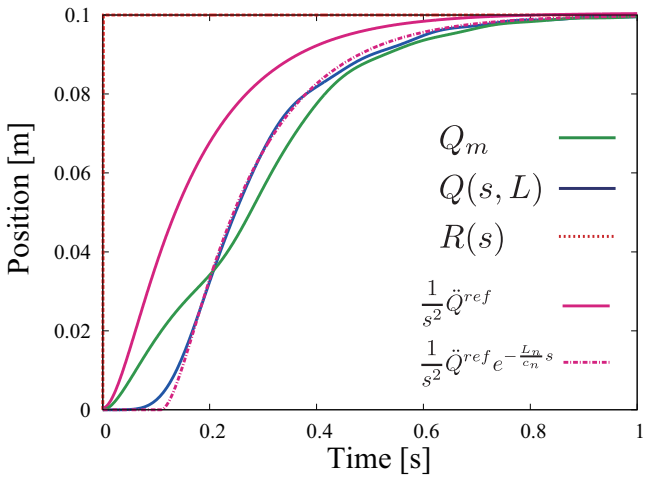

Fig. 6-7: Enlarged view of Fig. 6-6.

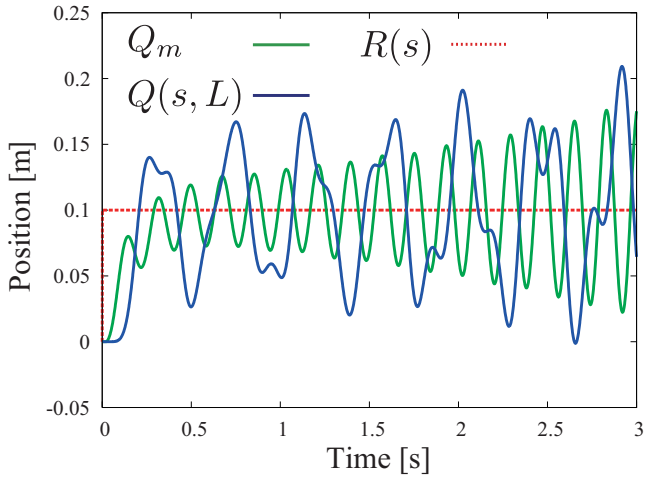

Fig. 6-8: Simulation results by DOB (with input-output time delay).

command. The proposed method is compared with the method based on DOB.

Firstly, for confirming the performance of the reflected wave rejection, the simulations in the case that there is no time delay are conducted. The simulation results are shown in Figs. 6-5 and 6-6. From Fig. 6-5, it is found that vibration from the resonant system occurs on the response of tip position $Q(s, L)$. On the other hand, from Fig. 6-5, it turns out that vibration caused by the resonance is well suppressed by the reflected wave rejection and CDOB. Moreover, Fig. 6-7 shows the enlarged view of the proposed method without time delay shown in Fig. 6-6. It can be seen that response of the tip position $Q(s, L)$ and

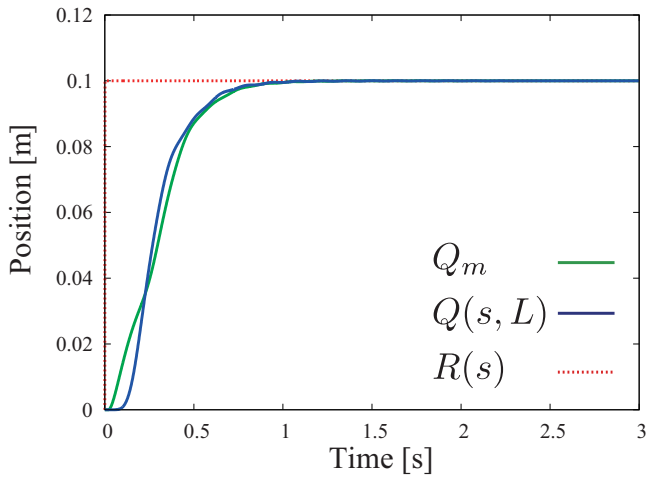

Fig. 6-9: Simulation results of the proposed method (with input-output time delay).

delayed position $\frac{1}{s^2}\ddot{Q}^{ref}e^{-\frac{L}{c}s}$ are corresponded, The fact implies that the resonant system is transformed into an equivalent time-delay system whose time delay is $\frac{L}{c}s$ by the reflected wave rejection.

Next, the simulation results in the case that there is time delay are shown in Figs. 6-8 and 6-9. From Fig. 6-8, time delay causes the vibration on the response of both motor and tip position. On the other hand, from results of the proposed method shown in Fig. 6-9, vibration caused by time delay from the resonant and time-delay system is well suppressed. Fig. 6-10 shows the enlarged view of Fig. 6-9. From Fig. 6-9, it can be also seen that response of the tip position $Q(s, L)$ corresponds to the delayed position $\frac{1}{s^2}\ddot{Q}^{ref}e^{-\left(\frac{L}{c}s+T_i+T_l\right)}$. Moreover, CDOB is able to suppress the effect of time delay which is sum of the time delays from the resonant and time-delay systems.

From these results, validity of the proposed method which is composed of the reflected wave rejection and the CDOB is verified.

Variation of Delays

In this part, simulation in the case when input-output time delays are changed is conducted. Equivalent time delay of the resonant system shown in Table 6.1 is used. The other parameters equal to same value shown in Table 6.1.

Fig. 6-11 shows simulation results of the tip-position response when the input-output time delays are changed. In Fig. 6-11, sum of input-output time delays are changed from 0 ms to 1000 ms. From Fig. 6-11, it is found that the value of input-output time delays do not affect the transient response of

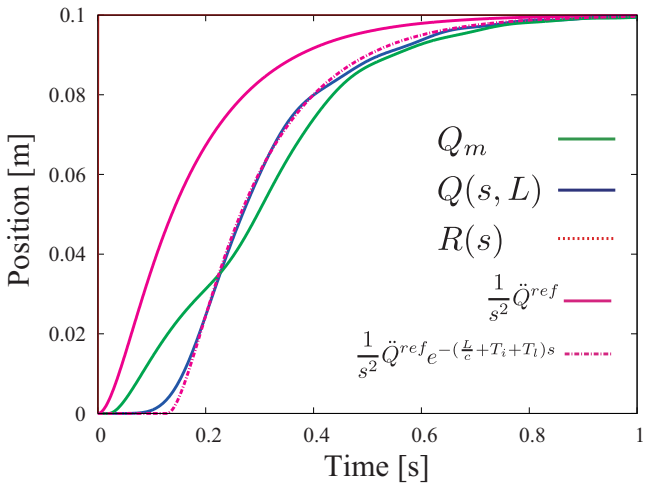

Fig. 6-10: Enlarged view of Fig. 6-9.

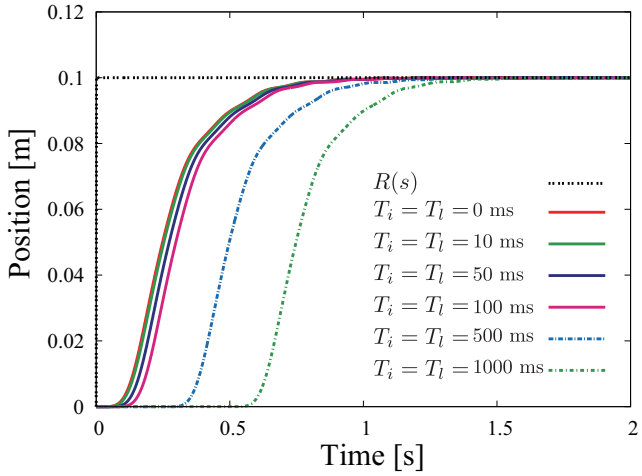

Fig. 6-11: Simulation results of the tip position response when the input-output time delays are changed.

the tip position if cut-off frequency is set enough high value. These results imply that time delay is well compensated by a CDOB.

6.2.2 Experiments

Experimental Setup

In order to verify the effectiveness of the proposed method, experiments of position control are conducted in a two-mass resonant system. The control software was written in C language under RTAI 3.7.

Table 6.2: Experimental parameters for reflected wave rejection for integrated system.

Parameter	Description	Value
T_s	Sampling time	0.1 ms
K_{tn}	Nominal force coefficient	3.33 N/A
M_n	Nominal mass	0.245 kg
k	Spring coefficient	200 N/m
c	Propagation velocity of wave	1.42 m/s
a	Length of a spring	0.05 m
$\frac{L}{c}$	Propagation time of wave	35 ms
$T_i + T_l$	Input-output time delays (Round trip delay)	40 ms
K_p	Proportional gain	200
K_d	Differential gain	30
g_{pd}	Cut-off frequency of the pseudo derivation	2000 rad/s
g_{dis}	Cut-off frequency of DOB	2000 rad/s
g_r	Cut-off frequency of reflected wave rejection	2000 rad/s
g_w	Cut-off frequency of CDOB	1000 rad/s

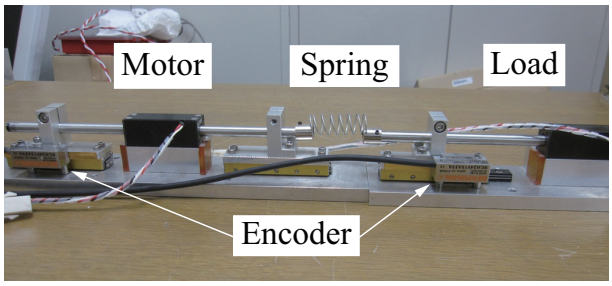

Fig. 6-12: Experimental setup.

The experimental setup is shown in Fig. 6-12. The experimental setup deals with linear motion as shown in Fig. 2-1. The right motor is used as load and is not controlled. On the other hand, the left motor is controlled according to the control program. Position information of each motor is obtained by linear encoders (resolution capability: 0.1 μm).

Experimental parameters are shown in Table 6.2. As roots of the characteristic equation in (6.3) are

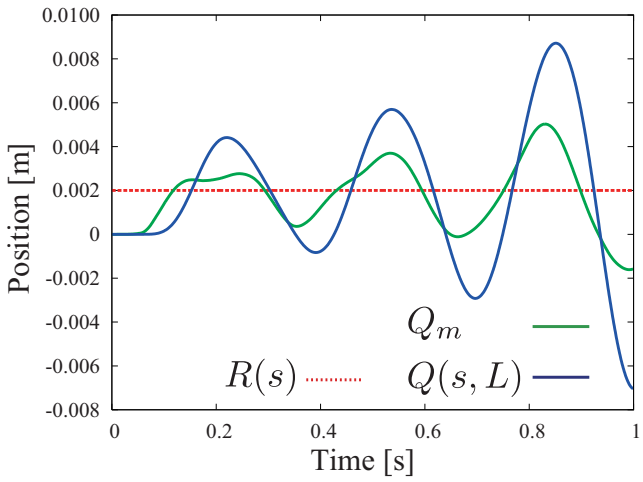

Fig. 6-13: Experimental results by PD controller with DOB.

multiple roots on the real axis, position and velocity gains should be set as

$$K_d = 2\sqrt{K_p}. \tag{6.4}$$

input-output time delays are artificially generated in a computer, and jitter is not considered in the experiments.

Performance of the proposed method is compared with those of a method using PD controller with a DOB and a method using both a resonance ratio control and a CDOB. Each control gain is set to make the time-constants of the proposed and compared methods same. A DOB and a reaction force observer in the compared methods are implemented in the remote side. In the resonance ratio control, a reaction force feedback is conducted at remote side. The nominal plant model which is implemented in the CDOB is the two-mass resonant system including the reaction force feedback. It is noted that the compared method does not use the tip position information.

Experimental Results

The experimental results of the PD controller with DOB are shown in Fig. 6-13. In Fig. 6-13, it can be seen that the system becomes unstable because of input-output time delay.

The experimental results of the resonance ratio control with CDOB are shown in Fig. 6-14. In similar to the results of the PD controller with the DOB, the system becomes unstable. The reason is that error of plant model in the CDOB makes the system unstable.

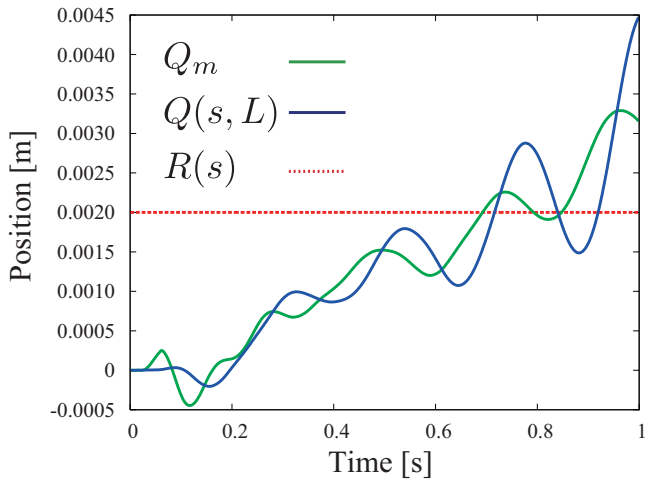

Fig. 6-14: Experimental results by resonance ratio control with CDOB.

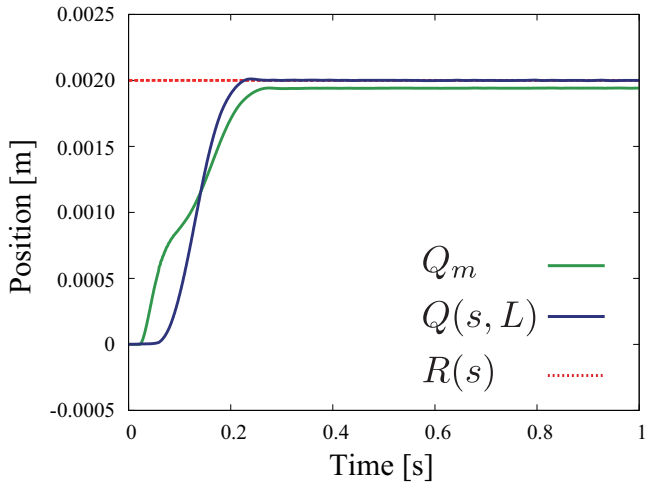

Fig. 6-15: Experimental results by the proposed method.

On the other hand, in results of the proposed method shown in Fig. 6-15, the system is kept stable and vibration is well suppressed. From Fig. 6-15, a steady state error is observed at the tip position because of the disturbance acting on the tip which is composed of coulomb and viscous frictions.

6.3 System Integration by Using Reflected Wave Rejection Implemented at Controller Side

6.3.1 Structure of Reflected Wave Rejection

In the previous part, the reflected wave rejection is implemented at remote (plant) side as shown in Fig. 6-4. Although it is better to implement it at local (controller) side, it is difficult to implement the typical reflected wave rejection if there are input and output delays. Therefore, a novel reflected wave rejection scheme under existence of these delays is proposed.

First of all, the transfer function from Q_m to $Q(s,L)$ is transformed into

$$\begin{aligned} Q(s,L) &= 2e^{-T_w s}\frac{1}{1+e^{-2T_w s}}Q_m \\ &= 2e^{-T_w s}\left(1-e^{-2T_w s}+e^{-4T_w s}-e^{-6T_w s}+\cdots\right)Q_m \\ &= 2e^{-T_w s}\left[Q_m-e^{-2T_w s}Q_m+e^{-4T_w s}\left(1-e^{-2T_w s}+e^{-4T_w s}\cdots\right)Q_m\right]. \end{aligned} \tag{6.5}$$

In the aforementioned transformation, the relation of geometric series $1/(1+r)=1-r+r^2-r^3\cdots$ is used. Furthermore, by using the relation of geometric series, (6.5) is transformed into

$$Q(s,L)=2e^{-T_w s}\left[Q_m-e^{-2T_w s}Q_m+\frac{1}{2}e^{-3T_w s}Q(s,L)\right]. \tag{6.6}$$

Here, let's re-define a reflected wave as the following equation:

$$Q'_{rfl} = -e^{-2T_w s}Q_m+\frac{1}{2}e^{-3T_w s}Q(s,L). \tag{6.7}$$

The re-defined reflected wave corresponds to a wave at the end of negative feedback (i.e. $e^{-T_w s}Q(s,L)$) shown in Fig. 2-7. By using (6.7), the relation between Q_m, $Q(s,L)$ and Q'_{rfl} is represented as

$$Q(s,L) = 2e^{-T_w s}\left[Q_m+Q'_{rfl}\right]. \tag{6.8}$$

As well as the conventional reflected wave rejection, the reflected wave Q'_{rfl} will be canceled out by the feedforward of the estimated reflected wave. However, because there are input and output delays, the compensation value for eliminating the reflected wave from the resonant system must include the inverse system of the time delays. In the proposed method, the compensation value including the inverse systems are calculated as

$$\begin{aligned} \ddot{Q}'^{comp}_{rfl} &= e^{+T_i s}\hat{Q}'_{rfl} \\ &= \frac{g_r}{s+g_r}\left(-e^{-(2T_{wn}-T_{mn}-T_{in})s}Q_{dm}+\frac{1}{2}e^{-(3T_{wn}-T_{ln}-T_{in})s}Q_d(s,L)\right) \end{aligned} \tag{6.9}$$

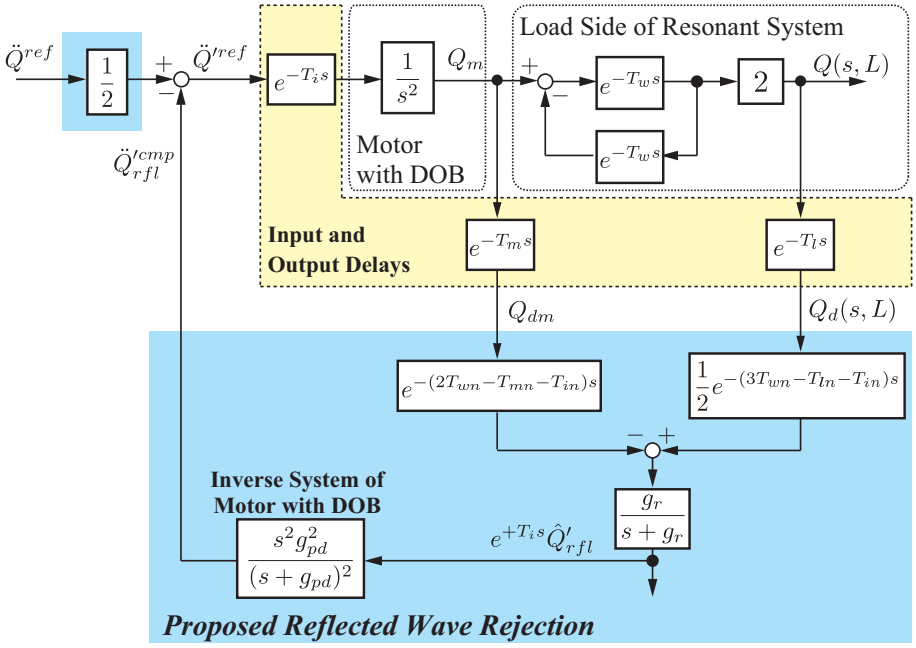

Fig. 6-16: Block diagram of the proposed reflected wave rejection.

where $\hat{Q}'_{rfl}$, T_{in}, T_{mn}, and T_{ln} denote the estimated reflected wave, and the nominal time delays, respectively. It is noted that, in order to calculate the above compensation value, following conditions must be satisfied,

$$2T_w > T_m + T_i \tag{6.10}$$

$$3T_w > T_l + T_i. \tag{6.11}$$

If the time delays satisfy the above conditions, the proposed reflected wave rejection can be implemented. Compared with the application range of the conventional method against value of time delay (at least $T_w > T_l$ should be satisfied), it is found that the application range is extended.

The block digram of the proposed reflected wave rejection is shown in Fig. 6-16. In Fig. 6-16, $\ddot{Q}'^{cmp}_{rfl}$ denotes the compensation value in acceleration dimension, and it is calculated as

$$\ddot{Q}'^{cmp}_{rfl} = s^2 \frac{g_{pd}^2}{(s+g_{pd})^2} e^{+T_i s} Q^{cmp}_{rfl}. \tag{6.12}$$

In (6.12), the inverse system of the motor with DOB is approximately implemented by using the pseudo derivation. Finally, the acceleration reference injected to the motor is calculated as

$$\ddot{Q}'^{ref} = \frac{1}{2}\ddot{Q}^{ref} - \ddot{Q}^{cmp}_{rfl}. \tag{6.13}$$

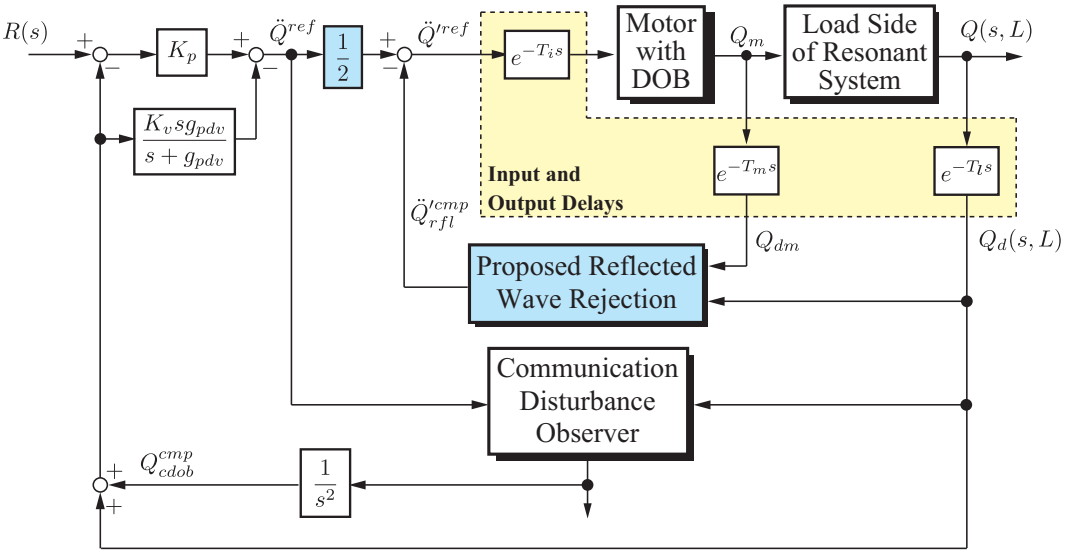

Fig. 6-17: Whole block diagram of the proposed position control system.

It is noted that 1/2 in the right hand of (6.13) means that cancellation of the superposition of the wave at $x = L$ represented by the block "2" shown in Fig. 2-7. If the cut-off frequencies g_r and g_{pd} in the proposed reflected wave rejection are ideally high value, the transfer function from the acceleration reference to the tip position is represented as

$$\frac{Q(s,L)}{\ddot{Q}^{ref}} = \frac{1}{s^2} e^{-(T_w+T_i)s}. \tag{6.14}$$

From (6.14), it is found that the vibration is suppressed because the time delay has been omitted from the denominator of the transfer function.

By using the proposed reflected wave rejection, the resonant system with input-output time delay can be regarded as an equivalent time-delay system described as (6.14). Then, the position-control system of (6.14) is constructed by using the position controller with a CDOB [78]. The acceleration reference is calculated as

$$\ddot{Q}^{ref} = K_p \left(R(s) - Q_d(s,L) - Q^{cmp}_{cdob} \right) - K_v \frac{s g_{pdv}}{s+g_{pdv}} (Q_d(s,L) + Q^{cmp}_{cdob}) \tag{6.15}$$

where $R(s)$, K_p, K_v, g_{pdv} and Q^{cmp}_{cdob} denote the position command, the position gain, the velocity gain, the cut-off frequency for calculation of velocity, the compensation value of CDOB, respectively. In the proposed system, the P control with a velocity minor loop is used as a position controller. The whole block diagram of position control of the integrated resonant and time-delay system is shown in Fig. 6-17.

Table 6.3: Simulation parameters for reflected wave rejection without use of tip position for integrated system.

Parameter	Description	Value
T_s	Sampling time	0.1 ms
T_i	Input delay	7.5 ms
T_m	Output delay at motor	7.5 ms
T_l	Output delay at load	7.5 ms
T_w	Propagation time of wave	40 ms
K_{tn}	Nominal thrust force coefficient	3.0 N/A
M_n	Nominal mass of motor	0.245 kg
w_1	First order resonance frequency	39.5 rad/s
w_2	Second order resonance frequency	103.0 rad/s
K_p	Position gain	900
K_v	Velocity gain	80
g_{dis}	Cut-off frequency of DOB	500 rad/s
g_r	Cut-off frequency of reflected wave rejection	500 rad/s
g_{cdob}	Cut-off frequency of CDOB	1000 rad/s
g_{pd}	Cut-off frequency of pseudo derivation for reflected wave rejection	500 rad/s
g_{pdv}	Cut-off frequency of pseudo derivation for position controller	500 rad/s
dQ, $dQ(s, L)$	Position sensor resolutions	65536 pulse/rev

Finally, if the cut-off frequency of the CDOB is enough large value, the transfer function from position command $R(s)$ to the tip position $Q(s, L)$ is represented as

$$\frac{Q(s,L)}{R(s)} = \frac{K_p}{s^2 + K_v s + K_p} e^{-(T_w+T_i)s}. \tag{6.16}$$

It is found that because there is no time delay in the denominator of the fully closed-loop transfer function, vibrations on the integrated resonant and time-delay system are suppressed.

6.3.2 Simulation

Simulation Setup

In order to verify the validity of the proposed method, simulation of position control on a three-mass resonant system is conducted. Plant and control parameters used in this simulation are shown in Table

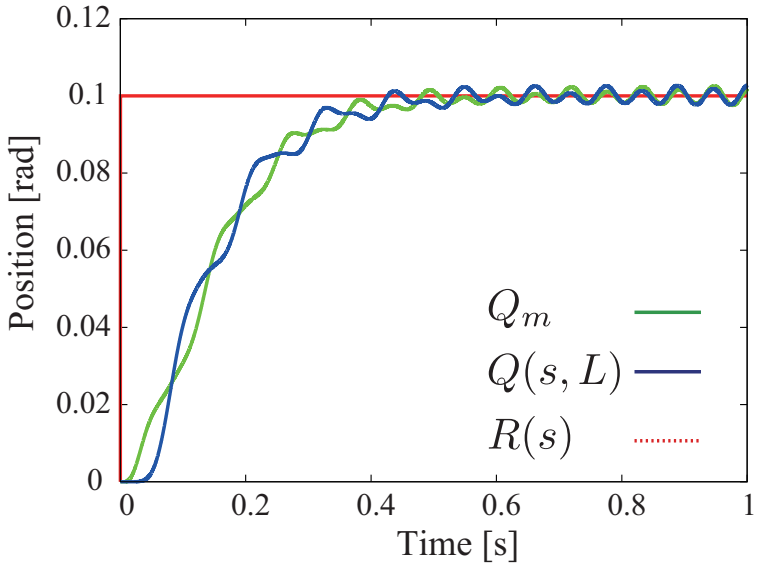

Fig. 6-18: Simulation results of the conventional reflected wave rejection.

6.3. The control goal of the simulation is that the tip position corresponds to the position command (a step of 0.1 rad) without vibration and destabilization. Performance of the proposed method is compared with that of the method based on the conventional reflected wave rejection. The difference between the proposed and conventional methods is only in the structures of the reflected wave rejections, but the other control parameters are same.

Simulation Results

The simulation results of the conventional and proposed methods are shown in Figs. 6-18 and 6-19. From the results of the conventional method, the vibration can be observed because the performance of the reflected wave rejection degrades due to the existence of the delays. On the other hand, it is found that the residual vibration is well suppressed with the proposed approach.

6.3.3 Experiments

Experimental Setup

To verify the effectiveness of the proposed method, a position control of flexible arm is performed. Experimental setup is shown in Fig. 6-20. The definitions of angles q_m and $q(t, L)$ are accordance with those described in section 2.2.2. The control goal is that the tip position of a flexible arm $q(t, L)$

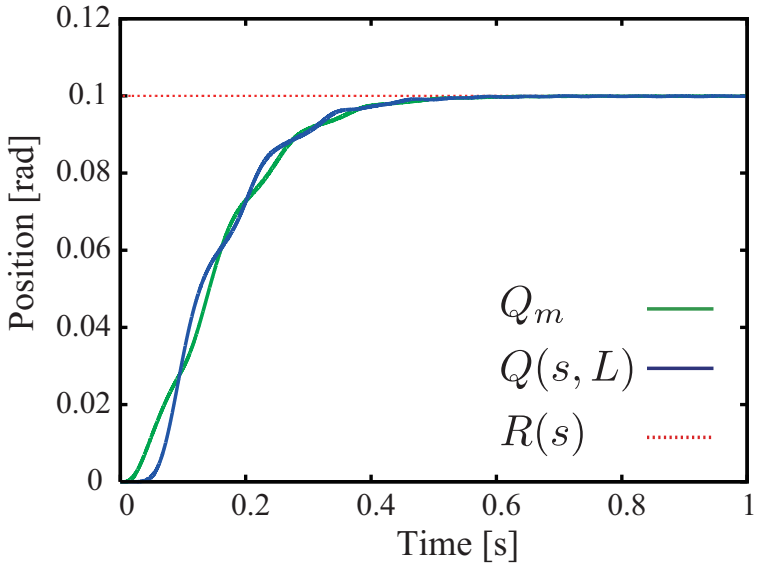

Fig. 6-19: Simulation results of the proposed reflected wave rejection.

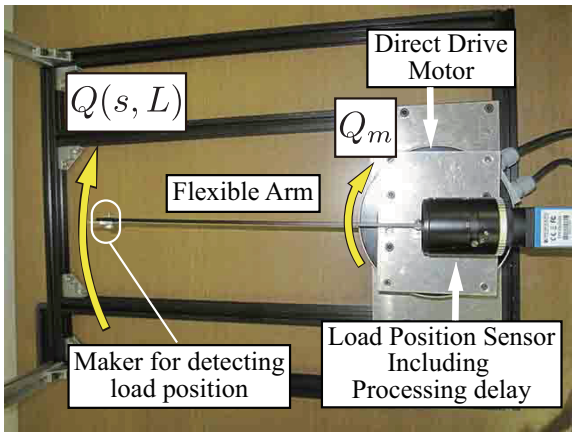

Fig. 6-20: Experimental Setup.

corresponds to the position command $r(t)$ without vibrations. The flexible arm is mounted on the direct drive rotary motor (encoder resolution: 20 bit/rev). The tip position $q(t, L)$ is obtained by the vision sensor (frame rate: 100 Hz). Equivalent resolution of vision sensor is 1.09×10^{-4} rad. Control program is written by C language under Real time application interface 3.8 (RTAI 3.8) on Linux.

Experimental parameters are shown in Table 6.4. Output delay at load side includes processing time of vision sensor ($T_l = 20$ ms). The delays T_i and T_m are artificially generated in the computer. The jitters of input and output delays are not considered in this experiment. In this experiment, a step position

Table 6.4: Experimental parameters for reflected wave rejection without use of tip position for integrated system.

Parameter	Description	Value
T_s	Sampling time	0.1 ms
T_i	Input delay	5.0 ms
T_m	Output delay at motor side	5.0 ms
T_l	Output delay at load side	20 ms
T_w	Propagation time of wave	9.6 ms
K_{tn}	Nominal thrust force coefficient	3.0 N/A
M_n	Nominal mass of motor	0.245 kg
w_1	First order resonance frequency	104.0 rad/s
L	Length of flexible arm	0.3 m
K_p	Position gain	10000.0
K_v	Velocity gain	400
g_{dis}	Cut-off frequency of DOB	1000 rad/s
g_r	Cut-off frequency of reflected wave rejection	200 rad/s
g_{cdob}	Cut-off frequency of CDOB	1000 rad/s
g_{pd}	Cut-off frequency of pseudo derivation for reflected wave rejection	200 rad/s
g_{pdv}	Cut-off frequency of pseudo derivation for calculation of velocity	1000 rad/s

command ($r(t) = 0.05$ rad) is applied to the control system. It is noted that, because output delay T_l is larger than propagation time of wave T_w, the typical reflected wave rejection shown in Fig. 3-2 can not be implemented in this experiment.

Experimental Results

The experimental results of the proposed method are shown in Fig. 6-21. From Fig. 6-21, the residual vibration on tip position is well suppressed by the proposed method although there exist input and output time delays. However, it is observed that there is steady state error because of the friction acting on motor and degradation of performance of disturbance rejection when the CDOB is used. Although the disturbance compensator is not implemented in this system for the sake of simplicity, the elimination or reduction of steady state error is possible by using the method about disturbance rejection in CDOB [80, 81].

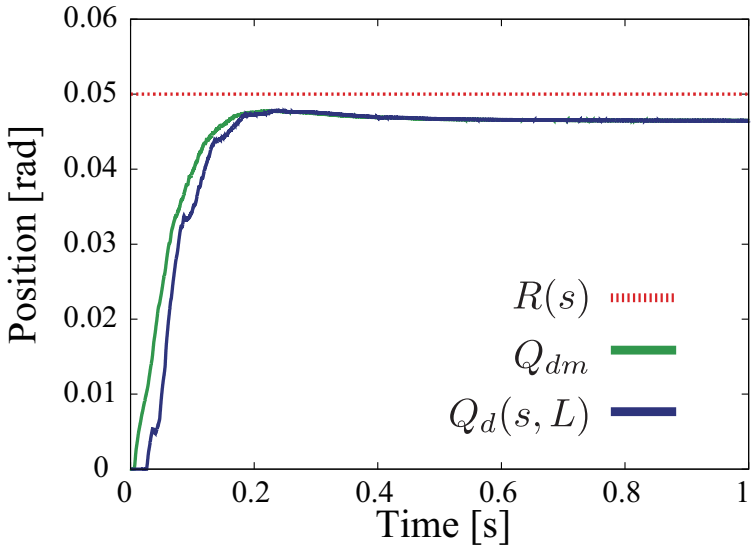

Fig. 6-21: Position response of the proposed method.

Then, validity of the proposed reflected wave rejection is confirmed.

6.4 System Integration by Using Reaction-Force-based Reflected Wave Rejection Implemented at Controller Side

6.4.1 Structure

The method for integrated system described in previous part needs to use the tip-position information. However, in general, it is difficult to obtain the tip-position information because of problem on sensor mounting. Therefore, this part proposes a reaction-force-based reflected wave rejection, which uses only motor position information. First of all, the reflected wave is rewritten by using a reaction force acting on the motor instead of tip position. The reaction force is represented as

$$\begin{aligned} F^{reac}(s,0) &= -\kappa \frac{\partial Q(s,0)}{\partial x} \\ &= \frac{\kappa}{c} \frac{1 - e^{\frac{2L}{c}s}}{1 + e^{\frac{2L}{c}s}} Q(s,0) \end{aligned} \tag{6.17}$$

where $F^{reac}(s,0)$ and κ denote the reaction force acting on the motor and the stiffness of the flexible arm, respectively. By using (6.17) and transfer function from Q_m to $Q(s,L)$, the reflected wave shown

in (6.7) is transformed into

$$Q'_{rfl} = -\frac{1}{2}e^{-2T_w s}Q_m - \frac{1}{2}e^{-2T_w s}\frac{1}{Ws}F^{reac}(s,0) \tag{6.18}$$

where W denotes the characteristic impedance which is represented as

$$W = \sqrt{\rho\kappa} \tag{6.19}$$

where ρ represents the mass density of flexible arm. As well as the conventional reflected wave rejection, the estimated reflected wave including the inverse system of input delay is calculated as

$$e^{+T_i s}\hat{Q}'_{rfl} = \frac{g_r}{s+g_r}\left(-\frac{1}{2}e^{-T_{rfl}s}Q_{dm} - \frac{1}{2W_n s}e^{-T_{rfl}s}\frac{s}{s+g_{hpf}}\hat{F}_d^{reac}(s,0)\right) \tag{6.20}$$

where g_{hpf} and $\hat{F}_d^{reac}(s,0)$ denote the cut-off frequency of high-pass filter and the delayed reaction force due to output time delay, respectively. T_{rfl} stands for the delay implemented in the reflected wave rejection, which is represented as

$$T_{rfl} = 2T_{wn} - T_{mn} - T_{in}. \tag{6.21}$$

It is noted that, for implementation of (6.20), the delays must be satisfied following condition,

$$2T_{wn} > T_{mn} + T_{in} \tag{6.22}$$

In this research, the reaction force is estimated by the reaction-force observer (RFOB) [15]. However, the reaction force estimated by RFOB often includes the disturbance, such as friction, other than reaction force. Therefore, a high-pass filter is applied to the estimated force for eliminating DC component of such disturbance in (6.20). Finally, the compensation value is calculated by using inverse system of the position controlled motor as follow,

$$Q'^{comp}_{rfl} = \frac{g_{inv}^2}{s^2 + 2g_{inv}s + g_{inv}^2}\frac{s^2 + K_v s + K_p}{K_p}e^{+T_i s}\hat{Q}'_{rfl} \tag{6.23}$$

where g_{inv} denotes the cut-off frequency of second order low-mass filter which makes the inverse system be proper.

Whole block diagram of the proposed method is shown in Fig. 6-22. In Fig. 6-22, block of "reflected wave rejection" denotes the calculation based on (6.20). It is noted that the control system shown in previous part is a fully closed-loop control system, but the control system shown in Fig. 6-22 is a semi-closed-loop control system. In the case of the proposed method, tip-position information can not be used

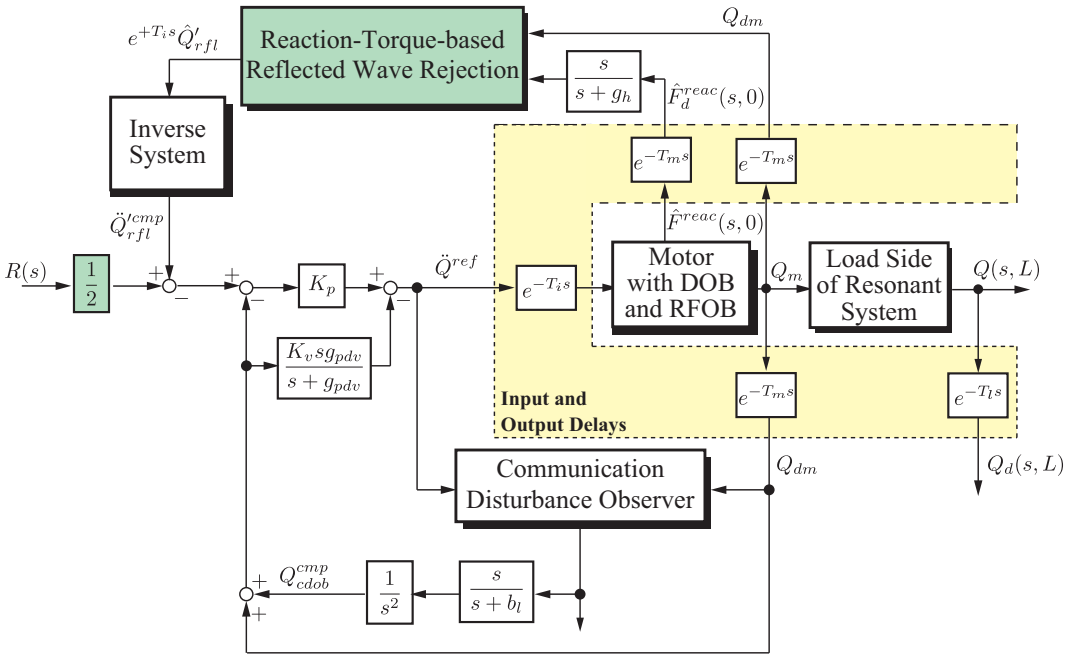

Fig. 6-22: Whole block diagram of the proposed position control system.

for control of the integrated system. According to the above, CDOB designed for position controlled motor without consider load side of resonant system is located in inner loop. In outer loop, vibration suppression of mechanical resonances is achieved by the proposed reflected wave rejection. The compensation value (6.20) for the reflected wave is fed back to the position command with multiplying the inverse system of the position controlled motor without delay. Because the CDOB with band-pass filter is implemented at inner loop, the cut-off frequencies b_l and g_h must be satisfied following conditions,

$$b_l < g_h. \tag{6.24}$$

If the condition (6.24) is not satisfied, the drift effect occurs due to the integrator in the proposed reflected wave rejection. Finally, the acceleration reference which is transmitted to the plant is represented as

$$\ddot{Q}^{ref} = K_p\left(\frac{1}{2}R(s) - Q_{dm} - Q_{cdob}^{cmp} - Q_{rfl}^{\prime cmp}\right) - K_v\frac{sg_{pdv}}{s+g_{pdv}}(Q_{dm} + Q_{cdob}^{cmp}). \tag{6.25}$$

Table 6.5: Experimental parameters for reaction-force-based reflected wave rejection for integrated system.

Parameter	Description	Value
T_s	Sampling time	0.1 ms
T_i	Input delay	5.0 ms
T_m	Output delay at motor side	5.0 ms
T_l	Output delay at load side	20 ms
T_w	Propagation time of wave	12.5 ms
K_{tn}	Nominal torque coefficient	1.18 Nm/A
M_n	Nominal mass of motor	0.0029 kgm^2
w_1	First order resonance frequency	125 rad/s
W	Characteristic impedance	3.1 Ns/m
L	Length of flexible arm	0.3 m
K_p	Position gain	ω_1^2
K_v	Velocity gain	$2\omega_1$
	(CDOB based method)	$3\omega_1$
g_{dis}	Cut-off frequency of DOB	1000 rad/s
g_r	Cut-off frequency of reflected wave rejection	300 rad/s
g_h	Cut-off frequency of CDOB	1000 rad/s
g_l	Cut-off frequency of CDOB	25 rad/s
g_{hpf}	Cut-off frequency of high-pass filter	50 rad/s
g_{pd}	Cut-off frequency of pseudo derivation for reflected wave rejection	300 rad/s
g_{pdv}	Cut-off frequency of pseudo derivation for calculation of velocity	2000 rad/s

6.4.2 Experiments

Experimental Setup

To verify the effectiveness of the proposed method, a position control of flexible arm is performed. Experimental setup is same flexible arm system as shown in Fig. 6-20. The control goal is that the tip position of a flexible arm $q(t, L)$ corresponds to the position command $r(t)$ without vibrations. The flexible arm is mounted on the direct drive rotary motor (encoder resolution: 20 bit/rev). The tip position $q(t, L)$ is obtained by a vision sensor (frame rate: 100 Hz). Equivalent resolution of tip position obtained by the vision sensor is 1.09×10^{-4} rad. Control program is written by C language under Real time

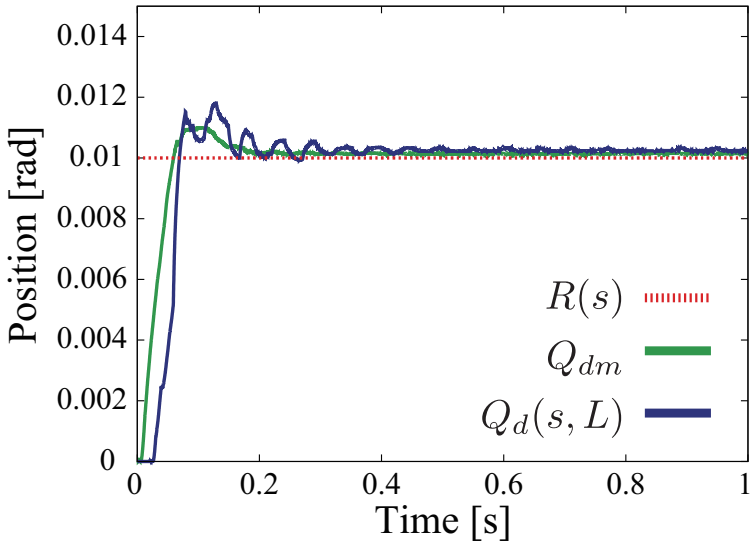

Fig. 6-23: Experimental results (without reflected wave rejection).

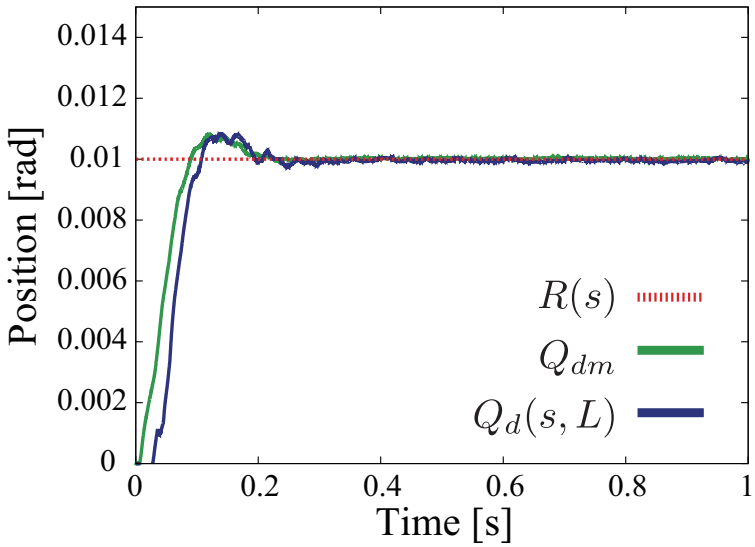

Fig. 6-24: Experimental results by the conventional reflected wave rejection.

application interface 3.8 (RTAI 3.8) on Linux.

Experimental parameters are shown in Table 6.5. Output delay at load side includes processing time of vision sensor ($T_l = 20$ ms). The input and output delays without the image processing delay is artificially generated in the computer. The jitters of input and output delays are not considered in this experiment. In this experiment, a step position command ($r(t) = 0.01$ rad) is applied to the control system.

The proposed method is compared with the conventional reflected wave rejection shown in Fig. 6-17.

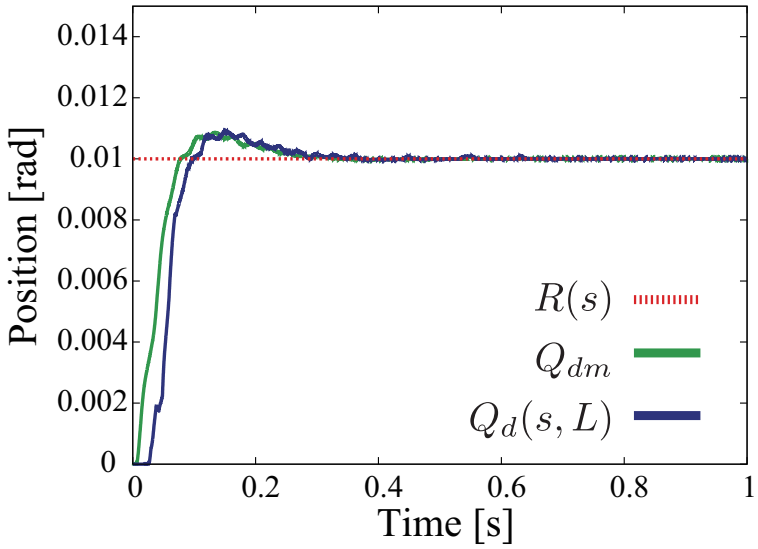

Fig. 6-25: Experimental results by the proposed reflected wave rejection.

Experimental Results

The experimental results are shown in Figs. 6-23–6-25. Fig. 6-23 shows the experimental results of the CDOB based method which does not implement vibration suppression for mechanical resonances. It is found that time delay is compensated and the system is stabilized, but vibration occurs at load side due to mechanical resonances.

Figs. 6-24 and 6-25 shows the results of the conventional and proposed reflected wave rejections. It turns out that the vibrations due to time delay and mechanical resonance are well suppressed by both two methods. Therefore, the proposed method achieves same vibration suppression performance as the conventional reflected wave rejection although the tip-position information is not used for control. In both two methods, the undesired overshoots are observed on the position responses. It is because the CDOB's filter degrades the transient performance instead of the performance of disturbance suppression. It is noted that, in these experiments, the results of the conventional and proposed reflected wave rejections do not have steady state error because those methods implements the high-pass filters in the CDOBs, which can suppress impulse disturbances. If there exists a step disturbance, steady state errors occur in responses of both methods.

Validity of the proposed reflected wave rejection is confirmed by these experimental results.

6.5 Summary of Chapter 6

This chapter explained the reflected wave rejection for an integrated resonant and time-delay system. In basic concept of the proposed approach, the mechanical resonant system implements the reflected wave rejection. Hence, the resonant system can be regarded as equivalent time-delay system because the transfer function of wave equation with reflected wave omitted is expressed as a time delay. Then, a second-order system (i.e. motor dynamics) with sum of actual and equivalent time delays is an equivalent plant model for the integrated system. The time delay in the above mentioned equivalent plant can be compensated by typical time-delay compensation methods at the same time. In addition, the basic concept for control of the integrated system was extended to the reflected wave rejection for integrated system which can be implemented at local (controller) side. Finally, the reaction-force-based reflected wave rejection for the integrated system was derived, which has advantage that control system can be implemented by using only motor position.

Chapter 7

Robust Control of Wave System

7.1 Introduction of Chapter 7

This chapter explains a wave-based disturbance observer for robust enhancement against disturbance. In the previous chapters, suppression of the disturbance acting on the tip is not considered in design of control with the reflected wave rejection. On the the other hand, it is noted that the disturbance acting on the motor is suppressed by the disturbance observer. Sensitivity function of typical reflected wave rejection shown in Chapter 3 implies that disturbance acting on the tip induces a steady state error. Hence, to realize robust control system, additional disturbance compensator should be implemented. The wave-based disturbance observer proposed in this chapter is an extension of arm disturbance observer [98] which is used in the field of control of a two-mass resonant system.

The contents of this chapter are as follows. Section 7.2 explains the modeling of the wave system considering disturbance acting on the tip. Section 7.3 describes the structure of wave-based disturbance observer. The control of wave system with reflected wave rejection and wave-based disturbance observer is analyzed in Section 7.4. Section 7.5 explains force control of wave system using wave-based disturbance observer as force estimator [100]. Finally, this chapter is summarized in Section 7.6.

Henceforth, the disturbance acting on the tip position is called a load disturbance.

7.2 Modeling of Wave System Considering Load Disturbance Position

The resonant system dealt with in this chapter is a one-link flexible arm shown in Fig. 7-1. In Fig. 7-1, $q(t,x)$, q_m, L, and f_l^{ext} denote the distributed position at x in t, the motor position, the length of

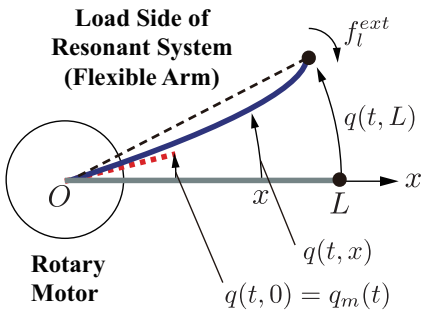

Fig. 7-1: Modeling of the resonant system based on wave.

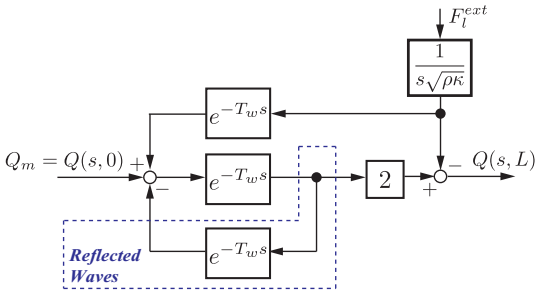

Fig. 7-2: Block diagram of resonant system modeled by wave equation.

the flexible arm, and the external load force acting on $x = L$, respectively. The controlled system is composed of a motor and one-link flexible arm. The control objective for the system is that the tip position $q(t, L)$ tracks the position command $R(s)$ without residual vibration and steady state error caused by the external force.

Firstly, modeling for the load side of the resonant system is explained. Load side of the resonant system means the one-link flexible arm without the motor located at boundary. It is assumed that the response of motor is not affected by the response of the load side because motor implements an acceleration control based on the DOB.

In this research, the resonant system is modeled by the wave equation, which is one of the distributed parameter model, in order to consider high-order vibrations. The wave equation is expressed as

$$\frac{\partial^2 q(t, x)}{\partial t^2} = c^2 \frac{\partial^2 q(t, x)}{\partial x^2} \tag{7.1}$$

where c denotes the propagation velocity of the wave. The boundary conditions for the resonant system

shown in Fig. 7-1 are represented as

$$q(t,0) = q_m(t) \tag{7.2}$$

$$\frac{\partial q(t,L)}{\partial x} = -\frac{1}{\kappa} f_l^{ext} \tag{7.3}$$

where κ denotes the spring coefficient per unit length. (7.2) means that the motor position, which is regarded as the input for the load side, is applied at $x = L$. It is noted that the motor position is not affected by the response of load side owing to the implementation of the DOB as shown in Chapter 2. On the other hand, (7.3) means that the external load force is applied at $x = L$. By using the above boundary conditions and wave equation, a transfer function can be derived as

$$Q(s,L) = G(s)Q_m + H(s)F_l^{ext} \tag{7.4}$$

where

$$G(s) = \frac{2e^{-T_w s}}{1+e^{-2T_w s}} \tag{7.5}$$

$$H(s) = -\frac{1}{s\sqrt{\rho\kappa}} \frac{1-e^{-T_w s}}{1+e^{-2T_w s}} \tag{7.6}$$

where s and ρ stand for the Laplace operator and the inertia/mass per unit, respectively. T_w stands for the propagation time of the wave, which is represented as $T_w = \frac{L}{c}$. From transfer functions (7.5) and (7.6), it turns out that there are time delay in the denominators of the transfer functions, and the tip position will vibrate. Block diagram of the load side of resonant system modeled as the wave equation is shown in Fig. 7-2. In Fig. 7-2, the negative feedback and block "2" mean the reflected waves. In addition, the reflected wave which is negative feedback part in Fig. 7-2 is a cause of the vibration. Therefore, if the reflected wave is rejected from the resonant system, the vibration will be suppressed as shown in the previous chapters.

If the reflected wave rejection is applied for the vibration suppression, the transfer function becomes

$$Q(s,L) = \frac{K_p}{s^2+K_v s+K_p} e^{-T_{wn} s} R(s) - \frac{1}{s\sqrt{\rho\kappa}}(1-e^{-2T_{wn} s}) F_l^{ext}. \tag{7.7}$$

According to the above equation, both transfer functions represented as (7.5) and (7.6) are stabilized by the reflected wave rejection. However, (7.7) implies that steady state error occurs by step disturbance F_l^{ext} because $\lim_{s\to 0}(1-e^{-2T_w s})/(s\sqrt{\rho\kappa}) = 2T_w/\sqrt{\rho\kappa}$.

7.3 Wave-based Disturbance Observer

As mentioned before, the vibration can be suppressed by using the reflected wave rejection-based vibration control under existence of disturbance acting on the tip. However, the reflected wave rejection does not have suppression of the external force and it leads to the steady state error. In addition, if there exists the error in T_{wn}, the performance of the reflected wave rejection degrades. Considering the above, this paper proposes the wave-based DOB for compensation of the external force and the parameter variation. Here, a load (arm) DOB is one of the DOB which is used in a two-mass resonant system. In other words, the wave-based DOB is a load (arm) DOB for wave equation which is resonant system comprising infinite numbers of mass and spring.

7.3.1 Structure

Before explaining the wave-based DOB, the load disturbance is defined. First of all, (7.4) is transformed into

$$\left(1+e^{-2T_w s}\right)Q(s,L) = 2e^{-T_w s}Q_m - \frac{1}{s\sqrt{\rho\kappa}}\left(1-e^{-T_w s}\right)F_l^{ext}. \tag{7.8}$$

Here, by introducing nominal time delays $e^{-T_{wn}s}$ and $e^{-2T_{wn}s}$, (7.8) can be transformed into

$$\left(1+e^{-2T_{wn} s}\right)Q(s,L) = 2e^{-T_{wn} s}Q_m - \frac{1}{s\sqrt{\rho\kappa}}\left(1-e^{-T_w s}\right)F_l^{ext} + Q^{err}. \tag{7.9}$$

where Q^{err} denotes the equivalent position response caused by the parametric uncertainty, and it is represented as

$$Q^{err} = 2e^{-T_w s}\left(1-e^{-(T_{wn}-T_w)s}\right)Q_m - e^{-2T_w s}\left(1-e^{-2(T_{wn}-T_w)s}\right)Q(s,L). \tag{7.10}$$

Finally, the following equation can be derived as

$$Q(s,L) = \frac{2e^{-T_{wn}s}}{1+e^{-2T_{wn}s}}Q_m - \frac{1}{1+e^{-2T_{wn}s}}Q_l^{dis} \tag{7.11}$$

where Q_l^{dis} is defined as a load disturbance in the wave system, which is represented as

$$Q_l^{dis} = \frac{1}{s\sqrt{\rho\kappa}}\left(1-e^{-T_w s}\right)F_l^{ext} - (1+e^{-2T_{wn}s})Q^{err}. \tag{7.12}$$

The above disturbance leads to degrade the vibration suppression performance. In addition, the disturbance induces the steady state error. To compensate the load disturbance represented as (7.12), the

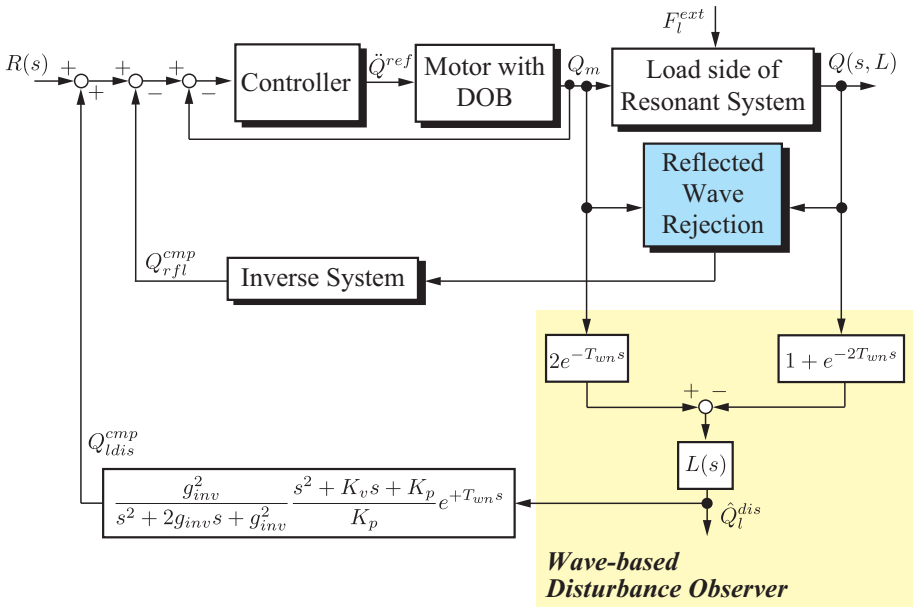

Fig. 7-3: Block diagram of load disturbance rejection based on the wave-based DOB.

wave-based DOB (WDOB) is proposed. The load disturbance is estimated through a low-pass filter $L(s)$, and the estimated load disturbance is represented as

$$\hat{Q}_l^{dis} = L(s)\left(2e^{-T_{wn}s}Q_m - (1+e^{-2T_{wn}s})Q(s,L)\right). \tag{7.13}$$

Block diagram of the load disturbance rejection based on the WDOB is shown in Fig. 7-3. The compensation value for the load disturbance, which is the estimated load disturbance multiplied inverse system of the resonant system without reflected wave and motor, is fed back to the position command. The compensation value is generated as

$$Q_{ldis}^{cmp} = \frac{g_{inv}^2}{s^2+2g_{inv}s+g_{inv}^2}\frac{s^2+K_vs+K_p}{K_p}e^{+T_{wn}s}\hat{Q}_l^{dis}. \tag{7.14}$$

Then, the actual load disturbance and estimated load disturbance are cancelled out. However, it is difficult to implement the control system shown in Fig. 7-3 due to difficulty of realization of the inverse system of time delay. If the inverse system of the time delay approximates "1", the compensation value is represented as

$$\tilde{Q}_{ldis}^{cmp} = \frac{g_{inv}^2}{s^2+2g_{inv}s+g_{inv}^2}\frac{s^2+K_vs+K_p}{K_p}e^{+T_{wn}s}\hat{Q}_l^{dis}. \tag{7.15}$$

By using the above compensation value, the steady state error caused by the external force can be eliminated, but the effect of parametric uncertainty can not be compensated well.

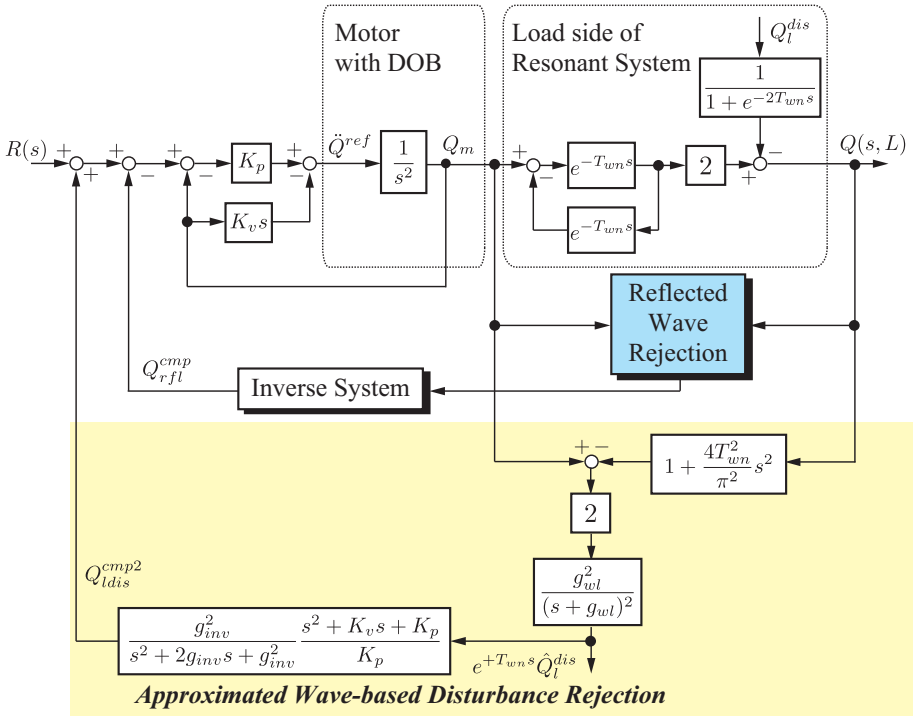

Fig. 7-4: Block diagram of the proposed control system with finite-approximated wave-based DOB for implementation (case of $n = 1$).

7.3.2 Implementation of Approximated WDOB

In this part, approximation of WDOB for robust enhancement of the parametric uncertainty is explained. In the approximation of WDOB, the compensation value for the load disturbance is directly calculated. the compensation value (7.14) without inverse system of the motor is represented as

$$\begin{aligned} e^{+T_{wn}s}\hat{Q}_l^{dis} &= e^{+T_{wn}s}L(s)\left(2e^{-T_{wn}s}Q_m - (1+e^{-2T_{wn}s})Q(s,L)\right) \\ &= L(s)\left(2Q_m - (e^{+T_{wn}s}+e^{-T_{wn}s})Q(s,L)\right). \end{aligned} \tag{7.16}$$

Here, the infinite product expansion of the hyperbolic cosine is introduced,

$$\begin{aligned} \cosh T_{wn}s &= \frac{e^{+T_{wn}s}+e^{-T_{wn}s}}{2} \\ &= \prod_{i=1}^{\infty}\left(1+\frac{T_{wn}^2}{\pi^2(n-\frac{1}{2})^2}s^2\right). \end{aligned} \tag{7.17}$$

By using the above, (7.16) is represented as

$$e^{+T_{wn}s}\hat{Q}_l^{dis} = 2L(s)\left[Q_m - \prod_{n=1}^{\infty}\left(1+\frac{T_{wn}^2}{\pi^2(n-\frac{1}{2})^2}s^2\right)Q(s,L)\right]. \tag{7.18}$$

Table 7.1: Simulation parameters for wave-based DOB.

Parameter	Description	Value
T_s	Sampling time	50 us
$\omega_1,\ \omega_2$	1st/2nd resonant frequencies	50, 150 rad/s
T_w	Propagation time of wave	$\pi/(2\omega_1)$ s
K_{tn}	Nominal force coefficient	1.18 Nm/A
J_n	Nominal inertia of motor	0.0035 kgm^2
K_p	Position gain	ω_{1n}^2
K_v	Velocity gain	$2.0\omega_{1n}$
T_{wn}	Nominal propagation time of wave	$\pi/(2\omega_{1n})$ s
g_{dis}	Cut-off frequency of DOB	3000 rad/s
g_r	Cut-off frequency of reflected wave rejection	2000 rad/s
g_{wl}	Cut-off frequency of WDOB	500 rad/s
g_{pd}	Cut-off frequency of pseudo derivation for velocity calculation	2000 rad/s
g_{inv}	Cut-off frequency of pseudo derivation for inverse system	1000 rad/s

If n equals to 1 in (7.18), approximated WDOB corresponds to the load DOB including the inverse system for a two-mass resonant system. Therefore, in other words, the WDOB is a generalized load DOB for the resonant system. In this part, the approximated WDOB with $n = 1$ is introduced, and the compensation value is represented as

$$Q_{ldis}^{cmp2} = \frac{g_{inv}^2}{s^2 + 2g_{inv}s + g_{inv}^2} \frac{s^2 + K_v s + K_p}{K_p} 2L_2(s) \left[Q_m - \left(1 + \frac{4T_{wn}^2}{\pi^2} s^2 \right) Q(s, L) \right] \quad (7.19)$$

where $L_2(s)$ denotes the low-pass filter which makes (7.19) be proper, and which is represented as

$$L_2(s) = \frac{g_{wl}^2}{(s + g_{wl})^2} \quad (7.20)$$

where g_{wl} denotes the cut-off frequency. The whole block diagram of the proposed method is shown in Fig. 7-4. Stability of the load disturbance compensations based on (7.14) and (7.19) are discussed in Section 7.4.

7.3.3 Numerical Results

Simulation Setup

In order to verify the effectiveness of the proposed method, simulations of position control on a three-mass resonant system are conducted. In this simulation, a step position command (0.005 rad/s) is applied to the controlled system. In order to check effect of the external force, the external force (0.01 Nm) is applied on the load side at $t = 0.25$. Simulation parameters are shown in Table 7.1. In order to check compensation of parameters, a nominal tip-position response, which is an equivalent time-delay system, in other words, is simulated. A nominal tip-position response is defined as

$$Q_l^{nom} = \frac{K_p}{s^2 + K_v s + K_p} e^{-T_{wn} s} R(s). \tag{7.21}$$

Simulation Results

Fig. 7-5 shows the simulation results of the reflected wave rejection when there is no difference between nominal and actual plant parameters. From Fig. 7-5, it is found that vibration on the load side is suppressed by the reflected wave rejection. In addition, the responses of tip position corresponds to the nominal equivalent time-delay system, which is written by a pink line. This means that the resonant system can be regarded as a equivalent time-delay system owing to the reflected wave rejection. After $t = 0.3$, steady state error is observed due to the external load force.

Fig. 7-6 shows the simulation results when the nominal 1st-order resonant frequency is 0.9 times as actual one. From Fig. 7-6(a), performance of vibration suppression degrades due to the parameter error. On the other hand, Fig. 7-6(b) shows that the wave-based observer compensates for both the parameter error and the external load force.

Fig. 7-7 shows the simulation results when the nominal 1st-order resonant frequency is 1.1 times as actual one. From Fig. 7-7(a), performance of vibration suppression degrades due to the parameter error as well as the results in Fig. 7-6(a). On the other hand, Fig. 7-6(b) shows that the wave-based observer compensates for the parameter error and the external load-force. Compared with results in Fig. 7-6, stability of the controlled system is decreased and vibration occurs. In actual implementation, it is better that nominal 1st-order resonant frequency is set smaller value than actual one from the point of view of the stability.

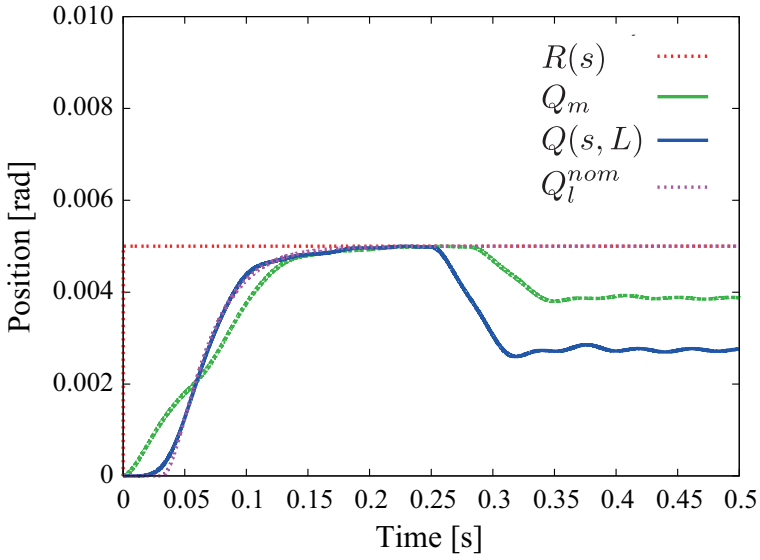

Fig. 7-5: Simulation results by the reflected wave rejection.

Table 7.2: Experimental parameters for wave-based DOB.

Parameter	Description	Value
T_s	Sampling time	50 us
$\tilde{\omega}_1$	Identified 1st resonant frequency	34.5 rad/s
ω_{1n}	Nominal 1st resonant frequency	$1.5\omega_1$ rad/s
T_w	Propagation time of wave	$\pi/(2\omega_{1n})$ s
K_{tn}	Nominal force coefficient	1.18 Nm/A
J_n	Nominal inertia of motor	0.0035 kgm^2
K_p	Position gain	ω_{1n}^2
K_v	Velocity gain	$3.0\omega_{1n}$
T_{wn}	Nominal propagation time of wave	$\pi/(2\omega_{1n})$ s
g_{dis}	Cut-off frequency of DOB	2000 rad/s
g_r	Cut-off frequency of reflected wave rejection	175 rad/s
g_{wl}	Cut-off frequency of WDOB	60 rad/s
g_{inv}	Cut-off frequency of pseudo derivation for inverse system	150 rad/s

7.3.4 Experiments

Experimental Setup

In this section, the experiments are conducted to verify the validity of the proposed method. The flexible arm system used in this experiments is same as the flexible arm shown in Fig. 3-15. The tip

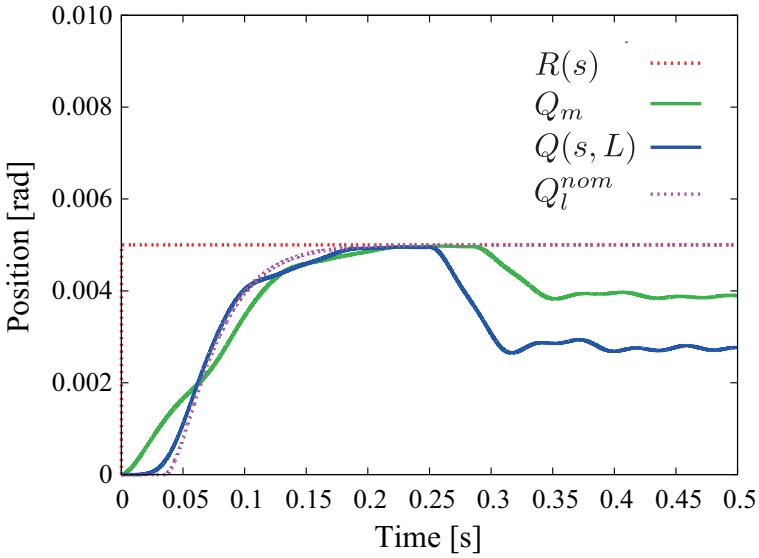

(a) Without WDOB

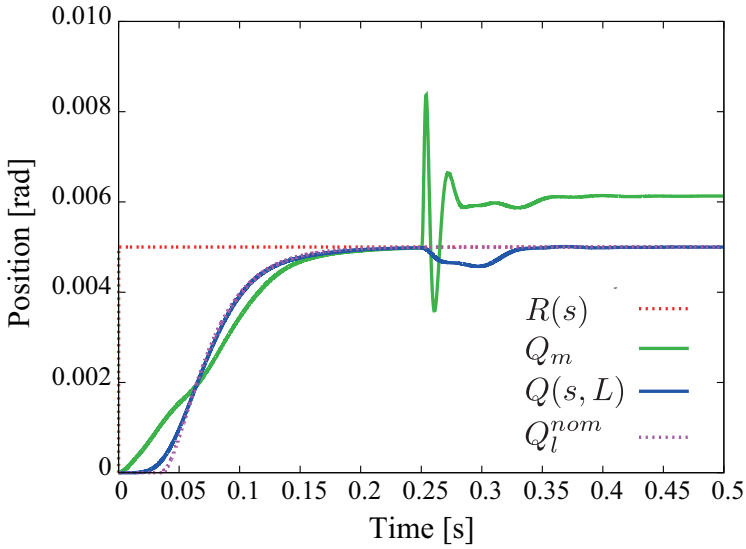

(b) With WDOB

Fig. 7-6: Simulation results by reflected wave rejection with/without wave-based DOB ($\omega_{1n} = 0.9\omega_1$).

position is obtained by using the position sensitive detector (PSD) and laser diode. The motor position is measured by position encoder. The real-time control system is realized by Linux OS with real-time application interface (RTAI 3.7).

The experimental parameters are shown in Fig. 7.2. In the experiments, a step command ($r(t) = 0.005$ rad) is applied to the system at $t = 2.0$.

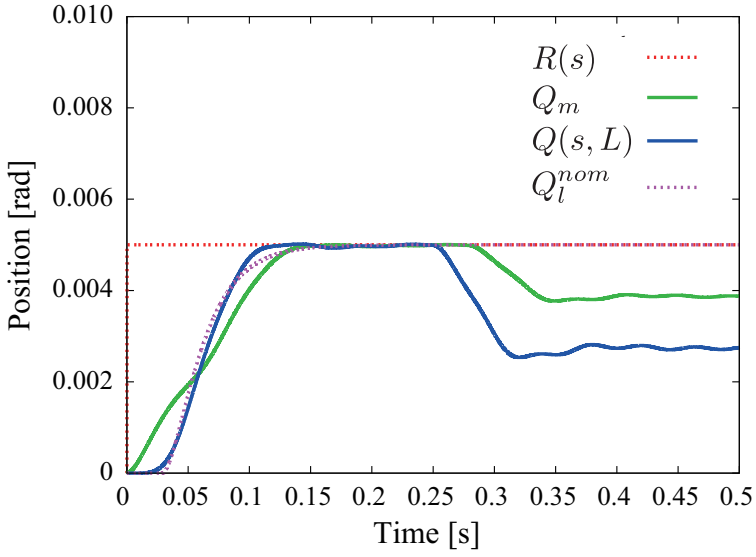

(a) Without WDOB

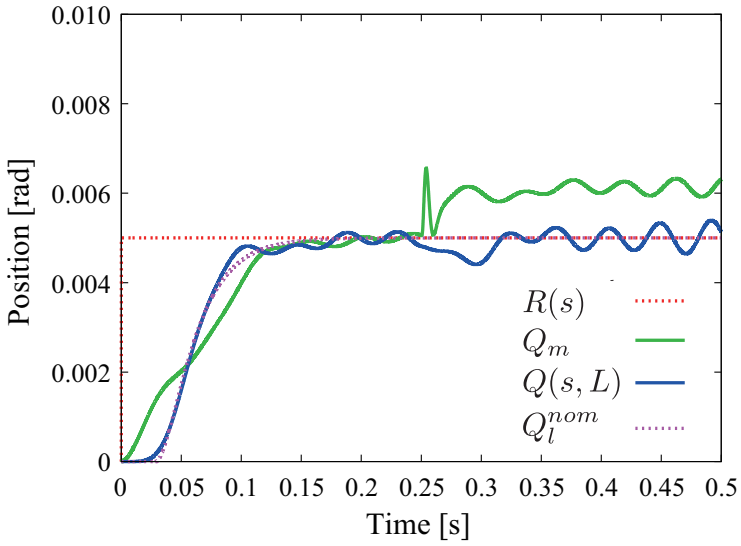

(b) With WDOB

Fig. 7-7: Simulation results by reflected wave rejection with/without wave-based DOB ($\omega_{1n} = 1.1\omega_1$).

Experimental Results

Experimental results of the reflected wave rejection with/without WDOB are shown in Fig. 7-8. From Fig. 7-8(a), the performance of the reflected wave rejection degrades because the nominal propagation time is different from the actual (identified) one. On the other hand, from Fig. 7-8(b), it is found that the WDOB compensates for the parametric uncertainty in the propagation time and the tip-position response

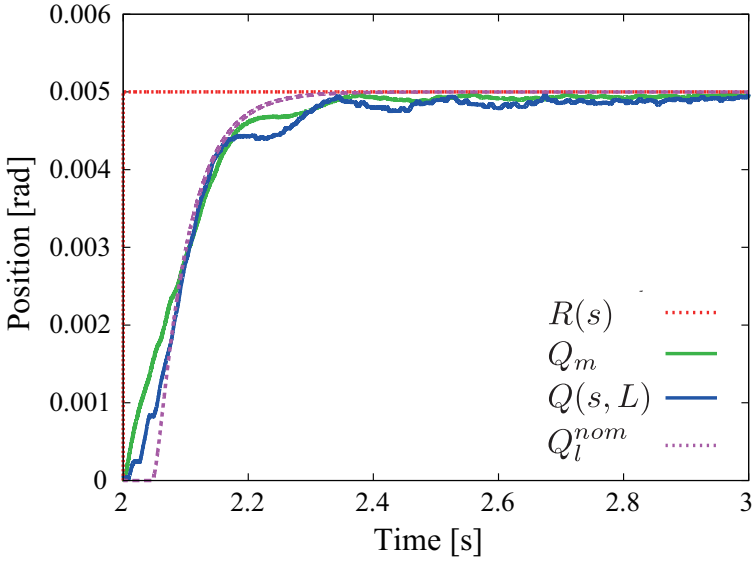

(a) Without WDOB

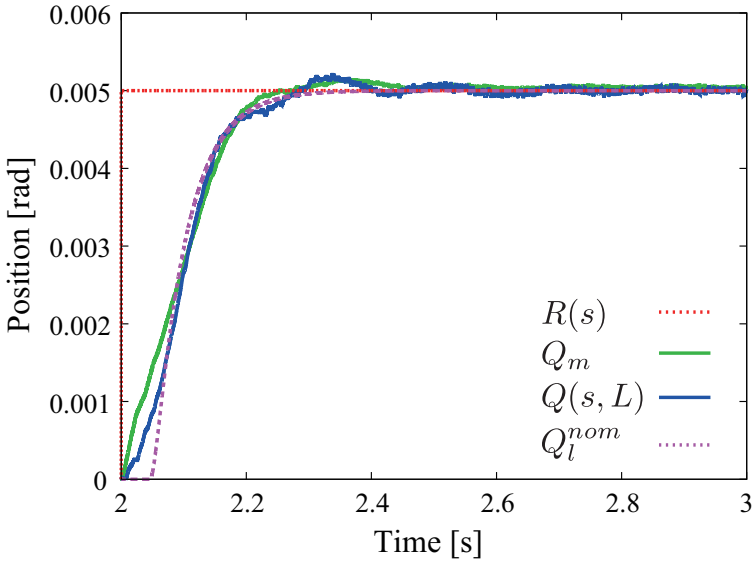

(b) With WDOB

Fig. 7-8: Experimental results by reflected wave rejection with/without WDOB.

$Q(s,L)$ is close to the response Q_l^{nom}. In addition, it also turns out that WDOB can eliminate the steady state error. The root mean square errors between $Q(s,L)$ and Q_l^{nom} of Figs. 7-8(a) and (b) are 2.1739×10^4 rad and 1.4703×10^4 rad, respectively. Therefore, the validity of the proposed method can be confirmed by the experimental results.

7.4 Analysis and Experimental Validation of WDOB-Based Disturbance Rejection with Approximation

7.4.1 Analysis based on Frequency Response

As mentioned in previous part, the reflected wave rejection-based control does not have load disturbance suppression performance at low-frequency area. This part analyzes sensitivity and complementary sensitivity functions of reflected wave rejection control with WDOB. The two methods are analyzed as follow,

- Method 1: WDOB, shown in Fig. 7-3, with an approximated inverse system $e^{T_{wn}s} \approx 1$,
- Method 2: Approximated WDOB, shown in Fig. 7-4, by using the finite-order model (7.19).

The open-loop transfer functions of the methods 1 and 2 are represented as

$$G_o^{WDOB} = \frac{1}{2}\frac{F_{r2}G_m}{1-F_{r2}L_w e^{-T_{wn}s}} G_w(s) G_m^{inv}\left[L_{inv}L_w(1+e^{-2T_{wn}s}) - F_{r1}e^{-T_{wn}s}\right] \quad (7.22)$$

$$\tilde{G}_o^{WDOB} = \frac{1}{2}\frac{F_{r2}G_m}{1-F_{r2}L_w} G_w(s) G_m^{inv}(L_{inv}L_w\tilde{G}_w^{inv} - F_{r1}e^{-T_{wn}s}) \quad (7.23)$$

where

$$F_{r1} = \frac{g_r}{s+g_r} \quad (7.24)$$

$$F_{r2} = \frac{2s+2g_r}{s+2g_r} \quad (7.25)$$

$$G_w(s) = \frac{2e^{-T_w s}}{1+e^{-2T_w s}} \quad (7.26)$$

$$G_m = \frac{K_p + K_d s}{s^2 + K_v s + K_p} \quad (7.27)$$

$$G_m^{inv} = \frac{s^2 + K_v s + K_p}{K_p + K_d s} \quad (7.28)$$

$$L_{inv} = \frac{g_{inv}^2}{s^2 + 2g_{inv}s + g_{inv}^2} \quad (7.29)$$

$$\tilde{G}_w^{inv} = \left(1 + \frac{4T_{wn}^2}{\pi^2}s^2\right). \quad (7.30)$$

By using the above, the sensitivity and complementary sensitivity function of each method can be calculated.

Fig. 7-9 shows the bode and Nyquist diagrams of sensitivity and complementary sensitivity functions of the methods 1 and 2. In case of Fig. 7-9, the cut-off frequency g_w is set as lower value than the

first-order resonant frequency ($g_w = 0.5\omega_1$). In this case, Fig. 7-9(a), both methods 1 and 2 realize good sensitivity function which has a gain at low-frequency area is small. Therefore, it is found that the load disturbance can be suppressed by both WDOB. In addition, from Figs. 7-9(a) and (b), complementary sensitivity function and stability does not degrade so much. Fig. 7-10 shows the bode and Nyquist diagrams of the methods 1 and 2 when the cut-off frequency g_w is set as higher value than the first-order resonant frequency ($g_w = 1.5\omega_1$). In this case, from Fig. 7-10(a) and (b), it is found that both complementary sensitivity and sensitivity functions of method 2 degrades. In addition, stability of method 2 gets worse than case of $g_w = 0.5\omega_1$ from Fig. 7-10(c). On the other hand, the method 1 dose not degrade the stability and sensitivity sensitivity function compared with case of $g_w = 0.5\omega_1$. However, complementary sensitivity function at low-frequency area degrades compared with case of $g_w = 0.5\omega_1$.

According the above analytical results, considering the stability, method 1 is superior to method 2. In contrast, under the condition of $g_w < \omega_1$, the method 2 has good robust performance. However, if there is variation in ω_1 and $g_w < \omega_1$ is not satisfied, the stability of method 2 becomes worse.

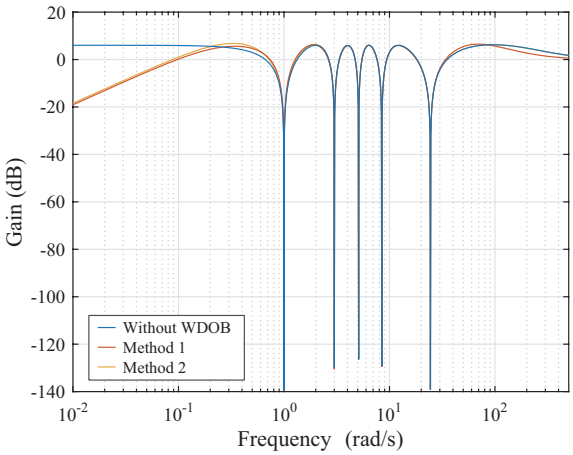

(a) Sensitivity function

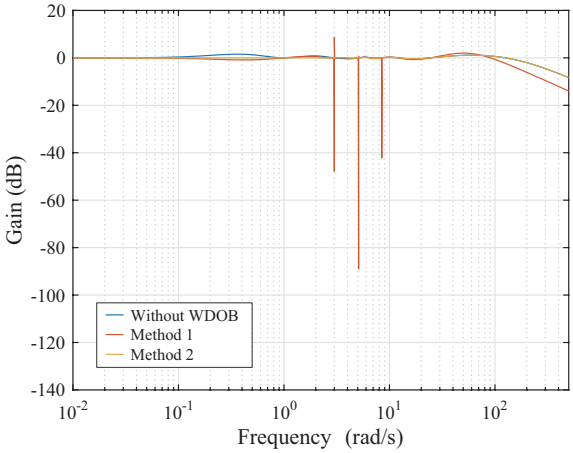

(b) Complementary sensitivity function

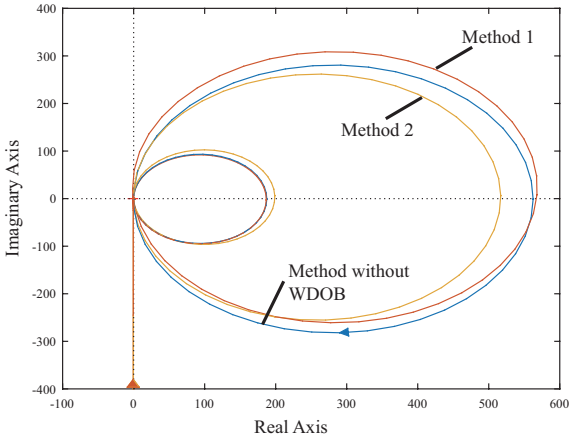

(c) Nyquist diagram

Fig. 7-9: Bode and Nyquist diagrams of reflected wave rejection with WDOBs ($g_w = 0.5\omega_1$).

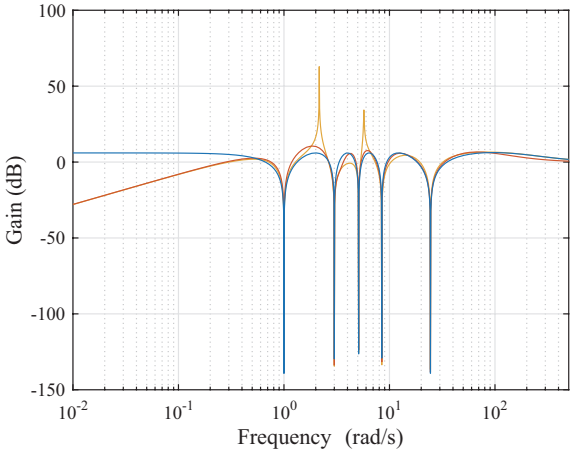

(a) Sensitivity function

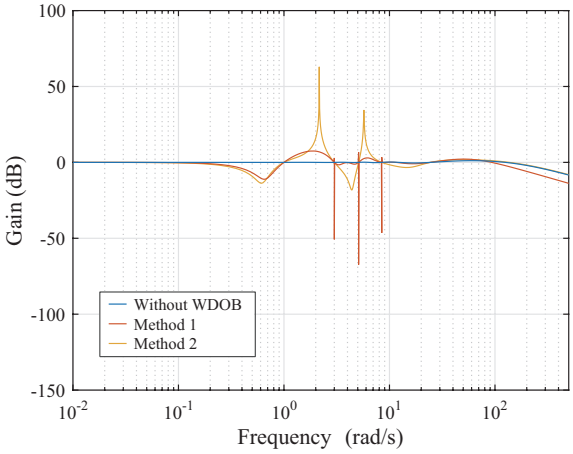

(b) Complementary sensitivity function

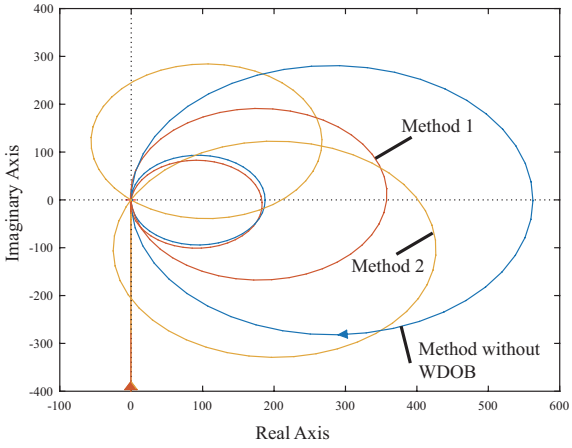

(c) Nyquist diagram

Fig. 7-10: Bode diagram of sensitivity and complementary function of reflected wave rejection with WDOBs ($g_w = 1.5\omega_1$).

Table 7.3: Parameters for experimental validation of wave-based DOB with approximations.

Parameter	Description	Value
T_s	Sampling time	50 us
$\tilde{\omega}_1$	Identified 1st resonant frequency	38.5 rad/s
ω_{1n}	Nominal 1st resonant frequency	$1.0\omega_1$ rad/s
T_w	Propagation time of wave	$\pi/(2\omega_{1n})$ s
K_{tn}	Nominal force coefficient	1.18 Nm/A
J_n	Nominal inertia of motor	0.0035 kgm^2
K_p	Position gain	ω_{1n}^2
K_v	Velocity gain	$3.0\omega_{1n}$
T_{wn}	Nominal propagation time of wave	$\pi/(2\omega_{1n})$ s
g_{dis}	Cut-off frequency of DOB	2000 rad/s
g_r	Cut-off frequency of reflected wave rejection	55 rad/s
g_{inv}	Cut-off frequency of pseudo derivation for inverse system	80 rad/s
ω_n	Poles design by state feedback control	48.0

7.4.2 Experimental Validation

Experimental Setup

In this part, the analytical results shown in previous part are confirmed by experiments. The experimental setup is same as the system shown in Fig. 3-15. In this experiment, the step command ($r(t) = 0.01$ rad) is applied to the control system.

Experimental parameters are shown in Table 7.3. In this experiment, performances of the method 1 and the method 2 are compared. The method 2 uses a first-order approximation ($n = 1$) in (7.18). In addition, the fully closed-loop state feedback control shown in Fig. 3-16 is also compared with the proposed method. The control gains in the fully closed-loop state feedback control are determined according to (3.42)–(3.48), and ω_n is set so that time constant equals to that of the proposed method.

Experimental Results

Fig. 7-11 shows the experimental results of method 1 and method 2 when the cut-off frequency of WDOB is lower than the first-order resonant frequency ($g_w = 20.0 \approx 0.5\omega_1$). It is found that the vibrations are well suppressed by the reflected wave rejection and steady state error is eliminated in both two methods. Fig. 7-12 shows the experimental results of method 1 and method 2 when the cut-off

frequency of WDOB is closed to the first-order resonant frequency ($g_w = 40.0 \approx 1.0\omega_1$). In this case, it can be observed that the response of method 2 becomes worse compared with Fig. 7-11(a). These experimental results correspond to the analytical results.

Next, the proposed method is compared with the fully closed-loop state feedback control. Experimental results of the fully closed-loop state feedback control are shown in Fig. 7-13. From Fig. 7-13, the time constant of the state feedback control is almost same as the response of proposed method shown in Fig. 7-12(a). Additionally, the steady state error does not occur owing to the integrator. However, it is found that the second order resonant frequency is excited, which means the spillover occurs. Hence, the fully closed-loop state feedback control shown in Fig. 3-16 is needed to design additional stabilization compensator for control of this plant, which makes the system complex.

According to the above, it is confirmed that, considering the stability, the method 1 should be used for the wave system because the spillover problem can be avoided.

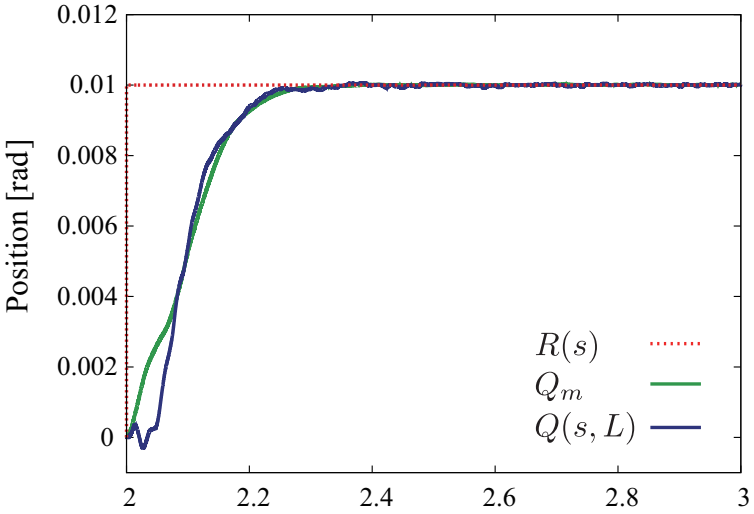

(a) Method 1

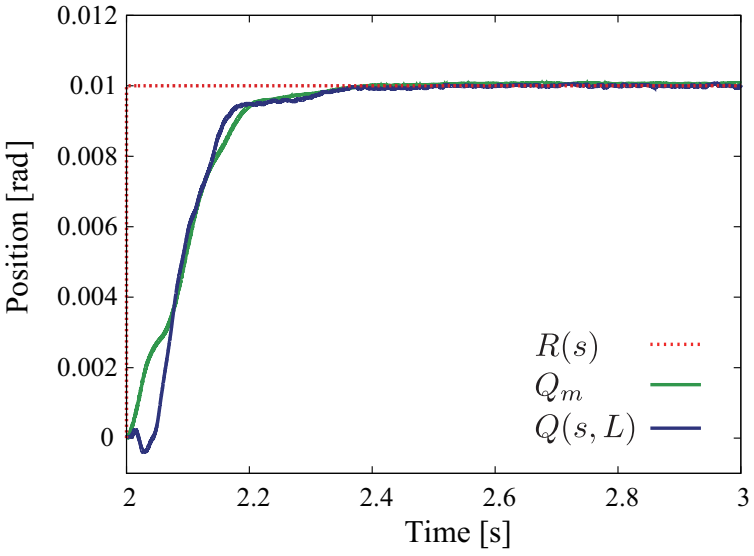

(b) Method 2

Fig. 7-11: Experimental results of position responses when cut-off frequency is $g_w = 20.0 \approx 0.5\omega_1$.

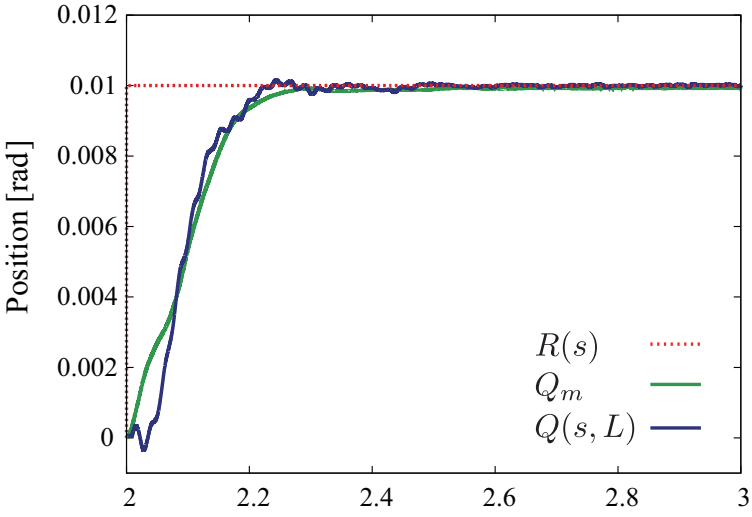

(a) Method 1

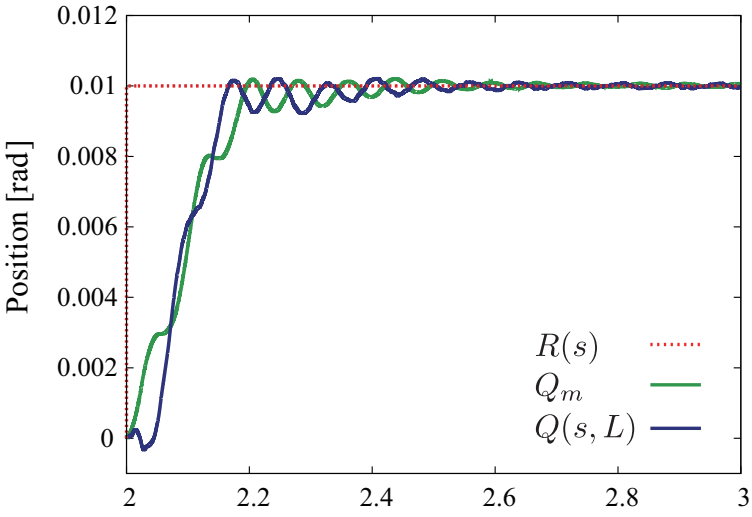

(b) Method 2

Fig. 7-12: Experimental results of position responses when cut-off frequency is $g_w = 40.0 \approx 1.0\omega_1$.

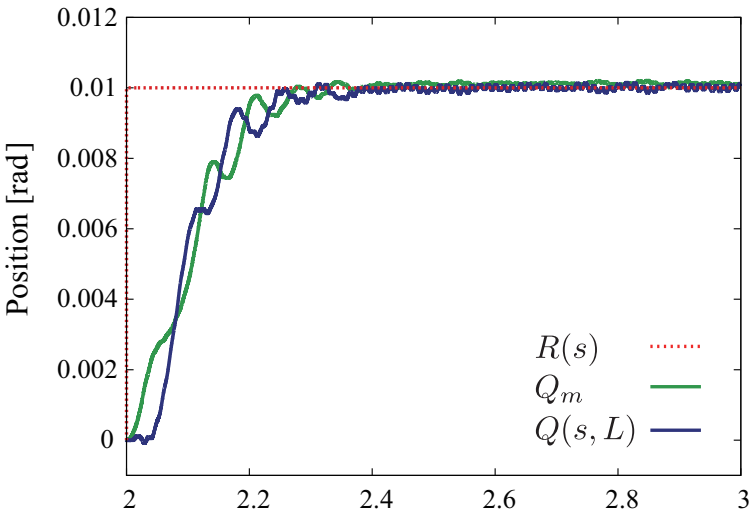

Fig. 7-13: Experimental results of state feedback control ($\omega_n = 1.2$).

7.5 Application to Force Control

The WDOB which is described in previous section can estimate the load disturbance including the load-external force. Therefore, by using the estimated load-external force, the force control of load-external force can be constructed. This section introduces how to design the force control system of wave system based on WDOB.

7.5.1 Estimation of Environmental Force Based on WDOB

In this section, estimation of the environmental force is explained. First of all, it is assumed that there is no modeling error of the propagation time of the wave. By using the assumption, the load disturbance can be represented as

$$Q_l^{dis} = \frac{1}{s\sqrt{\rho\kappa}} \left(1 - e^{-T_w s}\right) F_l^{env}. \tag{7.31}$$

Here, it is assumed that the environmental force is a step force ($sF_l^{env} = 0$). Therefore, (7.31) can be transformed into

$$\begin{aligned} Q_l^{dis} &= \frac{T_w s - \frac{1}{2}(T_w s)^2 + \cdots}{s\sqrt{\rho\kappa}} F_l^{env} \\ &= \frac{T_w - \frac{1}{2}T_w^2 s + \cdots}{\sqrt{\rho\kappa}} F_l^{env} \\ &\approx \frac{T_w}{\sqrt{\rho\kappa}} F_l^{env}. \end{aligned} \tag{7.32}$$

Therefore, the environmental force is estimated by

$$\begin{aligned} \hat{F}_l^{env} &= \frac{\sqrt{\rho\kappa_n}}{T_{wn}} \hat{Q}_l^{dis} \\ &= \frac{c_n\sqrt{\rho_n\kappa_n}}{L_n} \hat{Q}_l^{dis}. \end{aligned} \tag{7.33}$$

7.5.2 Force Control of Wave System

Structure

The whole block diagram of the proposed force control of wave system is shown in Fig. 7-14. K_f, F^{cmd}, and $Z_e(s)$ stand for the force gain and the force command, and the environmental impedance,

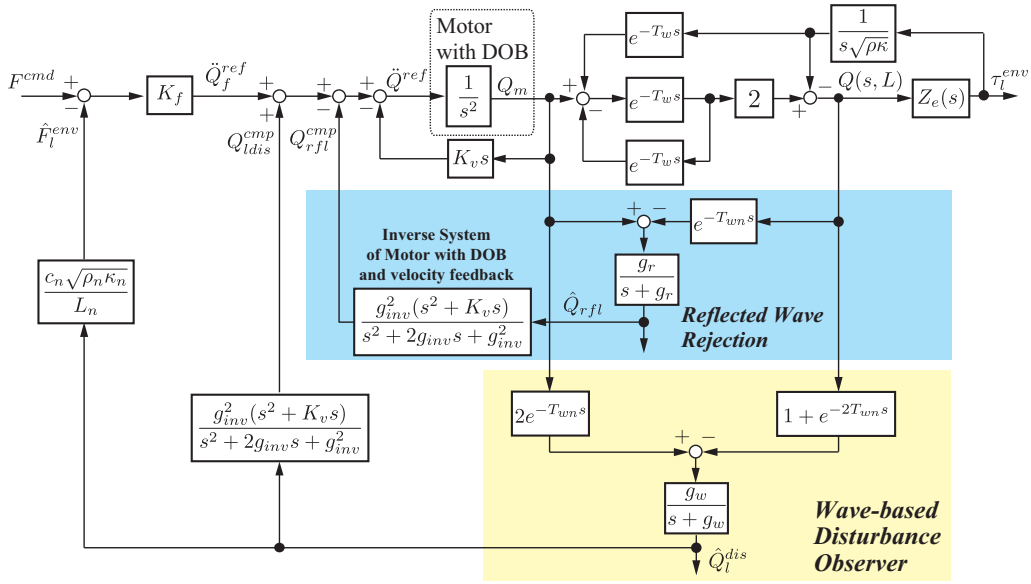

Fig. 7-14: Whole block diagram of the proposed force control of wave system.

respectively. The proposed force control utilizes the reflected wave rejection in inner loop, and the load disturbance rejection based on WDOB. The force controller represents a proportional controller, the acceleration reference applied to the motor is represented as

$$\ddot{Q}^{ref} = K_f(F^{cmd} - \hat{F}_l^{env}) - K_v s Q_m + \ddot{Q}_{ldis}^{cmp} - \ddot{Q}_{rfl}^{cmp}. \tag{7.34}$$

If the each cut-off frequency is enough high value, the transfer function from F^{cmd} to F_l^{env} is represented as

$$\frac{F_l^{env}}{F^{cmd}} = \frac{K_f Z_e(s)}{s^2 + K_v s + K_f Z_e(s) e^{-T_{wn} s}}. \tag{7.35}$$

From (7.35), there is a time delay in the denominator of the transfer function. Therefore, there exists possibility of making the controlled system unstable. It is noted that, if the environmental impedance can be known, we can utilize the time-delay compensation method (e.g. a CDOB). However, in general, environmental impedance is unknown parameter in force control systems.

Parameter Design

This part explains the design of control parameters (K_v and K_f). The control gains are determined based on open-loop transfer function. If the cut-off frequencies of reflected wave rejection and WDOB

are enough high values, the open-loop transfer function is derived as

$$G_o = \frac{K_f Z_e(s)}{s(s+K_v)} e^{-T_{wn}s}. \tag{7.36}$$

For the sake of simplicity, it is assumed that $Z_e(s) = K_e$ where K_e denotes the stiffness of the environment. If K_v equals to ∞, it can be approximated as $G_o \approx \tilde{G}_o = K_e K_f e^{-T_{wn}s}/s$. In this case, because $T_{wn} = \frac{\pi}{2\omega_1}$, phase delay at first-order resonant frequency equals to -180 degree. In addition, phase characteristics of the approximated transfer function is represented as

$$\angle \tilde{G} = -\frac{\pi}{2} - T_{wn}\omega. \tag{7.37}$$

Therefore, if the desired phase margin is set as P_m degree, the force gain should be set as

$$K_f = \frac{1}{K_e T_{wn}} \left(-\frac{\pi}{2} + P_m \frac{\pi}{180} \right). \tag{7.38}$$

In actual case, because the environment has often the damper term, the above gain is very conservative. Therefore, after conducting the performance test with gain (7.38), the force gain should be increased by cut and try. The design of the control gains are following procedure:1) The velocity is set as higher value than the first-order resonant frequency ω_1, 2) The maximum stiffness of the environment K_e is set, 3) The force gain is set as (7.38), 4) The force gain increases as long as relative stability of the control system is satisfied.

The advantage of the proposed method is that high-order resonances are suppressed by the reflected wave rejection. However, as mentioned in the above, bandwidth of the force control of the wave system is limited to up to the first-order resonant frequency. In addition, the maximum stiffness which can be dealt with in force control system is also limited. The method which increases the bandwidth of the force control is that the nominal value T_{wn} in the WDOB should be changed to smaller value than the actual one. However, it leads to violate the stability of the control system. The stability of the change of the nominal value will be considered in the future work.

7.5.3 Experiments

Experimental Setup

In order to verify the effectiveness of the proposed method, force control of the flexible arm is conducted. In this experiment, the step force command (0.05 Nm) is applied to the system and tip position contacts to an environment. A sponge is used as the environment in the experiments. Experimental setup

Table 7.4: Experimental parameters for force control of wave system.

Parameter	Description	Value
T_s	Sampling time	50 us
ω_{1n}	1st resonant frequency	40.1 rad/s
ω_{2n}	2nd resonant frequency	250.1 rad/s
T_w	Propagation time of wave	$\pi/(2\omega_1)$ s
K_{tn}	Nominal force coefficient	1.18 Nm/A
J_n	Nominal inertia of motor	0.0035 kgm^2
K_f	Force gain	100.0
K_v	Velocity gain	$1.5\omega_{1n}$
T_{wn}	Nominal propagation time of wave	$\pi/(2\omega_{1n})$ s
g_{dis}	Cut-off frequency of DOB	2000 rad/s
g_r	Cut-off frequency of reflected wave rejection	65 rad/s
g_{wl}	Cut-off frequency of WDOB	50 rad/s
g_{pd}	Cut-off frequency of pseudo derivation for velocity calculation	2000 rad/s
g_{inv}	Cut-off frequency of pseudo derivation for inverse system	150 rad/s
$\frac{c_n\sqrt{\rho k}}{L_n}$	Conversion gain for estimation of environmental force	4.22 Nm/rad

is shown in Fig. 7-15. The definitions of angles q_m and $q(t, L)$ are accordance with those described in section 2.2.2. The flexible arm is mounted on the direct drive rotary motor. The motor position q_m is obtained by the encoder (2^{20} pulse/rev.). The tip position $q(t, L)$ is obtained by the position sensitive detector (PSD). Control program is running on the Linux OS with RTAI 3.8.1.

Experimental parameters are shown in Table 7.4. The proposed method is compared with force control based on the resonant ratio control with load DOB [57]. The control parameters are adjusted by cut and try so that time constant of the conventional method are same as that of the proposed method. The parameters are shown in Table 7.5.

Experimental Results

Experimental results of force control are shown in Figs. 7-16 and 7-17. From Fig. 7-16, the first-order order resonance is well suppressed by the resonant ratio control. However, it is found that vibrations due to the second-order resonance are excited because the conventional method does not consider the high-

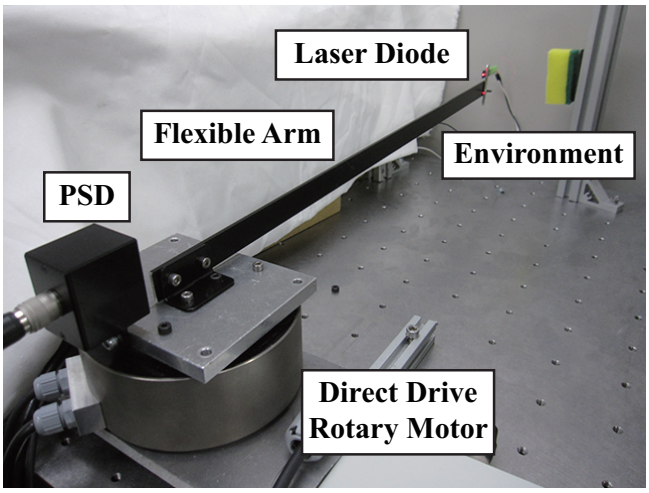

Fig. 7-15: Experimental setup.

Table 7.5: Control parameters for the conventional method.

Parameter	Description	Value
K_{sn}	Nominal spring coefficient	8.44 Nm/rad
J_{ln}	Nominal load inertia	K_{sn}/ω_{1n}^2 kgm^2
K_f	Force gain	500.0
K_v	Velocity gain	$4.0\omega_{1n}$
K_r	Reaction force gain	$5.0/J_{ln}$
g_{dis}	Cut-off frequency of DOB	2000 rad/s
g_l	Cut-off frequency of Load DOB	50 rad/s
g_{inv}	Cut-off frequency of pseudo derivation for inverse system	100 rad/s

order vibrations. Therefore, it is needed for the conventional method to decrease the force gain in order to suppress the vibration. On the other hand, Fig. 7-17 shows that the proposed method suppresses both first-order and second-order vibrations, although the time constant is same as that of the conventional method. Therefore, the validity of the proposed method is verified.

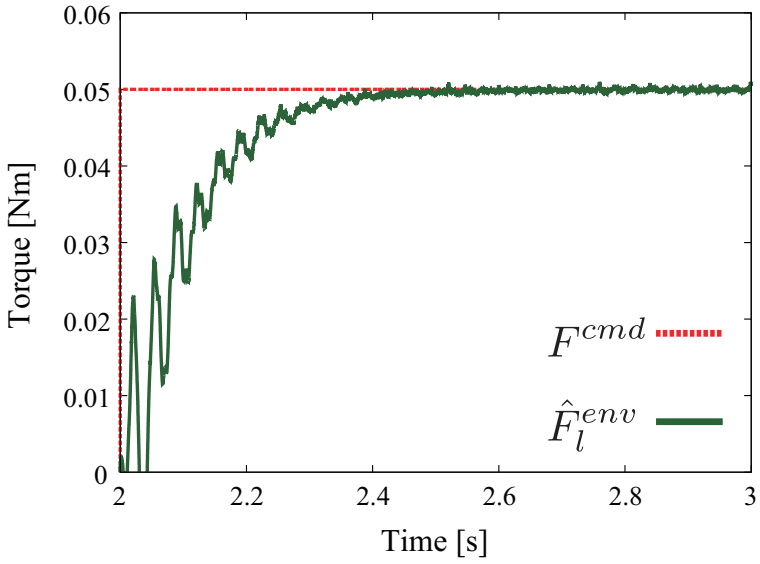

Fig. 7-16: Experimental results of the conventional force control by resonant ratio control [57].

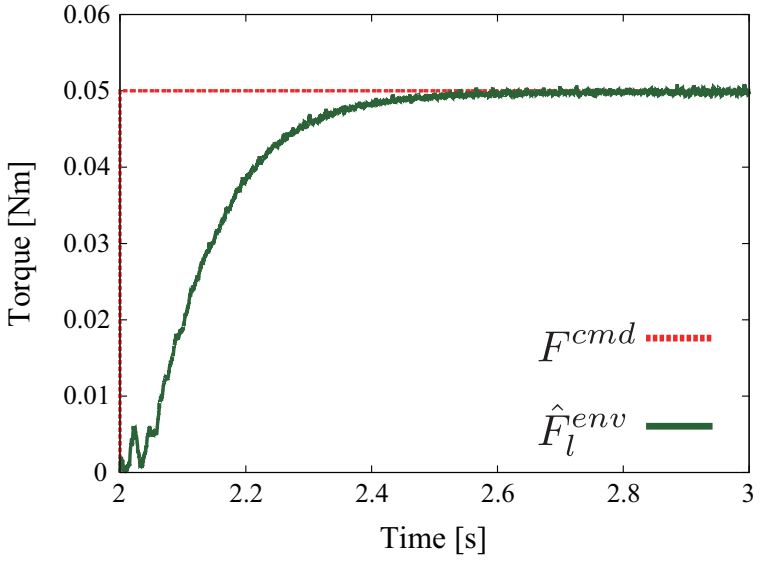

Fig. 7-17: Experimental results of force control by the proposed method.

7.6 Summary of Chapter 7

In this chapter, a wave-based disturbance observer (WDOB) was proposed for robust enhancement against the disturbance acting on the tip which is called load disturbance in this chapter. The WDOB is a extension of arm DOB which is used in the field of control of two-mass resonant system or multi-mass resonant system. However, there is difficulty in the implementation because the WDOB based disturbance compensation includes the inverse system of time delay $e^{+T_{wn}s}$. Hence, two approximation methods are described: one is to approximate the inverse system of time delay to 1, the other is use of finite-dimension approximation. The WDOB with those approximation is analyzed by the sensitivity and complementary sensitivity functions and Nyquist diagram. Although WDOB with finite-dimension approximation has better robust performance than approximation of $e^{+T_w s} \approx 1$ because the approximation includes the phase-lead effect of $e^{+T_w s}$, the cut-off frequency of WDOB should be set lower than maximum-order resonant frequency which is considered in the approximation, otherwise control system becomes unstable. Considering variation of resonant frequency, the WDOB with approximated inverse system of time delay 1 should be used.

Chapter 8

Conclusions

This dissertation proposed a control of wave systems based on the reflected wave rejection. Recent progress in performance of computer and control techniques has contributed to rapid and accurate control of industrial machines and robots. However, the rapid movements excites the mechanical resonances, which prevents the machines and robots from further improvement of rapidness and accuracy. Although typical vibration-control methods, such as control of a two-mass resonant system, have clear physical-meaning and simple control structure, the compensator considering spillover, which is to make the control system vibrate by neglected high-order vibrations, has to be designed. As a result, a total controller including stabilizing compensator for spillover has often become complex and high order. In addition, time delay included in communication system or DA converter decreases phase margin of the controlled system, and it also induces vibrations. Although time-delay can be neglected at low-frequency area, it should be considered at high-frequency area for realizing fast and accurate tracking control system. Therefore, in order to realize the further rapid and accurate motion of machines and robots, vibration suppression of mechanical resonance and time-delay compensation should be considered in control design. Under such background, in this dissertation, both the mechanical resonant and time-delay systems, which induce vibrations, are modeled as wave systems based on the wave equation. By using the wave equation in modeling of those systems, the infinite number of resonances (or poles) can be considered. In addition, the modeling based on the wave equation clarifies the similarity between those systems: the wave systems are composed of a position-input system and a wave-transmission system, a cause of vibration is a reflected wave in the wave systems. Therefore, to suppress the vibrations, the reflected wave rejection is proposed for both mechanical resonant and time-delay systems. The reflected wave

rejection is a core technique in this dissertation. In addition, owing to apply the reflected wave rejection to the mechanical resonant system, there exists only traveling wave in the system which implies that the mechanical resonant system can be regarded as an equivalent time-delay system. Hence, it is easy to integrate the mechanical resonant system and time-delay system. Then, the integrated resonant and time-delay system can be compensated by typical time-delay compensation methods (e.g. Smith predictor, communication disturbance observer). The above items are main contributions of this dissertation.

In Chapter 2, both mechanical resonant and time-delay systems were modeled by using a wave equation. As for the mechanical resonant system, application of a disturbance observer makes the transfer function simple, which is composed of time-delay elements. Structures of wave transmission in both systems were revealed from the transfer functions, and it was explained that there exists similarity between mechanical resonant and time-delay systems from the wave-transmission point of view. In addition, it was clarified that causes of vibrations are reflected waves in the wave systems.

In Chapter 3, a basic structure of how to eliminate the reflected wave from the wave systems to suppress the vibrations was proposed. The reflected wave rejection scheme is composed of a reflected wave estimator and a feedforward compensator for the reflected wave. Because the estimator and compensator use time-delay elements and the inverse system of motor, it is possible to implement the infinite-dimensional compensator without finite-dimensional approximation. Hence, the spillover problem can be avoided in the proposed method. Additionally, the effect of the reflected wave rejection is analyzed from both physical and control-theoretical points of view. From the theoretical point of view, the reflected wave rejection is equivalent to infinite series of phase lead and lag compensators. Therefore, its sensitivity function implies that the reflected wave rejection scheme has some robustness against variation of resonant frequencies, which is different from that of gain-stabilization method such as a notch filter.

In Chapter 4, the reflected wave rejection was applied to various mechanical resonant systems which have different boundary conditions and wave-transmission characteristics. In addition, the appropriate structures of reflected wave rejection for such resonant systems were proposed. First of all, the reflected wave rejection considering damper effect was proposed. Considering the damper in wave equation, time-delay elements change to time-delay-like elements whose time delay depends on frequency. For the implementation, a reaction-force-based reflected wave rejection with fractional-order low-pass filter was described. By using the proposed method, flexibility in control design improves because consideration of damper effect alleviates a restriction in wave model whose the poles (resonances) are located at regular

intervals on the imaginary axis. In the design of the reflected wave rejection, the compensation value generated by the typical reflected wave rejection is transformed by using a estimated reaction force from the wave system. Owing to the transformation, it is possible to calculate the compensation value for the reflected wave including damper effect by using the fractional-order low-pass filter. Finally, the reflected wave rejection considering mass on tip was proposed. In the industrial application, there exist cases that some loads are mounted on the drive system. Considering the above cases, the tip mass was considered in boundary condition at the end of wave system. The effect of mass produces a transfer function having all-pass characteristic. Therefore, a proposed reflected wave rejection in this part includes the all-pass filter generated by effect of mass. In addition, considering amplifying noise effect by the derivation, positive delay-feedback structure is introduced.

In Chapter 5, the reflected wave rejection for time-delay system is proposed. The relevance between the proposal and typical time-delay compensation methods, which are Smith predictor and communication disturbance observer, were clarified. It turned out that, from the point of view of wave, the proposal and typical time-delay compensation methods are same because the compensation value for time delay in each method is same, but the disturbance suppression performance and robust stability against variation of time delay are different. Furthermore, based on the similarity between resonant and time-delay systems mentioned in Chapter 2, time-delay compensation by an equivalent elastic force feedback was also proposed. It can be interpreted that a cause of vibration in time-delay system is robustness of the position-input system against the wave-transmission system. This interpretation comes up from a resonance ratio control which is one of vibration control of a two-mass resonant system. In such field, mass/inertia ratio between motor and load is strongly related to vibration-suppression performance, and vibration increases at load side when mass of motor is heavier than mass of load. If the disturbance observer is implemented to motor, which means that equivalent mass/inertia against torsional force becomes infinity, vibration occurs heavily. Considering such condition, the resonance ratio control conducts a reaction-force feedback to decrease equivalent mass of the motor. Because the equivalent elastic force (reaction force) can be defined in the wave system by wave equation, the idea is applied to the time-delay system. It is confirmed that equivalent elastic force feedback stabilizes the time-delay system by both simulations and experiments.

In Chapter 6, the reflected wave rejection for an integrated resonant and time-delay system was proposed. For realization of the precise control system, not only mechanical resonances but also time delay, for example time delays in a communication system and a DA converter, should be considered. For an

integrated resonant and time-delay systems, there is a case that it is difficult to stabilize the system by simple combination use of vibration control and time-delay compensation. Hence, compensation of the integrated resonant and time-delay systems based on the reflected wave rejection was proposed. In the proposed method, the resonant system is transformed into an equivalent time-delay system, in which there only exists traveling wave, by reflected wave rejection in inner loop. Hence, equivalent transfer function of the integrated system becomes the second order system, which represents the motor dynamics, with sum of time delays which are input-output time delay and transmission delay of the wave. As for the outer loop, actual and equivalent time-delays are simultaneously suppressed by the typical time-delay compensation. Based on the basic structure, the reflected wave rejection which uses a reaction force from the wave system instead of load position was also proposed.

Chapter 7 explained a wave-based disturbance observer for enhancing robustness against disturbance acting on the tip position and modeling error. The wave-based disturbance observer is an extension of arm disturbance observer which is used in control of a two-mass resonant system. For the implementation of wave-based disturbance observer, inverse system of time-delay element is needed to be implemented. Hence, two approximation methods are introduced: one is simple approximation $e^{+T_{wn}s} \approx 1$, the other is use of finite-dimensional approximation. The first-order finite-dimensional approximation of the wave-based disturbance observer is completely same as the arm disturbance observer. Additionally, the wave-based disturbance observer with those approximations were analyzed by use of sensitivity and complementary sensitivity functions. Finite-dimensional approximation of the wave-based disturbance observer performs better robust performance which means that nominal performance is maintained under existence of modeling error. However, finite-dimensional approximation-based wave-based disturbance observer needs to set the cut-off frequency of the observer lower value than maximum-order resonant frequency which is considered in the observer. If the cut-off frequency becomes higher value than the maximum-order resonant frequency due to variation of the resonant frequency, the stability of the control system becomes drastically worse. Therefore, considering the stability of the controlled system, it can be said that the wave-based disturbance observer with the approximation $e^{T_{wn}s} \approx 1$ should be used. Moreover, in Chapter 7, the force control of wave system by using the wave-based disturbance observer as estimator for force acting on tip position was proposed. If the modeling error of the wave system in the observer design does not exist, the wave-based disturbance observer can be used as the observer for the external force acting on the tip position. The proposed force control of wave system is composed of the reflected wave rejection and wave-based disturbance observer. In the inner loop, the reflected wave

rejection suppresses the vibrations of wave system, and wave-based disturbance observer compensates for the disturbance acting on the tip. Equivalent system of inner loop becomes the simple model which is a second-order system with time-delay. In the outer loop, feedback of the estimated force acting on the tip is conducted. Because the equivalent time delay decreases the phase margin of the control system, the force controller implements the phase lead compensator and local velocity feedback for increasing the phase margin. As for the improvement of force-control bandwidth, it is possible to set the nominal transmission time of the wave to higher value than actual value in the wave-based load disturbance observer.

Although this dissertation succeeded in developing the fundamental theory for the control of wave systems based on the reflected wave rejection, there exist issues which should be solved to extend applicability and generality of the proposed method as the future work. Firstly, because this dissertation has dealt with one-dimensional wave equation with respect to space which only considers x direction, the control of wave systems based on the reflected wave rejection should be extended to control of multi-dimensional wave systems which are governed by multi-dimensional wave equations. For example, there is a two-dimensional wave equation which expresses dynamics of a membrane. The flexible arm dealt with in this dissertation can be expressed by the two-dimensional wave equation whose input is applied at boundary line which is orthogonal to x axis (i.e. y axis). If the input at the boundary does not satisfy uniformity and stiffness on y axis is not enough high, the dynamics on y axis can not be neglected. In the case, in order to construct higher control-performance system, the interference between dynamics on different axes should be considered. Secondly, control of wave systems with multi-input-multi-output (MIMO) should be studied. For example, there is a roll-to-roll system involving a flexible plastic or a metal foil. The roll-to-roll system requires realization of both tension control and winding control. One of the solutions is control design based on modal transformation for the two different functions. Hence, control design of wave systems with appropriate modal transformation will be studied for MIMO systems. Finally, a control of multi-degrees-of-freedom (multi-DOF) system will be studied for realization of multi-DOF motions. In the case, relationship between kinematics and flexible structure should be considered. As stated above, although there exist the future work for improvement of versatility of the proposed method, the contents described in this dissertation are expected to make a contribution to progress in the academic field dealing with control engineering for realizing high-performance control systems.

References

[1] M. Iwasaki, K. Seki, and Y. Maeda : "High-Precision Motion Control Techniques: A Promising Approach to Improving Motion Performance," *IEEE Industrial Electronics Magazine*, Vol. 6, No. 1, pp. 32–40, March, 2012.

[2] T. Oiwa and M. Katsuki : "Survey of Questionnaire on Ultra–precision Positioning," *Journal of the Japan Society for Precision Engineering*, Vol. 74, No. 10, pp. 1027–1032, October, 2008. (in Japanese)

[3] M. Tomizuka : "Zero Phase Error Tracking Algorithm for Digital Control," *ASME Journal of Dynamic Systems, Measurement, and Control*, Vol. 109, No. 1, pp. 65–68, March, 1987.

[4] H. Fujimoto, Y. Hori, and A. Kawamura : "Perfect Tracking Control based on Multirate Feedforward Control with Generalized Sampling Periods," *IEEE Transactions on Industrial Electronics*, Vol. 48, No. 3, pp. 636–644, January, 2001.

[5] T. T. Phuong, Y. Yokokura, K. Ohishi, and C. Mitsantisuk : "FPGA-based High Performance Bilateral Control of Different Master-Slave Mechanism Using High Order Disturbance Observer," *Proceedings of the 2013 IEEE International Conference on Mechatronics, ICM '13–VICENZA*, pp. 534–539, March, 2013.

[6] Real-Time Application Interface : `https://www.rtai.org/` (June 1st, 2015).

[7] C. K. Lin, T. H. Liu, and S. H. Yang : "Nonlinear Position Controller Design with Input–Output Linearisation Technique for an Interior Permanent Magnet Synchronous Motor Control System," *IET Journal of Power Electronics*, Vol. 1, No. 1, pp. 14–26, March, 2008.

[8] T. Mita, M. Hirata, and S. B. Villas-Boas : "Design of H_∞ Controllers for Plants Having Poles on the $j\omega$ Axis – H_∞ Motion Control –," *IEEJ Transactions on Industry Applications*, Vol. 115, No. 10, pp. 1253–1262, October, 1995.

[9] V. I. Utkin : "Sliding Mode Control Design Principles and Applications to Electric Drives," *IEEE Transactions on Industrial Electronics*, Vol. 40, No. 1, pp. 23–36, February, 1993.

[10] A. Šavanovic, M. Elitas, and K. Ohnishi : "Sliding Modes in Constrained Systems Control," *IEEE Transactions on Industrial Electronics*, Vol. 55, No. 9, pp. 3332–3339, September, 2008.

[11] A. Šabanovic : "SMC Framework in Motion Control Systems," *International Journal of Adaptive Control and Signal Processing*, Vol. 21, pp. 731–744, May, 2007.

[12] K. Ohishi, K. Ohnishi, and K. Miyachi : "Torque-Speed Regulation Of DC Motor Based On Load Torque Estimation Method," *Proceedings of the IEEJ International Power Electronics Conference, IPEC–TOKYO*, pp. 1209–1216, March, 1983.

[13] K. Ohnishi, M. Shibata, and T. Murakami : "Motion Control for Advanced Mechatronics," *IEEE/ASME Transactions on Mechatronics*, Vol. 1, No. 1, pp. 56–67, March, 1996.

[14] H. Kobayashi, S. Katsura, and K. Ohnishi : "An Analysis of Parameter Variations of Disturbance Observer for Motion Control," *IEEE Transactions on Industrial Electronics*, Vol. 54, No. 6, pp. 3413–3421, December, 2007.

[15] T. Murakami, F. Yu, and K. Ohnishi : "Torque Sensorless Control in Multidegree of Freedom Manipulator," *IEEE Transactions on Industrial Elements*, Vol. 40, No. 2, pp. 259–265, April, 1993.

[16] S. Katsura, Y. Matsumoto, and K. Ohnishi : "Analysis and Experimental Validation of Force Bandwidth for Force Control," *IEEE Transactions on Industrial Electronics*, Vol. 53, No. 3, pp. 922–928, June, 2006.

[17] S. Katsura, K. Irie, and K. Ohishi : "Wideband Force Control by Position-Acceleration Integrated Disturbance Observer," *IEEE Transactions on Industrial Electronics*, Vol. 55, No. 4, pp. 1699–1706, April, 2008.

[18] K. Ohnishi, N. Matsui, and Y. Hori : "Estimation, Identification, and Sensorless Control in Motion System," *Proceedings of the IEEE*, Vol. 82, No. 8, pp. 1253–1265, August, 1994.

[19] T. Yamaguchi, Y. Tadano, and N. Hoshi "Torque Ripple Suppression Control by Periodic Disturbance Observer with Model Error Correction," *IEEJ Transactions on Industry Applications*, Vol. 134, No. 2, pp. 185–192, February, 2014. (in Japanese)

[20] J. Itoh, T. Fujii, T. Hoshino, A. Odaka, I. Sato, and D. Tanaka : "Analysis of Dead–Time Compensation Method Using Disturbance Observer for Vector Control," *IEEJ Transactions on Industry Applications*, Vol. 128, No. 8, pp. 1005–1012, August, 2008. (in Japanese)

[21] Y. Yokokura, S. Katsura, and K. Ohishi : "Motion Copying System Based on Real-World Haptics," *Proceedings of the 10th IEEE International Workshop on Advanced Motion Control, AMC 08–TRENTO*, pp. 613–618, March, 2008.

[22] I. A. Smadi and Y. Fujimoto : "On Nonlinear Disturbance Observer Based Tracking Control for Euler-Lagrange Systems," *Journal of System Design and Dynamics*, pp. 613–618, March, 2008.

[23] M. Ruderman and M. Iwasaki : "Observer of Nonlinear Friction Dynamics for Motion Control," *IEEE Transactions on Industrial Electronics*, to be published.

[24] M. Ruderman : "Tracking Control of Motor Drives Using Feedforward Friction Observer," *IEEE Transactions on Industrial Electronics*, Vol. 61, No. 7, pp. 3727–3735, July, 2014.

[25] Y. Yokokura, S. Katsura, and K. Ohishi : "Stability Analysis and Experimental Validation of a Motion-Copying System," *IEEE Transactions on Industrial Electronics*, Vol. 56, No. 10, pp. 3906–3913, October, 2009.

[26] S. Katsura and K. Ohishi : "Modal System Design of Multirobot Systems by Interaction Mode Control," *IEEE Transactions on Industrial Electronics*, Vol. 54, No. 3, pp. 1537–1546, June, 2007.

[27] K. Yamaguchi, M. Hirata, and H. Fujimoto : "Nanoscale Servo Control," Tokyo Denki University Press, 2007.

[28] T. Atsumi, T. Shimizu, and H. Masuda: "Head-Positioning Control Using Resonant Modes in Hard Disk Drives," *IEEE Transactions on Industrial Electronics*, Vol. 10, No. 4, pp. 378–384, September, 2005.

[29] T. Atsumi and W. C. Messner : "Optimization of Head-positioning Control in a Hard Disk Drive Using the RBode Plot," *IEEE Transactions on Industrial Electronics*, Vol. 59, No. 1, pp. 521–529, January, 2012.

[30] K. J. Astrom and B. Wittenmark : "Computer–Controlled Systems," Prentice–Han Inc., 1984.

[31] K. Ohishi, N. Shimada, and T. Miyazaki : "High-performance Robot Motion Control Based on Zero-phase Notch Filter for Industrial Robot," *Proceedings of the 11th IEEE International Workshop on Advanced Motion Control, AMC '10-NAGAOKA*, pp. 626–630, March, 2010.

[32] T. Mori, K. Fuwa, and H. Kando: "Vibration Control of Flexible Structures via Optimal Servo Control System Using Notch Filter," *Transactions on the Society of Instrument and Control Engineers*, Vol. 44, No. 7, pp. 611–613, July, 2008.

[33] YASKAWA Electric Co., Ltd. : `http://www.e-mechatronics.com/product/servo/sgm7/feature/index.html` (June 1st, 2015).

[34] Mitsubishi Electric Co., Ltd. : `http://www.mitsubishielectric.co.jp/fa/products/drv/servo/pmerit/mr_j4/amp/machine.html` (June 1st, 2015).

[35] Servoland Co., Ltd. : http://www.servoland.co.jp/products/spec.html (June 1st, 2015).

[36] K. Ohno and T. Hara : "Adaptive Resonant Mode Compensation for Hard Disk Drives," *IEEE Transactions on Industrial Electronics*, Vol. 53, No. 2, pp. 624–630, April, 2006.

[37] T. Atsumi, T. Arisaka, T. Shimizu, and T. Yamaguchi : "A Method for Designing a Vibration-Servo-Control System to Reduce the Effect of Mechanical Resonant Modes in a Hard Disk Drive," *Transactions on the Japan Society of Mechanical Engineers Series C*, Vol. 68, No. 675, pp. 3298–3305, November, 2002. (in Japanese)

[38] S. Katsura and K. Ohnishi : "Absolute Stabilization of Multimass Resonant System by Phase-Lead Compensator Based on Disturbance Observer," *IEEE Transactions on Industrial Electronics*, Vol. 54, No. 6, pp. 3389–3396, December, 2007.

[39] K. Ono, H. Takekawa, and H. Yamaura : "Inphase Design of the Lowest Two Natural Modes of Vibrations of Swing-Arm for High Frequency Band Head Positioner," *Transactions on the Japan Society of Mechanical Engineers Series C*, Vol. 64, No. 620, pp. 1347–1355, April, 1998. (in Japanese)

[40] Y. Imaizumi, S. Urushihara, K. Ohishi, and T. Miyazaki : "Design of Robust Load Position Servo System for Two Ineratia Resonant System Based on the Estimated Load Imformation," *IEEJ Transactions on Industry Applications*, Vol. 130, No. 7, pp. 847–857, July, 2010.

[41] Shiang Chih Fu, S. Cheng ; "Analysis and Suppression of Torsional Vibrations for the Permanent Magnet Synchronous Motor-load System," *Proceedings of the IEEE International Conference on Systems, Man and Cybernetics, SMC '2009–SAN ANTONIO*, pp. 3359–3364, October, 2009.

[42] S. H. Song, J. K. Ji, S. K. Sul, and M. H. Park : "Torsional Vibration Suprresion Control in 2-mass System by State Feedback Speed Controller," *Proceedings of the 2nd IEEE Conference on Applications, ICA'93–VANCOUVER*, Vol. 1, pp. 129–134, September, 1993.

[43] M. Itoh: "Vibration Suppression Control for a Two-link Planar Manipulator: Simulation Study on State Feedback Control Using Angular–velocity of Final Gear Stage," *Proceedings of the IEEE International Conference on Mechatronics and Automation, ICMA'05–NIAGARA FALLS*, Vol. 1, pp. 382–387, July, 2005.

[44] S. Yamada and H. Fujimoto : "Vibration Suppression Control for a Two-inertia System Using Load-side High-order State Variables Obtained by a High-resolution Encoder," *Proceedings of the 40th Annual Conference of the IEEE Industrial Electronics Society, IECON '14–DALLAS*, pp. 2897–2903, October, 2014.

[45] S. Morimoto and Y. Takeda : "Two-Degrees-of-Freedom Speed Control of Resonant Mechanical System Based on H_∞ Control Theory," *IEEJ Transactions on Industry Applications*, Vol. 116, No. 1, pp. 65–70, January, 1996. (in Japanese)

[46] I. N. Kar, K. Seto, and F. Doi: "Multimode Vibration Control of a Flexible Structure Using H_∞-based Robust Control," *IEEE/ASME Transactions on Mechatronics*, Vol. 5, No. 1, pp. 23–31, March, 2000.

[47] M. Hirata, K. Z. Liu, and T. Mita : "Active Vibration Control of a 2-mass Spring System using μ-$Synthesis$," *IEEJ Transactions on Industry Applications*, Vol. 114, No. 5, pp. 512–519, March, 1993.

[48] S. Manabe : "Controller Design of Two-Mass Resonant System by Coefficient Diagram Method," *IEEJ Transactions on Industry Applications*, Vol. 118, No. 1, pp. 58–66, January, 1998.

[49] K. Yuki, T. Murakami, and K. Ohnishi : "Vibration Control of 2-mass Resonant System by Resonant Ratio Control," *Proceedings of the 1993 IEEE International Conference on Industrial Electronics, Control, and Instrumentation, IECON '93–MAUI*, Vol. 3, pp. 2009–2014, November, 1993.

[50] Y. Hori, H. Sawada, and C. Yeonghan : "Slow Resonance Ratio Control for Vibration Suppression and Disturbance Rejection in Torsional System," *IEEE Transactions on Industrial Electronics*, Vol. 46, No. 1, pp. 162–168, February, 1999.

[51] A. Al-Mamun, E. Keikha, C. S. Bhatia, and T. H. Lee : "Integral Resonant Control for Suppression of Micro-Actuator Resonance in Dual Stage Actuator," *IEEE Transactions on Magnetics*, Vol. 48, No. 11, pp. 4614–4617, November, 2012.

[52] Y. Seki, K. Saiki, and H. Fujimoto : "Self Resonance Cancellation Using Multiple Sensors for Ballscrew Driven Stage," *Proceedings of the 12th IEEE International Workshop on Advanced Motion Control, AMC '12–SARAJEVO*, pp. 1–6, March, 2012.

[53] M. Aoki, H. Fujimoto, Y. Hori, and T. Takahashi : "Robust Resonance Suppression Control Based on Self Resonance Cancellation Disturbance Observer and Application to Humanoid Robot," *Proceedings of the 2013 IEEE International Conference on Mechatronics, ICM '13–VICENZA*, pp. 623–628, Febraury, 2013.

[54] N. Takesue and J. Furusho: "A Consideration on Inertia-Ratio and Damping Property of Vibration of Two-Inertia System," *IEEJ Transactions on Industry Applications*, Vol. 121, No. 2, pp. 283–284, February, 2001.

[55] S. Katsura and K. Ohnishi : "Force Control of Flexible Manipulator Based on Resonance Ratio Control Using Position Sensitive Detector," *IEEJ Transactions on Industry Applications*, Vol. 126, No. 6, pp. 693–699, June, 2006.

[56] S. Katsura, J. Suzuki, and K. Ohnishi: "Pushing Operation by Flexible Manipulator Taking Environmental Information into Account," *IEEE Transactions on Industrial Electronics*, Vol. 53, No. 5, pp. 1688-1697, October, 2006.

[57] S. Katsura and K. Ohnishi : "Force Servoing by Flexible Manipulator Based on Resonance Ratio Control," *IEEE Transactions on Industrial Electronics*, Vol. 54, pp. 539–547, February, 2007.

[58] C. Mitsantisuk and K. Ohishi : "Resonance Ratio Control Based on Coefficient Diagram Method for Force Control of Flexible Robot System," *Proceeding of the 12th IEEE International Workshop on Advanced Motion Control, AMC '12–SARAJEVO*, pp. 1–6, March, 2012.

[59] M. Hosaka and T. Murakami : "Vibration Control of Flexible Arm by Multiple Observer Structure," *IEEJ Transactions on Industry Applications*, Vol. 124, No. 7, pp. 693–698, July, 2004.

[60] E. Saito and S. Katsura : "Vibration Control of Two-Mass Resonant System Based on Wave Compensator," *IEEJ Transactions on Industry Applications*, Vol. 132, No. 4, pp. 473–479, April, 2012. (in Japanese)

[61] O. Morgul : "Dynamic Boundary Control of a Euler-Bernoulli Beam," *IEEE Transactions on Automatic Control*, Vol. 37, No. 5, pp. 639–642, May, 1992.

[62] M. Krstic : "Dead-Time Compensation for Wave/String PDEs," *ASME Journal of Dynamic Systems, Measurement, and Control*, Vol. 133, No. 3, March, 2011.

[63] Y. Chait and M. Miklavcic : "A Natural Modal Expansion for the Flexible Robot Arm Problem Via a Self-Adjoint Formulation," *IEEE Transactions on Robotics and Automation*, Vol. 6, No. 5, pp. 922–928, October, 1990.

[64] Y. Hori and M. Chengbin: "Fractional order Control: Theory and Applications in Motion Control," *IEEE Industrial Electronics Magazine*, Vol. 1, No. 4, pp. 6–16, December, 2007.

[65] Y. Halevi: "Control of Flexible Structures Governed by the Wave Equation Using Infinite Dimensional Transfer Functions," *ASME Journal of Dynamic Systems, Measurement, and Control*, Volume 127, No. 4, pp. 579–589, December, 2005.

[66] H. Iwamoto and N. Tanaka: "Active Wave Feedback Control of a Flexible Beam Using Wave Filter: Theoretical Verification of Basic Properties," *Transactions on the Japan Society of Mechanical Engineers Series C*, Vol. 70, No. 689, pp. 46–53, 2004. (in Japanese)

[67] M. Saigo and N. Tanaka: "Torsional Vibration Suppression by Using Wave Absorbing Filter," *Transactions on the Japan Society of Mechanical Engineers Series C*, Vol. 71, No. 703, pp. 852–858, 2005. (in Japanese)

[68] N. Abe and A. Kojima : "Control of Time Delayed and Distributed Parameter Systems," Corona-sha, 2007. (in Japanese)

[69] J. P. Richard : "Time-delay Systems : an Overview of Some Recent Advances and Open Problems," *Automatica*, Vol. 39, No. 10, pp. 1667–1694, October, 2003.

[70] H. Morioka, A. Šabanovic, A. Uchibori, K. Wada, and M. Oka : "Application of Time-delay-control in Variable Structure Motion Control Systems," *Proceedings of the IEEE International Symposium on Industrial Electronics Society, ISIE '05–PUSAN*, pp. 1313–1318, June, 2001.

[71] K. Gu and S-I. Niculescu: "Survey on Recent Results in the Stability and Control of Time-Delay Systems," *ASME Journal of Dynamic Systems, Measurement, and Control*, Vol. 125, No. 2, pp. 158–165, 2003.

[72] M. Bowthorpe: "Smith Predictor-based Robot Control for Ultrasound-Guided Teleoperated Beating-Heart Surgery," *IEEE Transactions on Biomedical and Health Informatics*, Vol. 18, No. 1, pp. 157–166, January, 2014.

[73] R. Yang, G. Liu, P. Shi, C. Thomas, and M. V. Basin: "Predictive Output Feedback Control for Networked Control Systems," *IEEE Transactions on Industrial Electronics*, Vol. 61, No. 1, pp. 512–520, January, 2014.

[74] O. J. M. Smith : "A Controller to Overcome Dead Time," *The International Society of Automation Journal*, Vol. 6, No. 2, pp. 28–33, February, 1959.

[75] L. Repele, R. Muradore, D. Quaglia, and P. Fiorini: "Improving Performance of Networked Control Systems by Using Adaptive Buffering," *IEEE Transactions on Industrial Electronics*, Vol. 61, No. 9, pp. 4847–4856, September, 2014.

[76] H. Okajima, T. Asai, and S. Kawaji: "Tracking Performance Limitation for Plants with Input Delay in 2-DOF Internal Model Control Systems," *Transactions on the Society of Instrument and Control Engineers*, Vol. 45, No. 6, pp. 313–319, January, 2007. (in Japanese)

[77] K. Natori and K. Ohnishi : "An Approach to Design of Feedback Systems with Time Delay," *Proceedings of the 31st Annual Conference of the IEEE Industrial Electronics Society, IECON '05–RALEIGH*, pp. 1931–1936, November, 2005.

[78] K. Natori and K. Ohnishi : "A Design Method of Communication Disturbance Observer for Time-delay Compensation, Taking the Dynamic Property of Network Disturbance into Account," *IEEE Transactions on Industrial Electronics*, Vol. 55, No. 5, pp. 2152–2168, May, 2008.

[79] K. Natori, R. Oboe, and K. Ohnishi : "Stability Analysis and Practical Design Procedure of Time Delayed Control Systems with Communication Disturbance Observer," *IEEE Transactions on Industrial Informatics*, Vol. 4, No. 3, pp. 185–197, August, 2008.

[80] K. Natori, R. Oboe, and K. Ohnishi : "Robust Time Delayed Control Systems with Communication Disturbance Observer," *Proceedings of the 33rd Annual Conference of the IEEE Industrial Electronics Society, IECON '07–TAIPEI*, pp. 316–321, November, 2007.

[81] A. A. Rahman and K. Ohnishi : "Robust Time Delayed Control System Based on Communication Disturbance Observer with Inner Loop Input," *Proceedings of the 36th Annual Conference of the IEEE Industrial Electronics Society, IECON '10–GLENDALE*, pp. 1621–1626, November, 2010.

[82] T. Takehara, T. Kunitake, H. Hashimoto, and F. Harashima : "The Control for the Disturbance in the System with Time Delay," *Proceedings of the 4th International Workshop on Advanced Motion Control, AMC '96–MIE*, Vol. 1, pp. 349–353, March, 1996.

[83] A. Suzuki and K. Ohnishi : "Improvement in Steady-State Accuracy of Time-delayed Control Systems with Communication Disturbance Observer by Low-Frequency Model Error Feedback," *IEEJ Transactions on Industry Applications*, Vol. 133, No. 9, pp. 861–867, September, 2013. (in Japanese)

[84] D. Yashiro and K. Ohnishi : "A Communication Disturbance Observer with a Band-pass Filter for Delay Time Compensation," *Proceedings of the 19th IEEE International Symposium on the Industrial Electronics Society, ISIE '10-BARI*, pp. 3585–3589, July, 2010.

[85] E. Saito and S. Katsura : "Vibration Control of Flexible System With Communication Delay Using Wave Compensator," *Proceedings of the 12th International Workshop on Advanced Motion Control, AMC '12–SARAJEVO*, pp. 1–6, March, 2012.

[86] E. Saito and S. Katsura : "Vibration Control of a Two-Mass Resonant System Using Wave Compensator," *Proceedings of the Annual Conference, SICE '11–TOKYO*, pp. 2672-2677, September, 2011.

[87] E. Saito and S. Katsura : "Vibration Suppression of Resonant System by Using Wave Compensator," *Proceedings of the 37th Annual Conference of the IEEE Industrial Electronics Society, IECON '11–MELBOURNE*, pp. 4105–4110, November, 2011.

[88] E. Saito, R. Oboe, and S. Katsura : "Time Delay Compensation Method Based on Reflected Wave Rejection," *Proceedings of the 39th Annual Conference of the IEEE Industrial Electronics Society, IECON '13–VIENNA*, pp. 4274–4279, November, 2013.

[89] E. Saito and S. Katsura : "Vibration Control of Resonant System by Using Reflected Wave Rejection with Fractional Order Low-Pass Filter," *Proceedings of the IEEE International Conference on Mechatronics, ICM '13–VICENZA*, pp. 852–857, February, 2013.

[90] E. Saito and S. Katsura : "Load Position Sensorless Vibration Control of Resonant System Using Reflected Wave Rejection," *Proceedings of the 2012 ASME Dynamic Systems and Control Conference/11th Motion and Vibration Conference, DSCC/MOVIC '12–FORT LAUDERDALE*, pp. 1–5, October, 2012.

[91] E. Saito and S. Katsura : "Compensation of Integrated Resonant and Time Delay System by Using Wave Compensator," *Journal for Control, Measurement, Electronics, Computing and Communications, Automatika*, Vol. 54, No. 1, pp. 28–38, March, 2013.

[92] E. Saito, R. Oboe, and S. Katsura : "Vibration Suppression of Integrated Resonant and Time Delay System by Reflected Wave Rejection," *Proceedings of the 2014 International Power Electrnics Conference, IPEC2014-HIROSHIMA*, pp. 1679–1684, May, 2014.

[93] E. Saito and S. Katsura : "Reaction-torque-based Reflected Wave Rejection for Vibration Suppression of Integrated Resonant and Time-delay System," *Proceedings of the IEEE International Conference on Mechatronics, ICM '15–NAGOYA*, pp. 665–670, March, 2015.

[94] E. Saito and S. Katsura : "Position Control of Resonant System with Load Force Suppression Using Wave Observer," *IEEJ Journal of Industry Applications*, Vol. 3, No. 1, pp. 18–25, January, 2014.

[95] E. Kreyszig : "Advanced Engineering Mathematics," Wiley, 2005.

[96] J. Suzuki, T. Murakami, and K. Ohnish : "Vibration Control of Flexible Manipulator Taking Friction-depending Disturbance into Account," *IEEJ Transactions on Industry Applications*, Vol. 122, No. 3, pp. 235–240, March, 2002. (in Japanese)

[97] N. Hirose, M. Iwasaki, M. Kawafuku, and H. Hirai : "Robust Vibration Suppression of Resonant Modes by Feedback Compensation Realized Using Allpass Filters," *IEEJ Transactions on Industry Applications*, Vol. 129, No. 10, pp. 981–988, October, 2009. (in Japanese)

[98] M. Matsuoka, T. Murakami, and K. Ohnishi : "Vibration Suppression and Disturbance Rejection Control of Flexible Link Arm," *Proceedings of the 21st Annual Conference of the IEEE Industrial Electronics Society, IECON '95–ORLANDO*, Vol. 2, pp. 1260–1265, Novbemver, 1995.

[99] E. Saito and S. Katsura : “Time Delay Compensation by Using Equivalent Elastic Force Feedback,” *IEEJ The Papers of Technical Meeting on Industrial Instrumentation and Control, IIC14*, Vol. 2, pp. 93–98, March, 2014.

[100] E. Saito and S. Katsura : “Force Control of Wave System Based on Reflected Wave Rejection,” *Proceedings of the 2015 Annual Meeting of the Institute of Electrical Engineers of Japan*, Vol. 4, pp. 296–297, March, 2015. (in Japanese)

List of Achievements

Journals (As a first author)

[1] Eiichi Saito and Seiichiro Katsura, "Vibration Control of Two-mass Resonant System Based on Wave Compensator," *IEEJ Transactions on Industry Applications*, Vol. 132, No. 4, pp. 473–479, April, 2012. (in Japanese)

[2] Eiichi Saito and Seiichiro Katsura, "Compensation of Integrated Resonant and Time Delay System by Using Wave Compensator," *Journal for Control, Measurement, Electronics, Computing and Communications, Automatika*, Vol. 54, No. 1, pp. 28–38, March, 2013.

[3] Eiichi Saito and Seiichiro Katsura, "Position Control of Resonant System with Load Force Suppression Using Wave Observer," *IEEJ Journal of Industry Applications*, Vol. 3, No. 1, pp. 18–25, January, 2014.

[4] Eiichi Saito and Seiichiro Katsura, "Time Delay Compensation Using Equivalent Elastic Force Feedback," *IEEJ Journal of Industry Applications*, Vol. 4, No. 6, November, 2015. (to be published)

Journals (As a Co-author)

[1] Shunsuke Yajima, Eiichi Saito, and Seiichiro Katsura, "Controller Design for Reproduction of Grasping/Manipulation Motion of Grasping Objects with Different Diameters," *IEEJ Transactions on Industry Applications*, Vol. 2, No. 1, pp. 7–13, January, 2013.

[2] Takahiro Kosugi, Shunsuke Yajima, Eiichi Saito, and Seiichiro Katsura, "Mode Switching Bilateral Control for Master-Slave Systems with Different Motion Areas," *IEEJ Journal of Industry Applications*, Vol. 2, No. 5, pp. 473–479, September, 2013.

International Conference (As a first author)

[1] Eiichi Saito and Seiichiro Katsura, "Vibration Control of a Two-mass Resonant System Using Wave Compensator," *SICE Annual Conference, SICE '11-TOKYO*, pp. 2672–2677, September, 2011.

[2] Eiichi Saito and Seiichiro Katsura, "Vibration Suppression of Resonant System by Using Wave Compensator," *The 37th Annual Conference of the IEEE Industrial Electronics Society, IECON '11-MELBOURNE*, pp. 4105–4110, November, 2011.

[3] Eiichi Saito and Seiichiro Katsura, "Control of Bilateral Force Feedback System with Flexible Mechanism based on Resonant Ratio Control," *The 2011 IEEE/SICE International Symposium on System Integration, SII '11-KYOTO*, pp. 503-508, December, 2011.

[4] Eiichi Saito and Seiichiro Katsura, "Vibration Control of Flexible System with Communication Delay Using Wave Compensator," *The 12th International Workshop on Advanced Motion Control, AMC '12-SARAJEVO*, pp. 1–6, March, 2012.

[5] Eiichi Saito and Seiichiro Katsura, "A Filter Design Method in Disturbance Observer for Improvement of Robustness against Disturbance in Time Delay System," *The 21st IEEE International Symposium on Industrial Electronics, ISIE '12-HANGZHOU*, pp. 1650–1655, May, 2012.

[6] Eiichi Saito and Seiichiro Katsura, "Load Position Sensorless Vibration Control of Resonant System Using Reflected Wave Rejection," *The 2012 ASME Dynamic Systems and Control Conference/11th Motion and Vibration Conference, DSCC/MOVIC '12-FORT LAUDERDALE*, pp. 1–5, October, 2012.

[7] Eiichi Saito and Seiichiro Katsura, "Force Control of Two-Mass Resonant System with Vibration Suppression Based on Modal Transformation," *The 38th Annual Conference of the IEEE Industrial Electronics Society, IECON '12-MONTREAL*, pp. 2589–2594, October, 2012.

[8] Eiichi Saito and Seiichiro Katsura, "Vibration Control of Resonant System by Using Reflected Wave Rejection with Fractional Order Low-Pass Filter," *IEEE International Conference on Mechatronics, ICM '13-VICENZA*, pp. 852–857, February, 2013.

[9] Eiichi Saito and Seiichiro Katsura, "Bilateral Control of Two-Mass Resonant System Based on Concept of Multilateral Control," *The 22nd IEEE International Symposium on Industrial Electronics, ISIE '13-TAIPEI*, pp. 1–6, May, 2013.

[10] Eiichi Saito, Roberto Oboe, and Seiichiro Katsura, "Time Delay Compensation Method Based on Reflected Wave Rejection," *The 39th Annual Conference of the IEEE Industrial Electronics Society, IECON '13-VIENNA*, pp. 4274–4279, November, 2013.

[11] Eiichi Saito, Roberto Oboe, and Seiichiro Katsura, "Vibration Suppression of Integrated Resonant and Time Delay System by Reflected Wave Rejection," *The 2014 International Power Electrnics Conference, IPEC '14-HIROSHIMA*, pp. 1679–1684, May, 2014.

[12] Eiichi Saito and Seiichiro Katsura, "Reaction-torque-based Reflected Wave Rejection for Vibration Suppression of Integrated Resonant and Time-delay System," *IEEE International Conference on Mechatronics, ICM '15-NAGOYA*, pp. 665–670, March, 2015.

International Conferences (As a Co-author)

[1] Hidetaka Morimitsu, Eiichi Saito, and Seiichiro Katsura, "An Approach for Heat Flux Sensorless Heat Inflow Estimation Based on Distributed Parameter System of Peltier Device," *The 37th Annual Conference of the IEEE Industrial Electronics Society, IECON '11-MELBOURNE*, pp. 4069–4074, November, 2011.

[2] Rajitha Tennekoon, Janaka Wijekoon, Erwin Harahap, Hiroaki Nishi, Eiichi Saito, and Seiichiro Katsura, "Per Hop Data Encryption Protocol for Transmission of Motion Control Data Over Public Networks," *The 13th IEEE International Workshop on Advanced Motion Control, AMC '14-YOKOHAMA*, pp. 128–133, March, 2011.

[3] Fumito Nishi, Eiichi Saito, and Seiichiro Katsura, "Bilateral Transmission of Rubbing Motion into Ultra-fine Environments," *The 1st IEEJ International Workshop on Sensing, Actuation, and Motion Control, SAMCON '15-NAGOYA*, pp. 1–6, March, 2015.

Domestic Conference (As a first author)

[1] Eiichi Saito and Seiichiro Katsura, "Vibration Control of Two-Mass Resonant System Based on Wave Compensator," *The IEEJ Papers of Technical Meeting on Industrial Instrumentation and Control, IIC '11*, Vol. 3, pp. 59–64, March, 2011. (in Japanese)

[2] Eiichi Saito and Seiichiro Katsura, "Control of Multi Mass Resonant System Considering Wave Model," *The 2011 Annual Meeting of the Institute of Electrical Engineers of Japan*, Vol. 4, pp. 332–333, March, 2011. (in Japanese)

[3] Eiichi Saito and Seiichiro Katsura, "Vibration Control of a Two-Mass Resonant System Using Tip-Position Delayed Feedback," *Mechanical Engineering Congress 2011, MECJ '11*, No. J192031, pp. 1–5, September, 2011. (in Japanese)

[4] Eiichi Saito, Shutaro Yorozu, and Seiichiro Katsura, "Bilateral Control of A System Including Flexible Mechanism," *The 54th Administration Committee of Japan Joint Automatic Control Conference, JACC11*, No. 1I203, pp. 413–418, November, 2011. (in Japanese)

[5] Eiichi Saito and Seiichiro Katsura, "Robust Control of a Resonant System Using Wave Observer," *The IEEJ Papers of Technical Meeting on Industrial Instrumentation and Control, IIC '12*, Vol. 5, pp. 51–56, March, 2012. (in Japanese)

[6] Eiichi Saito and Seiichiro Katsura, "Improvement of Control Bandwidth in Bilateral Control with Flexibility Based on Load Disturbance Observer," *The 2012 Annual Meeting of the Institute of Electrical Engineers of Japan*, Vol. 4, pp. 313–314, March, 2012. (in Japanese)

[7] Eiichi Saito and Seiichiro Katsura, "Time Delay Compensation by Using Equivalent Elastic Force Feedback," *The IEEJ Papers of Technical Meeting on Industrial Instrumentation and Control, IIC '14*, Vol. 2, pp. 93–98, March, 2014. (in Japanese)

[8] Eiichi Saito and Seiichiro Katsura, "Force Control of Wave System Based on Reflected Wave Rejection," *The 2015 Annual Meeting of the Institute of Electrical Engineers of Japan*, Vol. 4, pp. 296–297, March 24–26, 2015. (in Japanese)

Domestic Conference (As a co-author)

[1] Shunsuke Yajima, Eiichi Saito, and Seiichiro Katsura, "A Controller Design for Reproduction of Multi Degree-of-Freedom Motion," *IEEJ The Papers of Technical Meeting on Industrial Instrumentation and Control, IIC '12*, Vol. 2, pp. 13–18, March, 2012. (in Japanese)

[2] Hidetaka Morimitsu, Eiichi Saito, and Seiichiro Katsura, "Construction of Bilateral Control System with Transformation of Thermal-Mechanical Information," *IEEJ The Papers of Technical Meeting on Industrial Instrumentation and Control, IIC '12*, Vol. 2, pp. 61–66, March, 2012. (in Japanese)

[3] Takahiro Kosugi, Shunsuke Yajima, Eiichi Saito, and Seiichiro Katsura, "Operability Improvement in Bilateral Teleoperation with Different Motion Areas," *IEEJ The Papers of Technical Meeting on Industrial Instrumentation and Control, IIC '12*, Vol. 2, pp. 67–72, March, 2012. (in Japanese)

Awards

[1] “IEEE IES 2012 Best Conference Paper Award”
IEEE Industrial Electronics Society
October 26th, 2012

[2] “FA Foundation Paper Award”
FA Foundation
December 13th, 2013

Career

[1] April, 2013∼
Research Fellow (DC1)
The Japan Society for the Promotion of Science